# DETECTION OF SHALLOW SUBSURFACE CAVITIES USING 2D & 3D ELECTRICAL RESISTIVITY TOMOGRAPHY ALONG THE RED SEA COAST, DUBA REGION, TABUK-SAUDI ARABIA


BY

**MUHAMMAD HAROON TAYYAB**


A Thesis Presented to the

DEANSHIP OF GRADUATE STUDIES

**KING FAHD UNIVERSITY OF PETROLEUM & MINERALS**

DHAHRAN, SAUDI ARABIA

In Partial Fulfillment of the
Requirements for the Degree of

## MASTER OF SCIENCE

In

**GEOPHYSICS**

**MAY 2017**

KING FAHD UNIVERSITY OF PETROLEUM & MINERALS

DHAHRAN- 31261, SAUDI ARABIA

**DEANSHIP OF GRADUATE STUDIES**

This thesis, written by **Muhammad Haroon Tayyab** under the direction of his thesis advisor and approved by his thesis committee, has been presented and accepted by the Dean of Graduate Studies, in partial fulfillment of the requirements for the degree of **MASTER OF SCIENCE IN GEOPHYSICS.**

Dr. Abdulaziz Al-Shaibani
Department Chairman

Dr. SanLinn Isma'il Kaka
(Advisor)

Dr. Salam A. Zummo
Dean of Graduate Studies

Dr. Abdullatif Al-Shuhail
(Member)

19/12/12
Date

Dr. Khalid Al-Ramadan
(Member)

# DEDICATION

I dedicate this work to my Mother (late), Father and my wife, without their prayers, motivation and support I may not be able to complete MS successfully.

To my Teachers for their guidance and tutelage.

# ACKNOWLEDGEMENTS

*"In the name of Allah, The Most Gracious and The Most Merciful"*

All praise belongs to Almighty Allah (s.w.t.) for bestowing me with courage and perseverance to carry out this work sincerely. I thank Almighty Allah for giving me opportunity to do my M.S. successfully at King Fahd University of Petroleum and Minerals, Dhahran.

I would like to express my deepest gratitude to King Fahd University of Petroleum and Minerals for providing me good academic platform during my M.S.

My deepest gratitude and appreciation goes to my thesis advisor and mentor Dr. SanLinn Ismail Kaka for his constant guidance, motivation and support during the course of my studies. His valuable suggestions broadened my horizon in the field of Engineering Geophysics and made this work interesting and challenging for me. I also wish to express my deep gratitude and appreciation to Dr. Abdullatif Al-Shuhail and Dr. Khalid Al-Ramadan for their reviews, guidance, and efforts serving on my thesis committee.

I am very grateful to my company INSPECTECH for providing me with the needed data for this study, and special gratitude goes to my Division Managers, Engr. Mustafa Dani, Engr. Chadi Said and Engr. Daher Mokdad, and all the colleagues for their encouragement and continuous support throughout the course of my Masters.

I would like to thank several individuals for their technical support; Dr. Bartolomeo Garofalo and Dr. Gianfranco Morelli from Geostudi Astier Srl. for their guidance and

assistance in inversion and interpretation parts of the thesis, and for providing their expert views and guidance.

I also wish to express my deep gratitude and appreciation to Mr. Abid Ali, Mr. Imran Hussain and Mr. Mohammad Ali for their assistance with data acquisition.

I am very thankful to Ayyaz Mustafa, Waleed Ejaz, Abdullah Alqubalee, Asif Abbas, Mustafa Al Marzouq, Amjad Ali and Syed Haroon Ali for their support during my Masters. I would also like to acknowledge all the Earth Sciences faculty members with whom I took courses during my M.S., who helped me a lot during my coursework. I also owe thanks to all the students and faculty with whom I interacted during my Master's program.

# TABLE OF CONTENTS

# LIST OF TABLES

# LIST OF FIGURES

# LIST OF ABBREVIATIONS

| | | |
|---|---|---|
| **CIRIA** | : | The Construction Industry Research and Information Association |
| **CRS** | : | Constant Resistance |
| **CST** | : | Constant Separation Traversing |
| **DC** | : | Direct Current |
| **DIC** | : | Depth of investigation characteristic |
| **EM** | : | Electromagnetic |
| **ERT** | : | Electrical Resistivity Tomography |
| **GPR** | : | Ground Penetrating Radar |
| **GPS** | : | Ground Positioning System |
| **IP** | : | Induced polarization |
| **NAPL** | : | Non-aqueous phase liquid |
| **RMS** | : | Root-mean-square |
| **RQD** | : | Rock Quality Designation |
| **SP** | : | Self-Potential |
| **SPT** | : | Standard Penetration Test |
| **UI** | : | User Interface |
| **VES** | : | Vertical Electrical Sounding |
| **VLF** | : | Very low frequency |

# NOMENCLATURE

| | |
|---|---|
| $\mathbf{B}$ | Magnetic induction [Wb/m$^2$] |
| $I$ | Electric current [A] |
| $K$ | Geometric factor [m] |
| $R$ | Resistance [Ω] |
| $V$ | Electric potential [V] |
| $Z$ | Electric impedance [Ω] |
| $a$ | Array “a” –spacing [m] |
| $d$ | Elevation; distance [m] |
| j | Electric current density [A/m$^2$] |
| $n$ | Array “n” -factor |
| $l$ | Dipole length [m] |
| $r$ | Dipole separation; distance [m] |
| $\Delta s$ | Sampling distance [m] |
| $t$ | Time [s] |
| $x$ | Cartesian coordinate; position [m] |
| $y$ | Cartesian coordinate; position [m] |
| $z$ | Depth; elevation [m] |
| η | Electrical Charge Density [Cb/m$^3$] |
| $\rho$ | Electrical Resistivity [Ωm] |
| $\rho_a$ | Apparent Resistivity [Ωm] |
| $\sigma$ | Electrical Conductivity [S/m] |
| $\nabla$ | Nabla Operator |

# ABSTRACT

FULL NAME : MUHAMMAD HAROON TAYYAB

THESIS TITLE : DETECTION OF SHALLOW SUBSURFACE CAVITIES USING 2D & 3D ELECTRICAL RESISTIVITY TOMOGRAPHY ALONG THE RED SEA COAST, DUBA REGION, TABUK-SAUDI ARABIA

MAJOR FIELD : GEOPHYSICS

DATE OF DEGREE : May, 2017

Poor rock quality and subsurface voids were encountered during a geotechnical investigation for a building construction along the Red Sea coast, in Duba Region, Tabuk, Saudi Arabia. Because of this, there were concerns about the integrity of the rock formation beneath the foundations of the proposed building. The subsoil conditions along the Red Sea coast in Saudi Arabia are complex due to existence of coralline limestone beds of Quaternary Age. The existence of natural voids and cavities in subsurface limestone poses severe hazard for civil engineering activities. To determine the extent of shallow voids through drilling was costly and time intensive. The construction project was thus halted and a geophysical investigation was undertaken to understand such heterogeneity, and detect the areas prone to ground subsidence through the collapse of cavities beneath the footprint of the proposed construction site.

The electrical resistivity survey was carried out for a rectangular area of approximately 4,500 $m^2$, to obtain a 3D image of the electrical characteristics of the subsurface in the top 15-20 m. The field data set consisted of twelve equidistant parallel 2D transects spaced at 3.36 m and two C-shaped 3D electric profiles along the periphery of the investigated area.

The electrode spacing was kept at 1.6 m for 2D and 2.5 m for 3D profiles, ensuring to capture high resolution image of the subsurface. The acquired data was processed and inverted using 2D and 3D inversion algorithms utilizing smoothness constrained least squares optimization routines, to convert the apparent resistivity pseudo-sections into a true resistivity model representing continuous distribution of calculated electrical resistivity in the subsurface.

The inverted resistivity data provided a clear image of weathered soils, the distribution of weak zones and the water table. Several low resistivity areas were identified and drilling of such anomalous areas subsequently led to the discovery of several weak zones or sediment-filled underground cavities. The electrical resistivity imaging result proved precise and efficient in delineating shallow subsurface voids and soil heterogeneity and thus recommend to carry out electrical resistivity investigation for complex geological sites.

# ملخص الرسالة

**الاسم الكامل**: محمد هارون طيب

**عنوان الرسالة: الكشف عن الكتل السطحية باستخدام المقاومة الكهربائية 2D و3D لتصوير على طول ساحل البحر الأحمر، منطقة ضبا-تبوك المملكة العربية السعودية**

**التخصص:** جيوفيزياء

**تاريخ الدرجة العلمية**: أبريل 2017

تربة صخرية ضعيفة و فراغات جوفية وجدت خلال تنفيذ اختبارات للتربة، حيث سيتم إنشاء مبنى على ساحل البحر الأحمر، منطقة ضبا- تبوك – المملكة العربية السعودية. بسبب ذلك، تولدت شكوك عن سلامة الصخورأسفل مستوى القواعد للمبنى المذكور.

حالة التربة الباطنية على طول ساحل البحر الأحمر في المملكة العربية السعودية, هي تربة معقدة بسبب وجود طبقة جيرية مرجانية تعود باصلها لآخر العصور الجيولوجية.

وجود مثل هذه الفراغات الجوفية والكهوف الطبيعية في الطبقة الجيرية يشكل خطرا شديدا للأعمال المتعلقة بالهندسة المدنية. وبما أن تحديد مدى حجم و امتداد الفراغات الجوفية المتواجدة في طبقة التربة القريبة من السطح، هو أمر يستنزف الكثيرمن المال و الوقت، تقرر تجميد البدء بأعمال الإنشاءات و الشروع بتنفيد دراسة جيوفيزيائية لفهم جيد لهذه التربة الغير متجانسة, وتحديد الأماكن التي من الممكن ان تكون عرضة لهبوطات أرضية في حال حدوث إنهيارات في الكهوف الجوفية أسفل قواعد المبنى المذكور.

لذلك, تم الشروع بتنفيذ عملية مسح للتربة باستخدام تقنية قياس المقاومة الكهربائية لمساحة تقدر ب 4500 مترمربع، بهدف الحصول على صور بالأبعاد الثلاثية تظهرخصائص التربة الكهربائية لعمق يصل الى 15-20 متر، و لأجل ذلك تم أخذ القراءات من الموقع عبر نصب خطوط 2D متوازية و متساوية البعد بقدر 3.36 مترو بعدد اثنا عشر خط, بالإضافة لخطين 3D بشكل الحرف C على طول حدود المنطقة المذكورة. حيث تمت المحافظة على تباعد ثابت للأقطاب الكهربائية بقدر 1.6 متر لخطوط ال 2D و 2.5 متر لخطوط ال 3D , بهدف الحصول على صور عالية الدقة للتربة. بعد ذلك تمت معالجة وتحويل القراءات بإستخدام لوغاريتمات تحويل 2D و 3D خاصة تقوم على البرمجة المسماة smoothness constrained least squares

optimization routines، بهدف تحويل ارقام المقاومة الظاهرية (pseudo-sections) الى أنموزج للتربة التحت- سطحية يحاكي الواقع ويمثل توزع متكامل ومتواصل لقيم المقاومة الكهربائية التي تمت معالجتها.

قدمت قراءات المقاومة الكهربائية المعالجة صورة واضحة تظهر التربة المتفككة/المتفتتة و توزع المناطق الضعيفة بالاضافة لمستوى المياه الجوفية. بالمقارنة مع نتائج فحوصات الثقوب فإن المناطق المتفككة/المتفتتة تم تأكيدها من خلال الحصول على نتئج غير طبيعية وضعيفة لقيم ال RQD التي تم الحصول عليها خلال تنفيذ الثقوب (Boreholes). عدة مناطق ذات قيم مقاومة كهربائية ضعيفة وجدت و تم الحفرفيها لاحقا مما كشف عن عدة مناطق ضعيفة و sediment filled underground cavities تم اسقاط نتائج قياس المقاومة الكهربائية على الصور الجوية مما أظهر تطابق جيد مع المعالم الطوبوغرافية والتغييرات الحاصلة في جيولوجيا السطح. ان النتيجة التي تماستخلاصها من خلال عملية فحص التربة باستخدام تقنية قياس المقاومة الكهربائية اظهرت انها تقنية دقيقة و تتسم بالكفاءة في تحديد الفراغات الجوفية القريبة من السطح و عدم التجانس في التربة، و يجب اخذها بعين الإعتبار عند استكشاف مواقع ذات طبيعة جيولوجية معقدة.

.

# CHAPTER 1

# INTRODUCTION

## 1.1 Background and Scope of Study

The existence of natural voids and cavities poses a major engineering hazard associated with construction areas underlain by carbonate rocks. Subsurface cavity refers to all subsurface structures such as sinkholes, voids, caves, cavities, karst and caverns. The most abundant natural cavities are formed by dissolution processes in carbonates (e.g. limestone and dolomite) and evaporites (e.g., salt, gypsum, and anhydrite). The subsoil conditions along the Red Sea coast in Saudi Arabia are complex due to existence of coralline limestone of Quaternary Age. The study area is overlain by coastal sediments and underlain by coralline limestone of Quaternary age. These coral beds are soft, porous and nonhomogeneous, often interspaced with large cavities.

Several problems are associated with subsurface karstic voids, such as building foundation collapse, road and highway subsidence, etc. Large void formation in a karst environment may lead to abrupt and catastrophic failure. Any of the above situations in a karst environment can be cost-intensive for the design of engineering structure. Often, the main targets in the subsurface are not met by boring within the karst areas. Misplaced borings often misrepresent the subsurface condition. Examining aerial photographs and satellite images is a classical technique of karst detection, and reasonably good maps have been produced over the past decade. However, such approach is spatially and temporally

discontinuous, representing only discreet information. Geological and geomorphological methods cannot be directly applied in many urban areas where rapid development has obscured surface features. Dependable hazard mapping, especially for detailed civil engineering studies, cannot rely solely on a limited source of information; other techniques are thus required for accurate study.

Subsurface voids represent disturbances of the close subsurface layered system in karst areas; such disturbances can be identified using geophysical techniques. Employing geophysical techniques to survey the area can be more effective, economic and less labor intensive, and can also reduce number of test bores to be drilled, as well as improve decision making in the position of test bores for more effective target verification and mapping.

In this study, the applicability of Electrical Resistivity Tomography (ERT) imaging is demonstrated for the investigation of shallow subsurface weathered zones, voids/cavities and soil heterogeneity, at a proposed construction site along the Red Sea coast in Tabuk Province, Kingdom of Saudi Arabia. Owing to the presence of soft and porous coralline limestone beds underlying the study area and visually observed karst holes at the surface, the investigation was aimed at imaging all possible geophysical anomalies that could be related to possible hazardous or subsidence prone areas.

## 1.2 Geophysical Application

Geophysical methods employ indirect, non-intrusive observations to characterize and map variations in the physical properties of what lies concealed beneath the ground surface. According to the Encyclopedia of Caves and Karstic Science, 2004, “All geophysical

techniques require contrasts of some physical properties (density, electrical resistivity, magnetic susceptibility and seismic velocity) between subsurface structures".

Although void space in rock may represent an enormous contrast in physical properties that can be advantageous to an investigator seeking concealed caves, underground karst openings are frequently small, irregular targets whose effects are easily masked by those of surface irregularities. In deep exploration, techniques that are useful usually are at the expense of resolution and accuracy; conversely, techniques capable of generating high-resolution images of shallow features are often based on high-frequency signals that are rapidly attenuated as they propagate through deeper soil and rock. It is conventional in geotechnical engineering practice to obtain subsurface information before embarking on any project. Mapping hidden karst is necessary when engineering projects are planned in rock formations known to contain caves, because karstic voids and collapses can compromise the integrity of building foundations, dams, and bridges. Drilling of boreholes is one of the methods of obtaining subsurface information. But if detailed subsurface information is needed, boreholes have to be closely spaced in order to produce a reliable image of the subsurface. Unfortunately, such drilling of multiple boreholes is time-consuming and uneconomical. More so, even though the subsurface information obtained at boring location is very accurate, the interpolation between boreholes can sometimes be erroneous due to significant variations in karst terrain. Use of geophysical tools as a control reduces the number of required boreholes and significantly decreases the ambiguity of the subsurface conditions.

## 1.3 Study Area

The study area is located in Duba region, Tabuk Province along the Red Sea coast, North-West (NW) of Saudi Arabia. It is part of Wadi Azlam in Al Muwaylih quadrangle. In the NW part of Saudi Arabia, large areas of Al Muwaylih quadrangle are overlain by basement crystalline rocks of Neoproterozoic Era. The area of investigation lies at the beach terrace made up of coralline limestone of Quaternary age along the Red Sea coast, at the downstream of Wadi Azlam. A portion of the general geology of NW Saudi Arabia is given in Figure 1.1 and the actual site location is shown by the Landsat image in Figure 1.2.

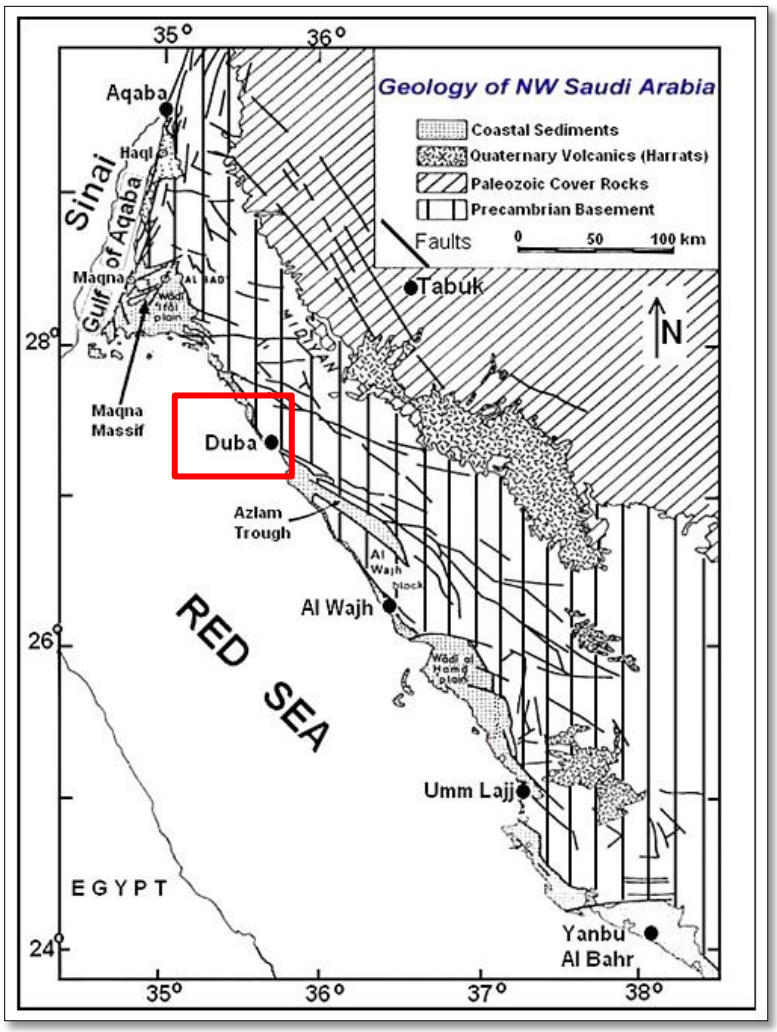


**Figure 1.1: Geology of North Western Saudi Arabia (Vazquez-Lopez and Motti 1981)**

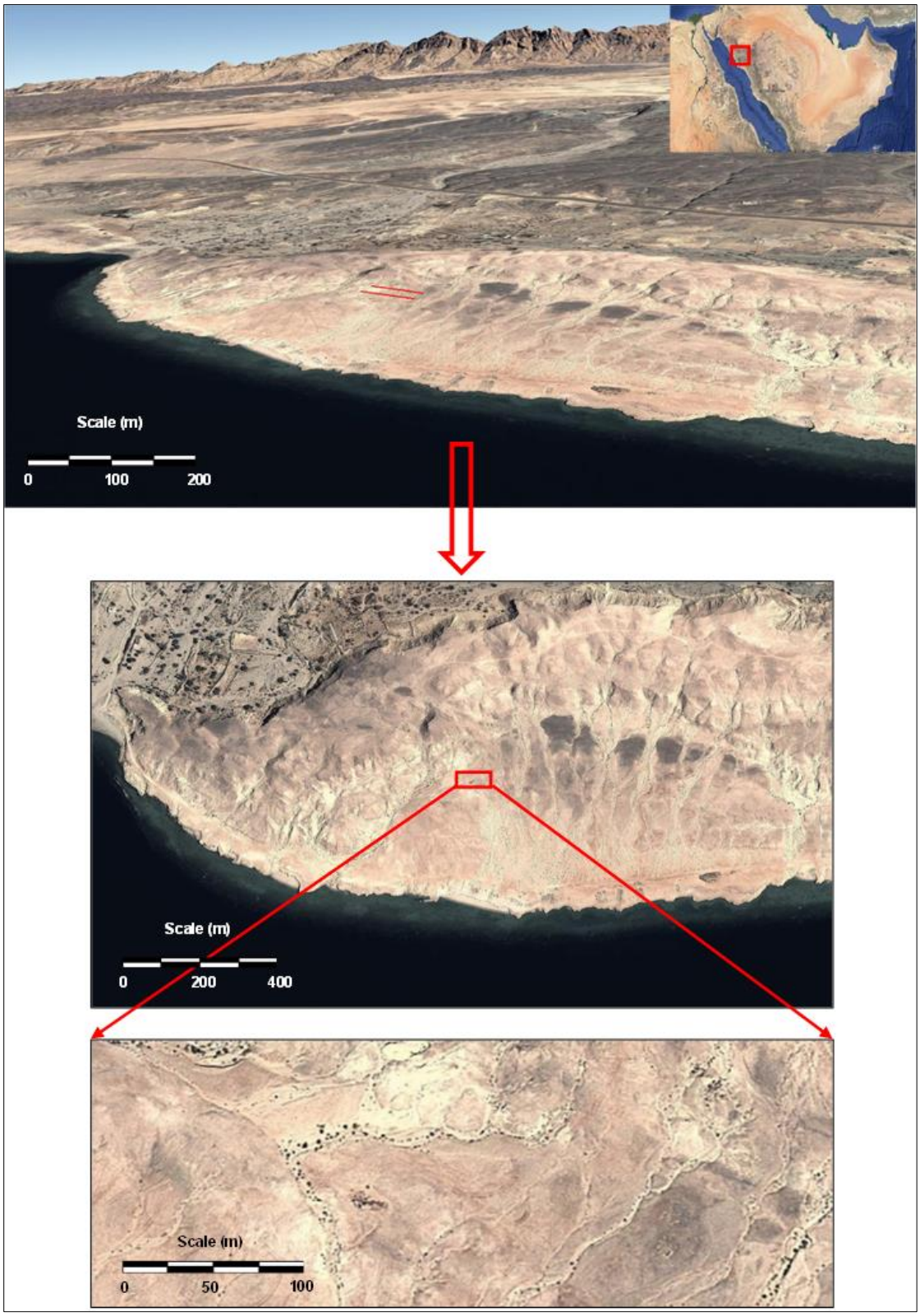


**Figure 1.2: Landsat image of the study area - Duba, Tabuk Province KSA**

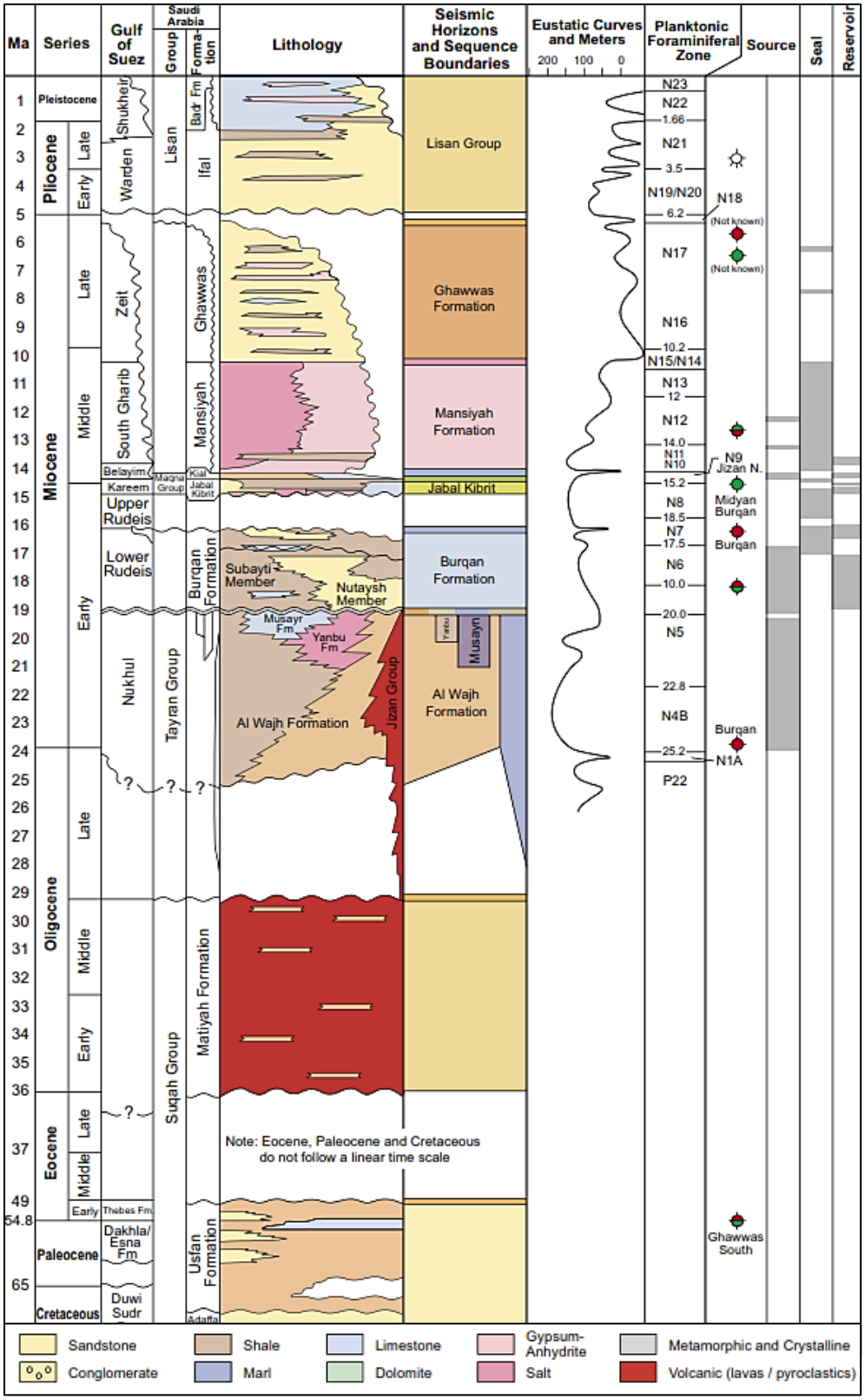


**Figure 1.3: Generalized Red Sea stratigraphic column (Hughes and Johnson 2005).**

Detailed geological maps of Al Muwaylih quadrangle were created by Davies and Grainger (1985). They display elevated and rough topography, and the overall breadth of the coastal plain gets tapered as we move from Al Wajh in the direction of Duba. Phanerozoic sedimentary rocks are present in both the Azlam Basin and the coastal plain, ranging in age from the Cretaceous to Quaternary. A Generalized Red Sea stratigraphic column is shown in Figure 1.3.

## 1.4 Problem Statement

An engineering construction site encountered voids and poor rock quality, with sporadic core recovery and low Rock Quality Designation (RQD) values, during an initial geotechnical investigation along the Red Sea coast, in Duba Region, Tabuk, Saudi Arabia. (Figure1.2); because of this, there were concerns about the integrity of the rock formation beneath the foundations of the proposed building. The project was thus halted and a geophysical investigation was carried out understand such heterogeneity.

This study was designed to detect and investigate the extent of voids and/or weathered zones beneath the area of construction site using electrical resistivity tomography (ERT), constrained with boreholes data. The ERT was chosen due to previous researchers' promising results (Anderson, et al., 2006; Garman, K. M. and Purcell, S. F., 2008; Abu-Shariah, M.I.I., 2009; El Mahmoudi et al., 2011; M. Farooq et al., 2012; J. Lopez 2013; Metwaly M. and AlFouzan F., 2013). It offers a rapid, less labor intensive and cost-effective imaging of the shallow subsurface with adequate resolution. Ground penetrating radar could not be applied in the area due to high salinity of the ground, which considerably attenuates the signal penetration.

## 1.5 Objectives

Keeping in view the subsurface stratigraphy (coralline limestone), as revealed by the borehole logs, the main objective of this study was to establish suitable procedures for the acquisition, processing and interpretation of ERT data in 2D and 3D surveys to investigate subsurface voids/cavities and shallow weathered zones, in terms of their lateral and vertical extension up to 20 m depth, beneath a proposed construction site.

The specific objectives of this study are to:

1. detect and map shallow subsurface cavities and weathered zones
2. evaluate their depth (roof and floor) and the lateral dimensions
3. detect different geologic layers and the water table
4. correlate ERT results with available geotechnical data and topographic features using aerial images, to reinforce and confirm the results

# CHAPTER 2

# ENGINEERING AND ENVIRONMENTAL GEOPHYSICS

## 2.1 Introduction

Recently, the use of geophysical methods for environmental and engineering applications has gained a wider acceptance than ever before. At the same time, the diversity of techniques, the use of varying terminology to describe the same method and the varying degrees of proficiency required for the interpretation of different types of geophysical data is likely to cause confusion amongst an increasingly non-specialist user community. It is therefore deemed beneficial to define the terminology and introduce basic concepts and methods of environmental and engineering geophysics in the context of site surveys.

### 2.1.1 Relevant Methods

Geophysical methods can be roughly categorized into three groups: surface, airborne and downhole methods. Only airborne and surface geophysical techniques can be regarded as non-invasive. Although downhole techniques have developed rapidly over recent years, particularly due to the success of tomographic imaging methods, they involve boreholes and are therefore invasive. Table 2.1 shows the most commonly used surface and airborne geophysical methods, along with their capabilities regarding the potential detection of typical environmental targets, their typical penetration depths and relative cost. All geophysical measurements rely on specific physical properties of the earth and before any geophysical surveying is considered, it is highly important to identify the appropriate

physical, chemical or geotechnical parameters which are deemed to provide the most relevant information about a particular problem on a site under investigation. One should also bear in mind that it is often contrasts due to spatial variation in those parameters that geophysical methods are sensitive to.

**Electrical and Electromagnetic**. Electrical and electromagnetic methods make use of electromagnetic energy in various parts of the spectrum and include a wide range of techniques which have proven to be extremely useful for environmental and engineering applications. The relevant physical parameters are electrical resistivity (or conductivity) and dielectric permittivity. Resistivity is a fundamental and diagnostic property that can be determined with a range of alternative techniques. It is linked with geotechnical parameters such as porosity, permeability or moisture content and hydrological parameters such as hydraulic conductivity, therefore these properties can be determined indirectly using these methods.

**Seismic and Acoustic.** Seismic and acoustic methods make use of acoustic energy and are particularly useful in engineering applications. They can be divided into refraction and reflection methods. While refraction seismic has historically been the preferred choice in shallow site investigations, there has been a major shift since 1980s towards using high-resolution seismic reflection surveying for this purpose. The physical properties relevant to seismic methods are the elastic wave velocities and related parameters such as elastic moduli and density. Seismic attenuation can give information about petrophysical properties. Shear and surface wave techniques are also commonly used for geotechnical evaluation.

**Potential Feld**. Potential field methods make use of the Earth's magnetic and gravitational fields and are used both for mapping and locating subsurface cavities. . Magnetic methods are based on measurements of the flux density of the geomagnetic field, which is affected by the magnetic susceptibility of geological or man-made materials. Gravity methods are based on measurements of acceleration due to gravity, which is affected by density variations in the subsurface. On a site investigation scale, is it generally required to conduct high-resolution microgravity surveys.

### 2.1.2 Literature Review

The range of geophysical techniques is vast and a detailed discussion of geophysical methodology is clearly beyond the scope of this thesis, except where it is directly relevant to the study conducted. The reader is referred to the extensive literature on applied geophysics in general (example Telford et al. 1990, Parasnis, 1997), Burger et al., 2005, S. Mareš, 2011, M. Everett, 2013) and environmental and engineering geophysics in particular (Reynolds, 1997, Sharma, 1997 and Stanislav, 2011). Government institutions, professional associations and other public bodies have published their own documentations on the use of geophysics for environmental and engineering applications. The Construction Industry Research and Information Association (CIRIA) has published comprehensive guidance about the role of geophysics in engineering investigations (McDowell, 2002). This document represents a revised and updated version of an earlier report by the Geological Society Engineering Group Working Party (Anon, 1988).

**Table 2.1: Summary information on the most commonly used surface and airborne geophysical methods (After U.S. Environmental Protection Agency, 1993).**

| Technique | Soil/geology | Leachate | Can detect Buried wastes | NAPLS | Penetration depth (m) [a] | Cost [b] |
|---|---|---|---|---|---|---|
| **Surface electrical and electromagnetic methods** | | | | | | |
| Self-potential | yes | yes (C) | yes | no | S t | L |
| DC resistivity* | yes | yes (C) | yes | possibly | S 60 km | L-M |
| Induced Polarisation | yes | yes (C) | yes | possibly | S km | L-M |
| Complex resistivity | yes | yes (C) | yes | yes | S km | M-H |
| Electromagnetic induction* | yes | yes (C) | yes | possibly | S 60/C 15 | L-M |
| Transient electromagnetics | yes | yes (C) | yes | no | S 150 | M-H |
| Metal detectors | no | no | yes | no | C/S 0-3 | L |
| VLF-resistivity | yes | yes (C) | yes | no | C/S 20-60 | M-H |
| Magnetotellurics | yes | yes (C) | no | no | S 1000+ | M-H |
| Ground penetrating radar* | yes | yes (C) | yes | yes | C 1-25 (100s) | M |
| **Surface seismic and acoustic methods** | | | | | | |
| Seismic refraction» | yes | yes | no | no | S 1-30 | L-M |
| Shallow seismic reflection | yes | no | no | no | S 10-30 | M-H |
| Continuous seismic profiling | yes | no | no | no | C 1-100 | L-M |
| Seismic shear/surface waves | yes | no | no | no | S 2 10s-100s | M-H |
| **Surface potential field methods** | | | | | | |
| Magnetometry* | no | no | yes (F) | no | C/S 0-20[c] | L-M |
| Gravity | yes | yes | no | No | S 100s+ | H |
| **Other surface geophysical methods** | | | | | | |
| Radiometry | no | no | yes (N) | no | C/S n/s | L |
| **Airborne geophysics** | | | | | | |
| Airborne electromagnetics | yes | yes (C) | yes | possibly | 0-100 | M |
| Aeromagnetics | yes | no | yes | no | 10s-100s | M |

*** = most commonly used methods at contaminated sites**

**(C) = detectable if contaminant(s) change electrical properties of ground water; (F) = ferrous metals only; (N) = nuclear**

**[a] : S = station measurement; C = continuous measurement. Depths are for typical shallow applications. n/s = near surface.**

**[b]: Ratings are very approximate. L = low; M = moderate; H = high.**

**[c]: For ferrous metal detection; greater depths possible for larger masses of metal.**

By analyzing research work focused around shallow cavities detection, it is evident that the main geophysical techniques used are the gravity, ground penetrating radar (GPR), seismic surveys, and ERT. The latter has gained a wide attention over the past few decades. ERT technique has been successfully employed in different situations by numerous investigators; Cardarelli et al. (2006a) used ERT technique in Rome to delineate

underground cavities. Smith, (1986), Militzer et al., (1979), Dutta et al., (1970); Greenfield, (1979) and Cook and Nostrand, (1954); used ERT to detect shallow underground caves. Thomas and Roth (1999) and Hutchinson et al. (2002) compared the efficacy of different geophysical methodologies for detection of voids and sinkholes. Anderson, et al., (2006); Hiltunen D. R. and Roth M. J. S., (2008); Garman, K. M. and Purcell, S. F., (2008); Loke, M. H., (2008); Zhou, et al. (2002); Zhou, et al., (2000); Hamzah, et al., (2006); Cardimona, S., (2008); Dong, et al., (2008) used ERT technique to successfully assess karst terrains. Gautman et al, (2000); Van Schoor, (2002); Zhou et al, (2002); Gibson et al, (2004) used ERT to plot subsurface karst features such as sinkholes and weathered areas. These investigations have demonstrated the efficiency of electric resistivity methods regarding mapping karst structures due to the large contrast in resistivity between filled cavities (low resistivity) and limestone bedrock. However, large subsurface heterogeneity in karst areas offers challenges for 2D geophysical exploration.

## 2.2 Site Investigation and Geophysics

The concepts of sustainability and risk prevention play an increasingly important role in the decision-making process of many modern societies today. One of the practical consequences of such political change is an increased demand for accurate and reliable site investigations. However, the importance of site investigations is not restricted to remedial action alone. The construction, maintenance and monitoring of facilities that constitute the infrastructure of today's industrialized countries (e.g. roads, buildings, plants, dams, landfills etc.) creates a constant need for increasingly detailed non-destructive investigations of highly engineered sites and structures from the very early stages of planning throughout the entire lifespan of these structures.

The term “site investigation” has a specific meaning in the context of environmental and engineering assessments. It summarizes the procedures undertaken to assess a site with regard to:

- its suitability for a particular purpose (e.g. the construction of civil engineering and building works),
- any risk that may be associated with the site (e.g. due to pollution/other hazards)
- or the structural integrity of the site (e.g. roads, dams, landfills).

It should be appreciated that a site investigation does not just comprise the collection of data, but also wider aspects such as the development, testing and refinement of conceptual models, the assessment and management of risk, and the management of health and safety aspects. Site investigations are commonly undertaken in a phased method:

- Stage 1: Desk study, site reconnaissance, walk-over surveys
- Stage 2: Detailed investigation
- Stage 3: Review, follow-up investigations, verification, appraisal of performance and monitoring

Major part of the fieldwork is typically carried out during stage 2 of the investigation.

## 2.3 The Relevance of Resistivity Methods

Amongst the geophysical portfolio, electrical methods in general and resistivity methods in particular play an important role in environmental and engineering site investigations. The versatility of resistivity as a diagnostic parameter makes resistivity methods applicable to a large variety of problems. Non-contacting techniques such as ground conductivity are extremely popular for reconnaissance purposes, for example to map out resistivity over

large areas of a site and to locate anomalous areas. Galvanic techniques such as DC resistivity (Section 3.1) are more laborious, but the stationary current flow bears some advantages, for example precise depth investigation.

A major breakthrough for resistivity methods was the development of electrical resistivity tomography (ERT), which made resistivity imaging possible, i.e. the creation of 2D or 3D images of the subsurface. This technique is now being used extensively for site investigations in the environmental and engineering sectors. One of the standard applications is the detection and mapping of contaminants and associated pathways. Such investigations are typically carried out on contaminated and derelict land and the results may be highly relevant for risk assessments under the contaminated land regime. For example, ERT was used by Ogilvy et al. (1999, 2002) to image the leachate distribution in landfills. Chambers et al. (1999) used ERT to characterize buried waste deposits in 3D on a site which is likely to be classified as contaminated land under the new regime.

Resistivity methods have also been successfully employed in a geohazards context, particularly for **cavity detection.** ERT is suitable for this purpose as empty (air-filled) cavities have a higher resistivity than undisturbed ground, whereas flooded (water-filled) cavities would result in lower values. Ogilvy et al. (2001) have demonstrated that shallow mineshafts can be expected to be detectable with 3D ERT.

One of the main objectives of this thesis is to demonstrate the applicability of ERT to an area suspected to have an associated engineering hazard due to presence of soft coralline limestone. Several problems are associated with subsurface karstic voids, such as building foundation collapse, road and highway subsidence, etc. Large void formation in a karst environment may lead to abrupt and catastrophic failure.

# CHAPTER 3

# PRINCIPLES OF ELECTRICAL RESISTIVITY SURVEY

Throughout the history of geophysics, the application of electrical and electromagnetic methods has revealed a tremendous amount of information about the physical properties of the subsurface on a global, regional and local scale. These methods have proven to be equally powerful at a range of depths from hundreds of kilometers to the near-surface (say 0-10 m). The shallow end of this depth scale is of interest in environmental and engineering site investigations. A wide range of electrical methods is available, a subset of which is sensitive to electrical resistivity, a fundamental and diagnostic physical property (Table 3.1). Electrical or electromagnetic methods that allow the direct or indirect measurement of resistivity are referred to as *resistivity methods*. Two of the most frequently employed resistivity methods in site investigations are direct current (DC) resistivity and the ground conductivity technique or coil-coil EM. DC resistivity uses stationary electric currents and is based on galvanic coupling, while ground conductivity is an electromagnetic method that operates in the frequency domain. Some resistivity methods such as VLF and radio-magnetotellurics utilize remote source signals. Other methods such as transient EM or the magnetometric resistivity technique are rarely used for environmental and engineering site investigations, but are of theoretical importance.

The remaining group of electrical methods (referred to as *non-resistivity methods*) comprises techniques which are concerned with effects of electric polarization (SP, IP). Another important electromagnetic method is ground penetrating radar (GPR). GPR is

based upon wave propagation and operates at much higher frequencies than the other methods. It is therefore mainly sensitive to dielectric properties, since resistivity variations merely cause wave attenuation. Although non-resistivity methods are not discussed here, they are equally important in environmental and engineering site investigations (Section 2.1.2).

**Table 3.1: Resistivity and non-resistivity electrical methods in environmental and engineering geophysics**

| Resistivity Methods | Non-resistivity Method |
|---|---|
| DC resistivity<br>Complex resistivity (SIP)<br>Ground conductivity and other FDEM<br>Very-low-frequency methods (VLF)<br>Radiomagnetotellurics (RMT)<br>Transient EM (TEM)<br>Magnetometric Resistivity (MMR) | Self-Potential (SP)<br>Induced Polarization (IP)<br>Ground Penetrating Radar (GPR) |

## 3.1 Direct Current (DC) Resistivity

The direct current (DC) resistivity method is the traditional way of measuring the resistivity of the subsurface. It has been in use for nearly a century and is a well-established technique. It has strong theoretical foundations, is applicable in many situations and can provide robust datasets for which sophisticated interpretation techniques are available. The technique employs an artificial source of direct or pseudo-direct electric current injected into the ground via galvanic contact through point electrodes, thus creating stationary

current flow in the earth. By measuring potentials at the surface in the vicinity of this current flow it is then possible to determine the effective resistivity of the subsurface for a given electrode geometry. From such measurements, a spatial distribution of intrinsic resistivity can be derived, which represents a physical model of the subsurface. This section reviews the physical and mathematical basis of the technique together with its use for electrical imaging and discusses practical problems and shortcomings.

### 3.1.1 Fundamental Theory of Resistivity

Complete theory of DC resistivity is set out in geophysical textbooks such as Parasnis (1997), Reynolds (1997), Telford et al. (1990) or Dobrin and Savit (1988). The fundamental assumption is that of a stationary and continuous electric current flow in a homogenous and isotropic conductive medium. The electric field E can thus be regarded as the gradient of a scalar potential,

$$E = -\nabla V \tag{3.1}$$

Since $\nabla$ x E $= 0$ for B $= 0$. This is far-reaching assumption because it excludes any variation of the field with time. Using Ohm's Law, we have

$$j = -\sigma \nabla V \tag{3.2}$$

Where j = electric current density, σ = electrical conductivity, V = electric potential, $\nabla =$ gradient.

Constant current flow in regions of finite conductivity does not allow for the accumulation of free charge, hence η = 0, so that the continuity equation yields ∇.j = 0. Therefore

$$\nabla\sigma \,.\, \nabla V + \sigma \nabla^2 V = 0 \tag{3.3}$$

which in regions with constant σ (∇σ = 0) reduces to Laplace's equation

$$\nabla^2 V = 0 \tag{3.4}$$

Potentials which satisfy this differential equation are possible solutions of the geoelectrical problem.

#### 3.1.1.1 The Four Electrode array

In practice, two electrodes are required in order to pass an electric current into the ground. The current electrodes are commonly referred to as $C_1$ and $C_2$ or, historically, A and B. Since the distance between the current electrodes is necessarily finite, the potential at any surface point nearby will be affected by both. As before, the potential due to $C_1$ observed at a potential electrode $P_1$ is:

$$V_1 = \frac{I\rho}{2\pi r_{11}} \tag{3.5}$$

The current at $C_2$ is of equal magnitude but opposite in direction, hence the potential due to $C_2$ observed at $P_1$ has to be

$$V_2 = \frac{I\rho}{2\pi r_{12}} \tag{3.6}$$

Overall, the superposition of both potentials is observed at $P_1$

$$V = V_1 + V_2 = \frac{I\rho}{2\pi}\left(\frac{1}{r_{11}} - \frac{1}{r_{12}}\right) \tag{3.7}$$

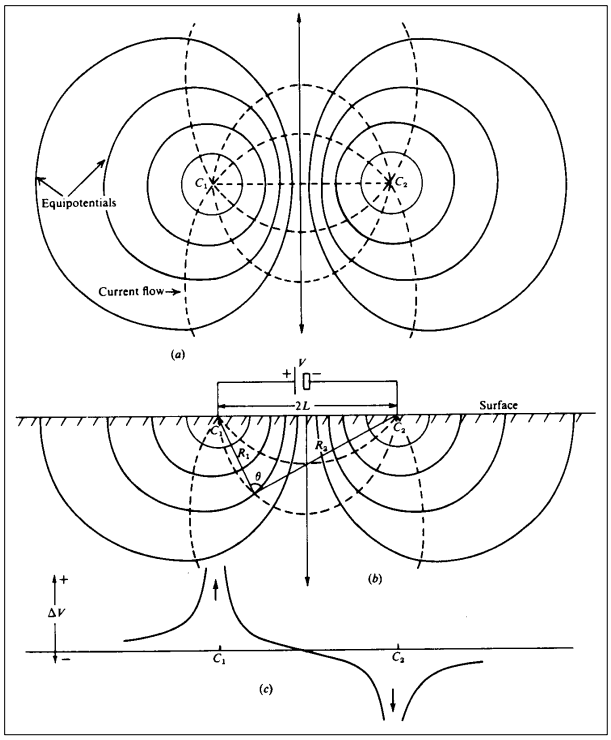


**Figure 3.1: Equipotentials and current flow lines for two point sources of current at the surface of a homogeneous medium (Telford et al., 1990).**

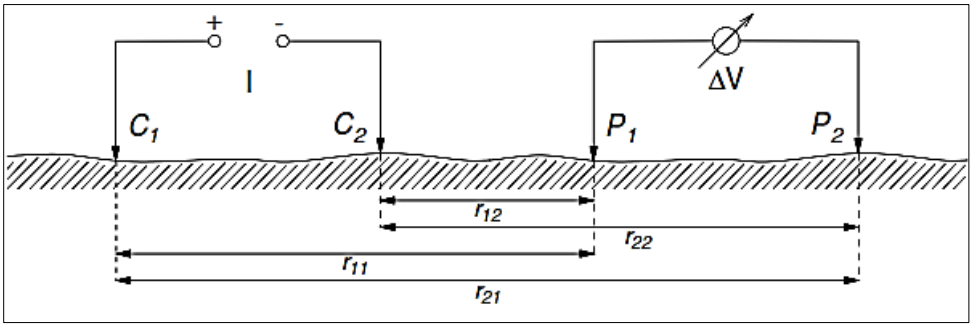


**Figure 3.2: The four-electrode array consisting of two current and two potential electrodes.**

The lines of constant potential (equipotentials) together with the current flow lines are shown in Figure 3.1. It is worth noting that (3.7) is the potential of a dipole with finite extent, sometimes referred to as a ***bipole***. If the distances $r_{11}$ and $r_{12}$ are large compared with the separation $C_1 C_2$, (3.7) is an approximation for the potential created by an ideal point dipole.

Similar to the current dipole, two electrodes are required to measure a potential difference between two points on the surface, referred to as $P_1$ and $P_2$ or, historically, M and N. This concept of a four-electrode array is shown in Figure 3.2. The potential difference (or voltage) observed between $P_1$ and $P_2$ is then given by the superposition of the individual potentials

$$\Delta V = \frac{I\rho}{2\pi}\left[\left(\frac{1}{r_{11}} - \frac{1}{r_{12}}\right) - \left(\frac{1}{r_{21}} - \frac{1}{r_{22}}\right)\right] \tag{3.8}$$

It is important to note that ΔV is essentially a function of three parameters: half- space resistivity, injected current and the geometry of the electrode spread.

### 3.1.1.2 The Concept of Apparent Resistivity

Practically, the potential difference ΔV can be measured for an array of known geometry and a known injection current. A resistivity can then be obtained by solving (3.8) for $\rho$. For a homogeneous isotropic subsurface (homogeneous half-space) this resistivity is equal to the bulk resistivity of the halfspace and hence constant for any injection current and electrode geometry

$$\rho = \frac{\Delta V}{I}.K \tag{3.9}$$

Where term

$$K = \frac{2\pi}{\left[\frac{1}{r_{11}} + \frac{1}{r_{22}} - \frac{1}{r_{12}} - \frac{1}{r_{21}}\right]} \tag{3.10}$$

denotes the *geometric factor*. On inhomogeneous ground, different values for $\rho$ are obtained if the array is moved or the electrode geometry is changed. The measured quantity is therefore referred to as the *apparent resistivity* $\rho_a$, indicating that it reflects the properties of a theoretical model (a homogeneous halfspace) which may not exist in practice.

### 3.1.2 Common Array Types

A number of array types are in common use with DC resistivity, each of which has specific advantages and disadvantages. These are mainly concerned with ease of use in the field, but also with the spatial resolution of subsurface inhomogeneities. The quality of results is also affected by the choice of geometry because signal-to-noise properties vary between array types. Furthermore, the results of a measurement can be degraded by mutual inductive coupling between cables. The intensity of this effect is also a function of array type.

#### 3.1.2.1 The Wenner Array

In the Wenner array the four electrodes are collinear, with the potential electrodes being located between the current electrodes (Figure 3.3a). The separation a between adjacent electrodes is constant, so that the geometric factor of the Wenner array becomes

$$K_{We} = 2\pi a \tag{3.11}$$

Although it has a simple geometry, this arrangement is often quite inconvenient for fieldwork because all four electrodes have to be moved to vary the depth of investigation.

#### 3.1.2.2 The Schlumberger Array

In the Schlumberger (or gradient) array, the potential electrodes are also located symmetrically between the current electrodes, however the current electrodes are placed much further apart (*AB* >> *MN*, Figure 3.3b). At an arbitrary point *P* on the line *AM NB* at a distance *x* from the center of the array

$$U = \Delta V = \frac{I\rho}{2\pi}\left(\frac{1}{S+x} - \frac{1}{S-x}\right) \tag{3.12a}$$

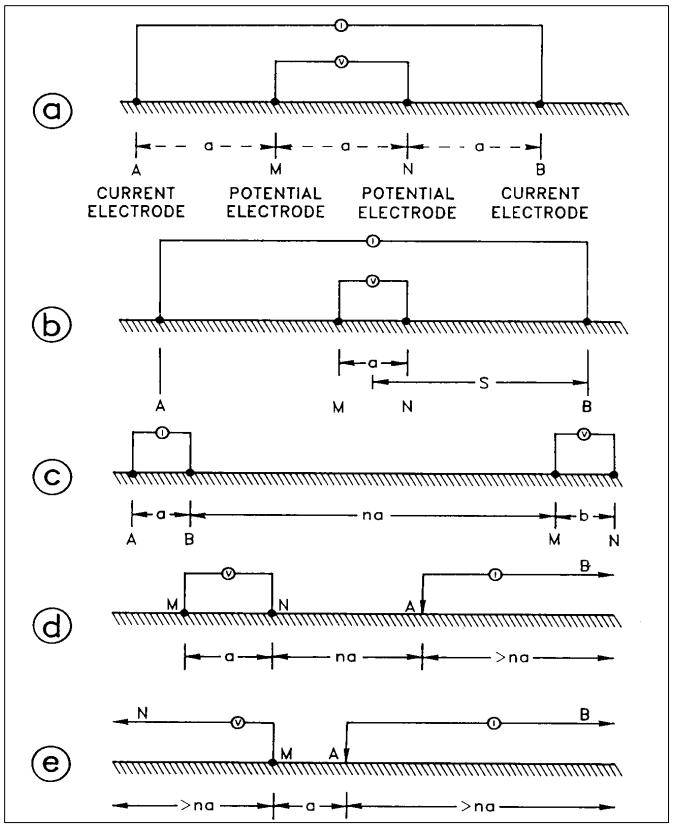


**Figure 3.3: Electrode array types commonly use in DC resistivity (Dobrin and Savit, 1988). (a) Wenner array; (b) Schlumberger array; (c) dipole-dipole array; (d) pole- dipole array; (e) pole-pole array. Parameters *a* and *n* (a and n-spacings) are often used in conjunction with regular grids of electrodes.**

$$\frac{dU}{dx} = -\frac{I\rho}{2\pi} = \frac{I\rho}{2\pi}\left(\frac{1}{(S+x)^2} - \frac{1}{(S-x)^2}\right) \qquad (3.12b)$$

where S is the half-length of the array. At the center ($x = 0$) therefore we have

$$\frac{dU}{dx} = -\frac{I\rho}{\pi S^2} \qquad (3.13)$$

and the apparent resistivity becomes

$$\rho_a = \frac{\pi S^2}{I}\left(-\frac{dU}{dx}\right) \qquad (3.14)$$

hence the name gradient array. If *MN* is sufficiently small, then *(- dU/dx)* = U/*a* and therefore one obtains for the geometric factor

$$K_{Sb} = \frac{\pi S^2}{a} \quad (3.15)$$

The Schlumberger array is usually used for vertical electric sounding survey for which the electrode spacing is expanded by simply increasing the distance of the current electrodes.

### 3.1.2.3 The dipole-dipole Array

The category of geometries where current and potential dipoles are separated from each other is called a dipole-dipole array. Specific terminology has become established for a number of dipole-dipole configurations (Figure 3.4). The inline (also known as axial or polar) and equatorial configurations of the dipole-dipole array.

The inline dipole-dipole array (Figure 3.3c, 3.4 top left) consists of two dipoles whose axes are on the same line. The separations *AB* and *MN* (i.e. the dipole lengths) are typically equal (*AB* = *MN* = *a*). In DC resistivity, the distance between the two dipoles is often defined as the distance BM which is normally expressed in terms of a multiple *n* of the separation *a*. The *n – factor* is often an integer. The geometric factor of the inline dipole-dipole array, expressed by *n* and *a*, is

$$K_{DDin} = \pi n(n+1)(n+2)a \quad (3.16)$$

In general, it is more convenient to define the distance between the two dipoles as the distance r between their respective midpoints. In order to distinguish between the two conventions, the symbol l will be used for the dipole lengths in the latter case.

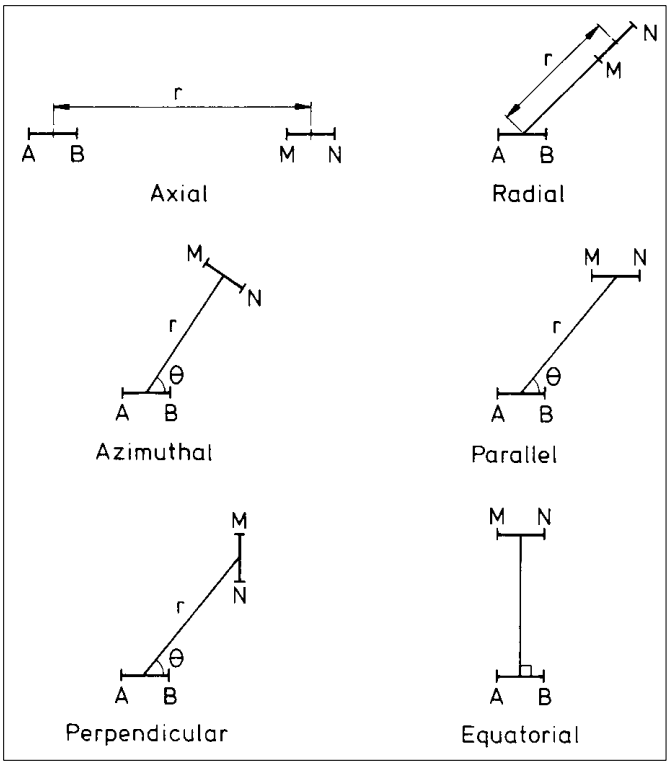


**Figure 3.4: Configurations of the dipole-dipole array (Parasnis, 1997).**

A dipole-dipole array can then be fully described by either the pair (*a*, *n*) or (*l*, *r*). The alternative geometric factor of the inline dipole-dipole array is then

$$K_{DDin} = \frac{2\pi}{\frac{2}{r} - \frac{1}{r-l} - \frac{1}{r+l}} = \pi r\left(1 - \frac{r^2}{l^2}\right) \tag{3.17}$$

The equatorial dipole-dipole array (Figure 3.4 bottom right) consists of dipoles which are parallel but not collinear and where the four electrodes form a rectangle. Its geometric factor is

$$K_{DDeq} = \frac{\pi}{\frac{1}{r} - \frac{1}{\sqrt{l^2+r^2}}} \tag{3.18}$$

assuming a symmetric array. A special case of the equatorial dipole-dipole array is the square array for which $r = l$ (Habberjam, 1979).

#### 3.1.2.4 The pole-dipole and pole-pole Arrays

If one of the current electrodes is removed to a great distance from the measurement area, the remaining current electrode can be regarded as a single current pole. This arrangement is referred to as a pole-dipole (or three-point) array (Figure 3.3d). Its geometric factor is

$$K_{PD} = 2\pi an(n+1) \tag{3.19}$$

If, in addition, one of the potential electrodes is also removed to a great distance, the remaining potential electrode can be regarded as a single potential pole and the array is referred to as a pole-pole array (Figure 3.3e). Here, the geometric factor is

$$K_{PP} = 2\pi a \tag{3.20}$$

## 3.2 Electrical Resistivity Tomography (ERT)

A great limitation of these basic field procedures is that their quantitative interpretation is restricted to simple geological structures such as a 1D layered earth (e.g. sedimentary beds) or lateral contrasts such as vertical boundaries (e.g. faults or dykes). The type and geometry of the anomaly must be known for the apparent resistivity to be diagnostic. Although these basic techniques have turned out to be extremely useful in some geological applications, they are insufficient in areas of complex geology and mostly inapplicable in a site investigation context where the subsurface is often highly heterogeneous and includes localized anomalous features. Here, two-dimensional (2D) or three-dimensional (3D) earth models must be considered, according to the degree of complexity. However, interpretation of the associated apparent resistivity datasets is then no longer trivial and more sophisticated techniques had to be developed for this purpose.

The construction of two-dimensional and three-dimensional images of the subsurface from resistivity data has become commonly known as electrical resistivity tomography (ERT). Sometimes the term "resistivity imaging" is also used. It is worth noting that imaging techniques can reflect different degrees of realism. In a looser sense of the term "imaging", basic visualization techniques such as pseudosections based on apparent resistivity data give simple images which contain spatial information but are not representative of the true distribution of intrinsic resistivity. Imaging in a stricter sense involves the creation of 2D or 3D models of "true" resistivity which can be regarded as "realistic" representations of the subsurface by virtue of its electrical properties. The procedure of deriving a true resistivity model from apparent resistivity field data is known as "resistivity inversion".

### 3.2.1 Multi-electrode DC Resistivity Field Survey

Electrical resistivity tomography surveys are nowadays conducted with multiplexed computer-controlled systems using a large number of electrodes connected to multicore cables at regular spacings (Barker, 1981; Griffiths and Turnbull, 1985; Griffiths et al., 1990).

**2D Resistivity Surveys**. Single lines or 2D grids (sequences of parallel lines) of electrodes are installed at the beginning of the survey and one or several multicore cables are connected to the electrodes. Data acquisition is then entirely automatic with a computer-controlled switching unit collecting data from a predefined sequence of electrode arrays with varying geometries (Figure 3.5). Early resistivity imaging was purely two-dimensional and the associated field technique comprised the installation of a single line along the profile to be investigated (Griffiths and Barker, 1993; Dahlin, 1993). Prior to the development of genuine 2D inversion algorithms, interpretation of such datasets was

limited. One simple interpretation technique is to create quasi-2D resistivity sections by extracting closely spaced VES from the 2D data, a procedure known as continuous vertical electric sounding (CVES) (Dahlin, 1993, 1996).

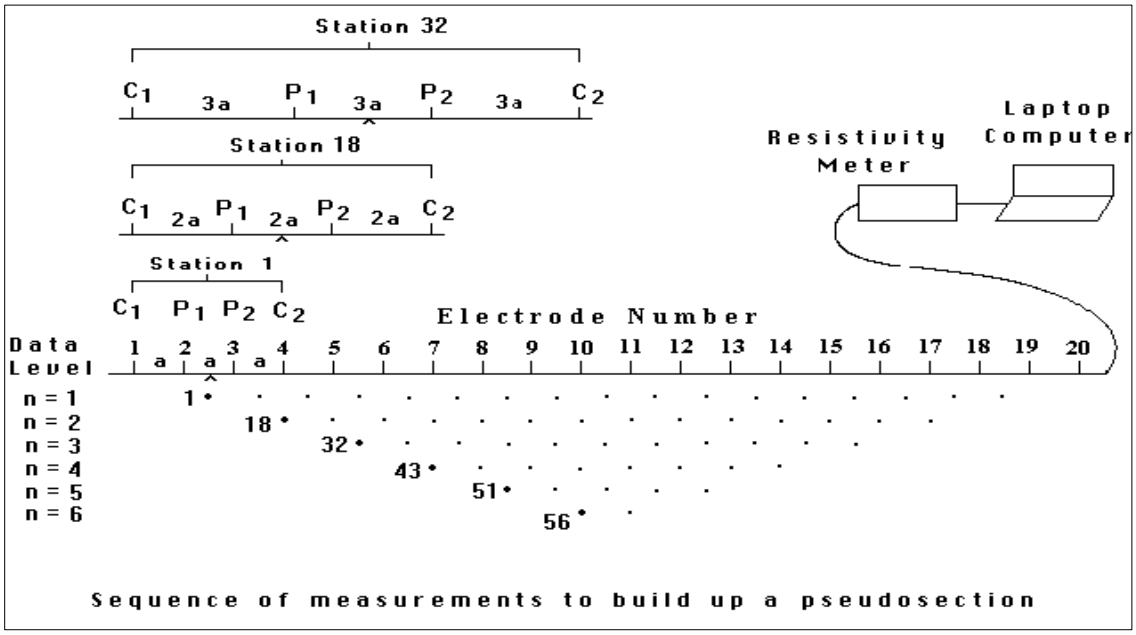


**Figure 3.5: Example of an ERT survey using a Wenner array with a set of evenly spaced electrodes to collect multi-offset data (Reynolds, 1997).**

**3D Resistivity Surveys.** Realistically, all geological structures are 3D in nature, therefore a full 3D resistivity survey and inversion provide the most accurate subsurface imaging (Loke and Barker, 1996b). It was only after the advent of increasingly sophisticated modelling and inversion algorithms that 3D imaging became technically feasible. Practical field techniques in conjunction with user-friendly interpretation were described by Loke and Barker (1996a). The initial suggestion involved the deployment of one multicore cable in snake-lines across a regular grid of electrodes (Figure 3.6). However, such a procedure is only viable for small grids of the order of 10 x 10 electrodes. For larger (or more detailed) 3D surveys, data are usually acquired along a sequence of parallel lines which involves the

installation of multiple cables or the use of roll-along techniques (Dahlin and Bernstone, 1997) in order to increase efficiency.

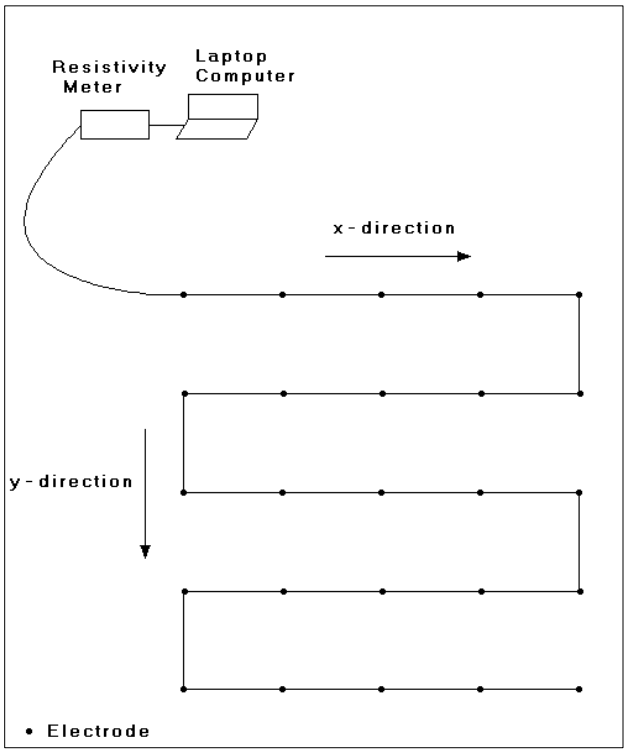


**Figure 3.6: Example of electrodes arranged along a multicore cable for a 3D ERT survey on a regular grid (Loke and Barker, 1996a).**

### 3.2.2 Resistivity Forward Modeling

For a given subsurface resistivity distribution, the objective of forward modelling is to calculate the apparent resistivity that would be measured by a survey over that structure. This procedure is an essential stage of any automated resistivity interpretation algorithm.

A solution of the forward problem involves solving the Laplace equation (3.4) numerically for arbitrary resistivity distributions. The most versatile implementations of resistivity forward modelling algorithms are based upon the finite difference (FD) method (Mufti, 1978; Dey and Morrison, 1979) or the finite element (FE) method (Coggon, 1971). A certain class of models, namely localized bodies in otherwise layered media, lends itself to

solutions based upon integral equations (Das and Parasnis, 1987). Although the associated algorithm is fast, the method is not suitable for modelling semi-infinite features. A method using alpha centers was suggested by Petrick et al. (1981).

### 3.2.3 Resistivity Inversion

Resistivity inversion is a mathematical process required to derive a model of the true spatial distribution of intrinsic resistivity in the region of interest from an apparent resistivity dataset. Early algorithms were limited to certain model geometries or comparisons with pre-calculated model responses (Pelton et al., 1978a; Tripp et al., 1984; Smith and Vozoff, 1984). Modern inversion techniques can deal with arbitrary resistivity distributions, are fully automated and frequently use non-linear optimizations methods to iteratively improve simple starting models in an attempt to achieve a *best fit* between model and measured data. As a consequence of the increased availability of computing power outside of mainframe environments in recent years, resistivity inversions are now routinely carried out on desktop PCs, even for large 2D and 3D datasets (Loke and Barker, 1996a).

A popular general geophysical inversion techniques is the Gauss- Newton least-squares inversion (Lines and Treitel, 1984) due to its robustness and variety of applications. One particular incarnation of this method, known as Occam's inversion, demands smoothness of the model as a general constraint (Constable et al., 1987; deGroot-Hedlin and Constable, 1990).

It is widely used in conjunction with electrical and electromagnetic techniques because smooth models tend to reflect the resolving power of these techniques best. Loke and Barker (1996b) have developed a fast and particularly versatile implementation of the

smoothness-constrained least-squares inversion. A quasi-Newton method is used to estimate the Jacobian matrix of partial derivatives during each iteration, resulting in a dramatic reduction of processor time and memory requirements. Both their 2D and 3D algorithms have proven to be robust under many circumstances and have been successfully applied to complex datasets obtained during environmental and engineering site investigations (Ogilvy et al., 2002, 1999; Chambers et al., 1999).

Several different algorithms for DC resistivity inversion have been described by Smith and Vozoff (1984), Li and Oldenburg (1994), Ellis and Oldenburg (1994b), Dabas et al. (1994) and Zhang et al. (1995). A detailed overview of relevant DC resistivity inversion techniques was given by Morelli and Labrecque, (1996).

### 3.2.4 Problems and Disadvantages

#### 3.2.4.1 Galvanic Contact

In Practice, the DC resistivity measurement requires galvanic contact with the ground. In theory, this contact is implicitly assumed to be of good quality. If this is not the case in practice, serious restrictions may result for the applicability of the technique. Indeed, a frequently encountered problem in DC resistivity is serious degradation of data quality which occurs when electrodes are being installed on highly resistive surfaces such as dry sands, gravels, rubble, ice, frozen soils or building materials. The term "poor galvanic contact" is used in these circumstances to describe a situation in which the resistive part of the contact impedance between the electrodes and the surface material becomes so large that it affects (or even prevents) current injection or potential measurement. Possible solutions that may improve galvanic contact comprise (Reynolds, 1997):

- wetting of electrodes with conductive fluid (e.g. water, saline solution, addition of bentonite);
- the use of multiple electrodes connected to the end of the current-carrying wire.

#### 3.2.4.2 Installation of Electrodes

A more practical problem with DC resistivity is that steel electrodes must be manually implanted in the survey area before measurements can commence. Strictly speaking, the technique must be regarded as intrusive, even if the electrodes require only minimal surface penetration. Not only is this procedure extremely cumbersome for large-scale surveys, but installation of electrodes may be impossible altogether. Metal stake electrodes are particularly unsuitable for installation on hard ground or artificial surfaces such as roads, pavements and other engineered structures. A practical way to install electrodes include

- drilling small-diameter holes prior to installation;
- using electrodes with larger contact area (e.g. disc electrodes) which do not penetrate the surface in conjunction with the use of conductive substances to enhance galvanic contact (e.g. mud, bentonite, saline solutions etc.);
- using non-polarizable electrodes which provide contact via an electrolytic solution and a porous membrane.

However, the successful mechanical installation of electrodes is no guarantee for a good quality electrical measurement. Mechanically hard surfaces are often associated with highly resistive materials, causing high contact impedances.

### 3.2.5 Geology -Resistivity Relationship

Changes in the resistivity of subsurface materials are mostly a function of lithology. Information about resistivity variations within the subsurface can be associated with different materials. The resistivity values of common earth materials are shown in Figure 3.7.

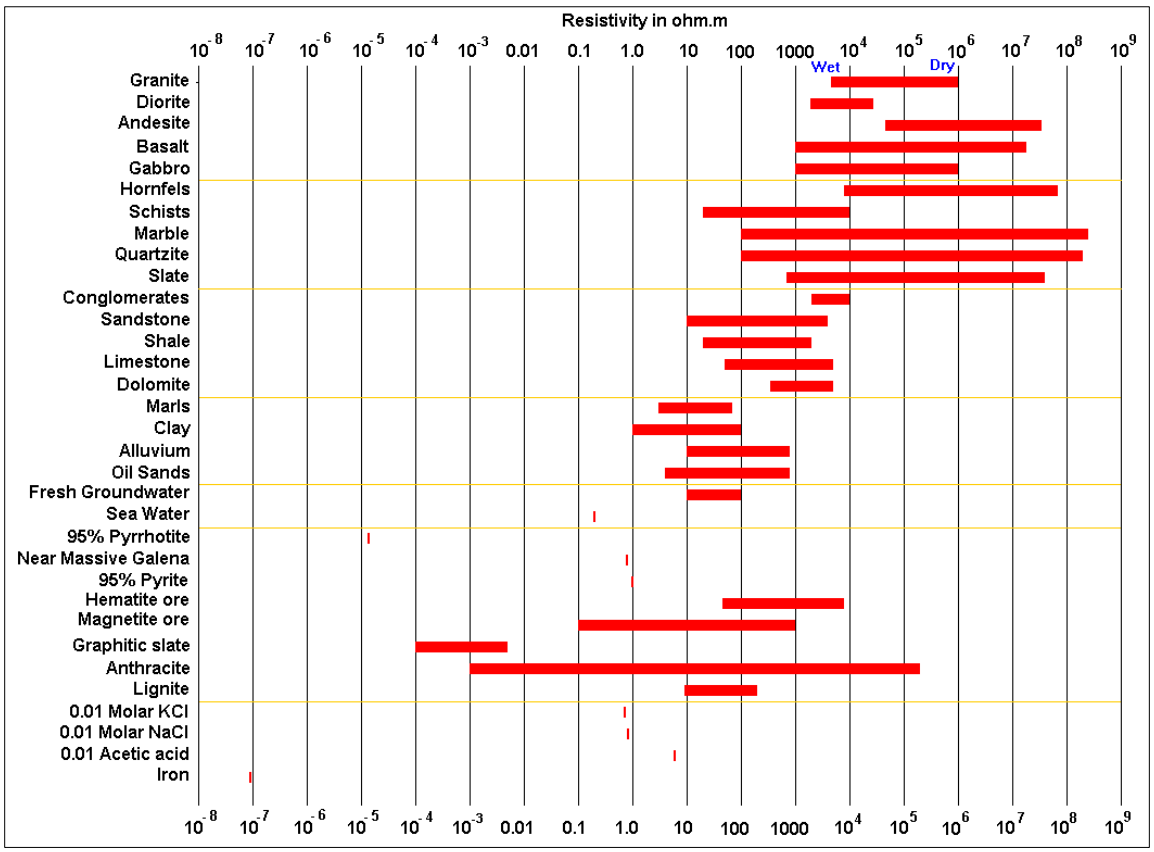


**Figure 3.7: Typical resistivity ranges of common Earth (rock and soil) materials (Loke 2004)**

From Figure 3.7, it can be noted that most materials are characterized by resistivity values that vary by several orders of magnitude. For example, limestone has resistivity values ranging from 50 ohm-m to $10^7$ ohm-m. Most minerals are considered to be insulators or resistive conductors. So in the majority of rocks, electrical current flow is accomplished by passage of ions in pore fluids (electrolytic conduction). The conductivity, which is the

inverse of resistivity, is mostly affected by porosity, saturation, salinity, lithology, clay content and to some degree by temperature. Accordingly, materials with constant mineralogical composition can possess different resistivity values, depending on all the above-mentioned parameters.

# CHAPTER 4

# DATA ACQUISITION AND ANALYSIS

In this chapter, details of ERT data acquisition and analysis are discussed. The high resolution ERT dataset was acquired using a network of electrode profiles laid along the study area. The data analysis comprises 2D and 3D tomographic inversions in the presence of smoothly varying topography.

The methodology adopted for this study consisted of three (3) main parts. First, the acquisition and analysis of 2D data to investigate different stratigraphic layers. Second, the acquisition of 3D data and merging with the 2D dataset to create a single global 3D inversion for final processing, in order to generate a 3D model and iso-resistivity volume to visualize the whole investigated area. Third, to correlate ERT results with borehole logs data and topographic features through aerial photograph, in order to avoid over interpretation and deal with the non-uniqueness of inverse problem.

2D resistivity data sets were acquired along 12 parallel profiles, covering a rectangular area of approximately 4,500 $m^2$, whereas the 3-D data sets were acquired along 2 C-shape profiles along the perimeter of the area, targeted to capture anomalies larger than 1 $m^3$. A fast multi-channel resistivity meter Syscal Pro (produced by Iris Instruments, France) was used.

After data acquisition, a full 2D and 3D inversion were performed to convert the apparent resistivity pseudo-sections into a true resistivity model representing continuous distribution

of calculated electrical resistivity in the subsurface. This was achieved by utilizing an industry-standard software ERTLab created by "Multi-Phase Technologies LLC, USA and Geostudi Astier srl, Italy". Forward resistivity calculations involved a Finite Element Method (FEM)-based iterative algorithm which models the subsurface by implementing network of hexahedrons to accurately integrate terrain topography. The inversion routines are based on the "smoothness constrained least squares optimization" technique. After data processing and inversion, electrical resistivity data obtained was plotted and correlated with the borehole logs in a way to optimize for modelling and interpretation of the subsoil underneath the survey area down to 20 m depth. The results of the survey are discussed in Chapter 5.

## 4.1 ERT Equipment and Data Acquisition

A 10-channel Syscal Pro resistivity meter (produced by IRIS instruments) was deployed for the field resistivity measurements, which combines a transmitter, a receiver and a switching unit in a single casing (Figure 4.1). The data was acquired at a sampling rate of 6000-7000 measurements per hour, with maximum 4 times stack within 1% error.

The equipment was powered by external 12 V battery, to avoid the use of AC generator and reduce any external source of disturbance. The maximum power applied is around 250 W (500 W with an external AC/DC converter), maximum voltages applicable to the transmitting electrodes around 800 V, and maximum current up to 2.5 A.

The electrical resistivity survey was carried out for a rectangular area of approximately 4,500 $m^2$, to obtain a 3D image of the electrical characteristics of the subsurface in the top

15-20 m. The survey area is characterized by smoothly varying topography. Figure 4.2 shows some photographs taken during data acquisition phase.

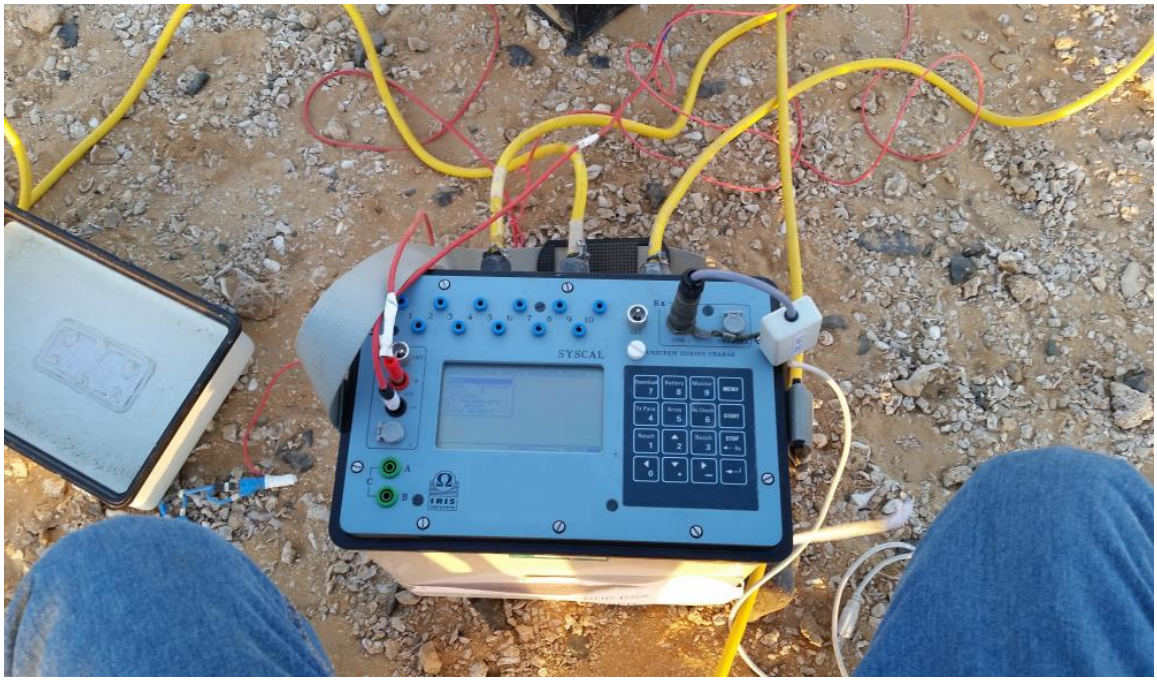


**Figure 4.1: Syscal-Pro employed for data acquisition.**

In order to obtain a high resolution subsurface image, the field data set consisted of 2 blocks of electric resistivity profiles: 2D and 3D. The 2D dataset consisted of twelve (12) equidistant parallel lines at 3.36 m spacing (equal division of 37.0 m width), each line was composed of three (3) multi-core cables with 24 electrode take-outs each, spaced at 1.6 m, making a total of 72 electrodes covering a total length of approximately 114 m. The schematic diagram of the 2D electrodes layout is shown in Figure (4.4).

The 3D data sets were acquired along two (2) C-shaped loop profiles along the perimeter of the area. Similarly, each loop was composed of 72 electrodes spaced at 2.5 m. The schematic diagram of the 3D electrodes layout is shown in Figure (4.5). A single spread of

multicore cables successfully covered the entire area, thus no roll-along technique was adopted.

Stainless steel electrodes were hammered into the ground and connected to each of the take-outs on the multicore cables with a copper clip, ensuring that a metallic connection was made between each take-out and electrode. Following the extent of dryness of the ground as at the time of this survey, electrodes were placed in shallow holes wetted with salt water to ensure proper contact impedance with the ground and reduce the source of noise from the topsoil. The overall effect was to provide up to 72 electrodes which could be individually addressed by the Syscal Pro.

Upon completion of electrodes and cable set-up, a contact resistance (CRS) test was carried out. The CRS test measures contact resistance by sending a current between two electrodes and simultaneously measuring the voltage between the two electrodes and the ground; the test begins at electrodes one and two, moves to two and three, and so on until all 72 electrodes are tested. The CRS test is done to ensure that all 72 electrodes in a single line are properly attached to the take-outs (i.e. metal to metal connection), so that the operator can monitor stake-electrode pairs where possible jumps in CRS values may occur (which may indicate a change in ground and/or soil conditions or that stakes were not planted deep enough, were planted in desecration cracks, or other physical problems), and to ensure that contact resistance values remained below 2,000 ohms. For the vast majority of data collected, the contact resistance values remained relatively low since the area was conductive. There were only several occasions where contact resistance values were greater than 2,000 ohms in which case small quantity of water was poured on the ground at the stake injection site and were retested and re-wetted until values were below 2,000

ohms. Once the CRS test was complete, the specially designed sequence file containing survey parameters including spacing values, array types, were uploaded to Syscal Pro and data collection began. Depending on the selected array type and number of resistivity profile to be recorded, data collection occurred over a period of 4 days with 8 hours of working shift each. The combined acquisition time for single line using pole-dipole and Wenner-Schlumber arrays was around 1 ¼ hours. The main time-consuming part of the survey was shifting electrodes and cables to the next location and performing the CRS test to check all the connection.

**Figure 4.2: Field data acquisition. Stainless steel stakes are inserted into the ground at a constant unit spacing; electrodes located along the yellow cables are connected to each stake, ensuring a metal-to-metal connection is made. Then, cables are connected to the IRIS 10 channel Syscal Pro earth resistivity meter where surveying is initiated.**

After initial trials with different array types to check the signal to noise ratio level, final dataset were acquired using two (2) electrode configurations: 2D pole-dipole and 2D

Wenner-Schlumberger arrays for 2D acquisition and 3D pole-dipole array for 3D acquisition. The general attributes of the two configurations used are as follow:

- The **Pole-Dipole** array has intermediate depth of penetration and resolution, and a very good signal to noise characteristics.
- The **Wenner-Schlumberger** array is a compromise between these two with good signal to noise, intermediate depth penetration of penetration and resolution, and good signal to noise characteristics.

The two array types collected all possible combinations of readings, with a global set of 1022 electrodes, resulting in a combined dataset of almost 64,000 measurements

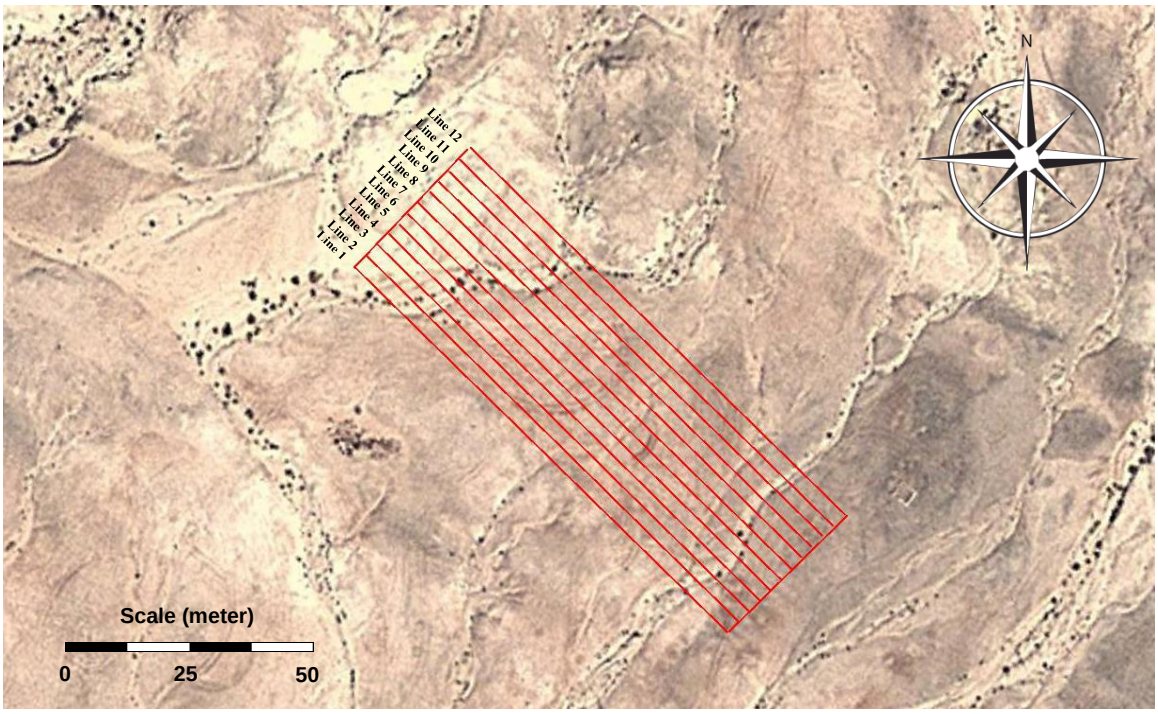


**Figure 4.3: Areal view showing the actual positions of ERT arrays spread out for data acquisition.**

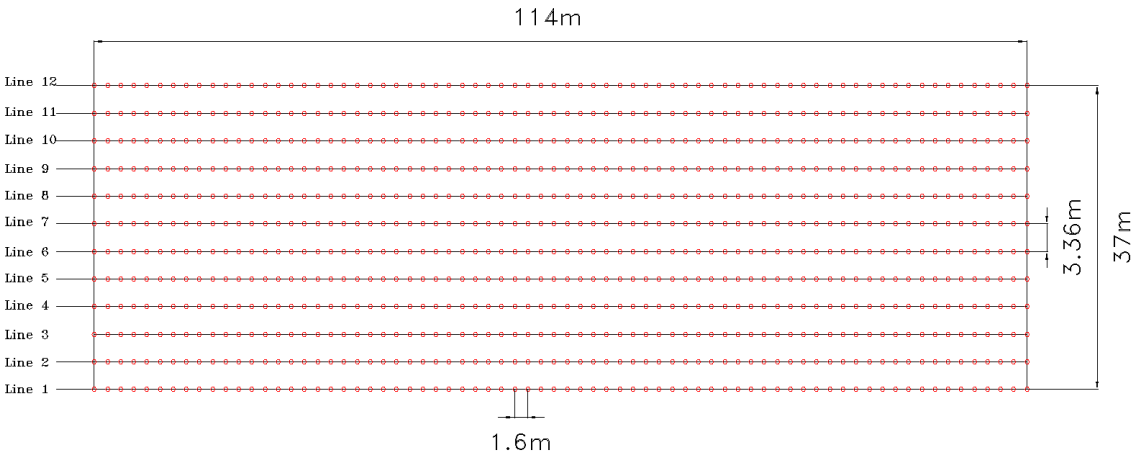


**Figure 4.4: Schematic diagram of 2D survey design showing positions and spacing of all ERT electrodes (red dots) employed for the 2D survey.**

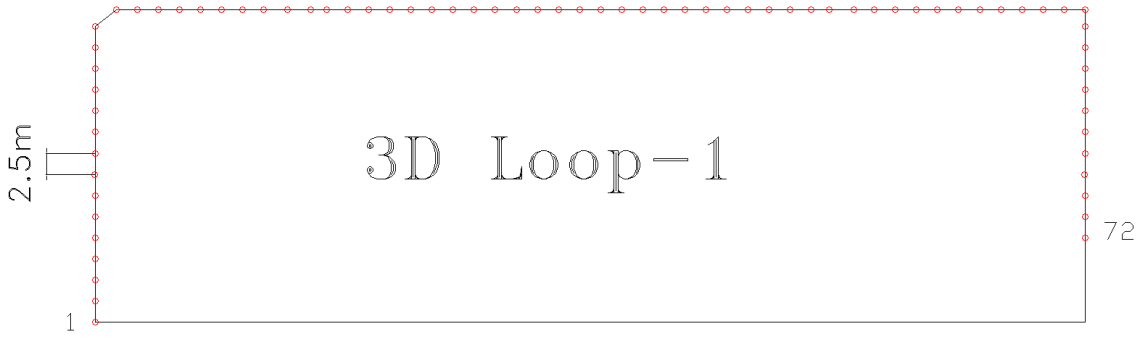


**Figure 4.5: Schematic diagram 3D survey design of - C-shaped loop (1) of electrodes (red dots) employed for 3D data acquisition**

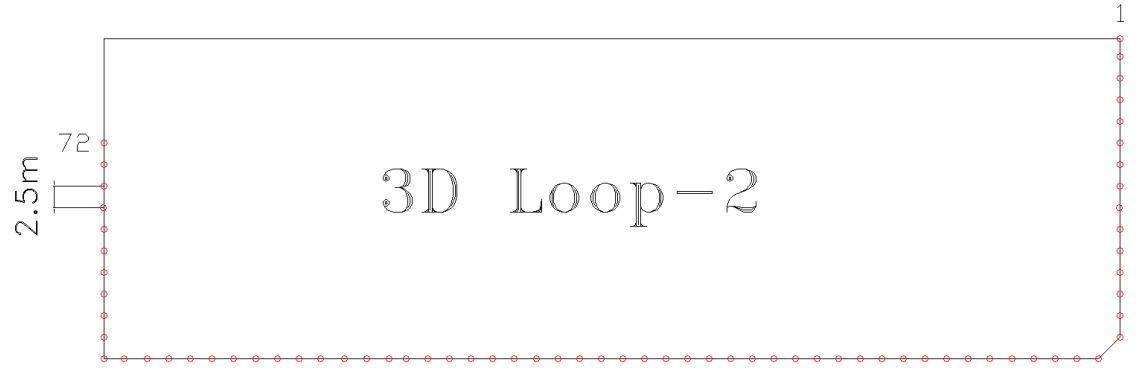


**Figure 4.4: Schematic diagram 3D survey design of - C-shaped loop (2) of electrodes (red dots) employed for 3D data acquisition**

## 4.2 ERT Data Processing and Analysis

The resistivity data sets collected in the field were converted into resistivity models for interpretation of subsurface conditions using the industry-standard software ERTLab™, jointly produced Multi-Phase Technologies LLC, USA and Geostudi Astier srl, Italy.

ERT data was processed using the following steps;

- Inspection of the resistivity data sets for presence of unreasonably high and low (negative) resistivity values called "bad data points" (Loke, 2004).
- Removal of "bad data points" to create global dataset ready for inversion
- Data inversion and compilation of results to visualize 3D resistivity model and 2D resistivity profiles that displays horizontal and vertical resistivity distribution.

### 4.2.1 Data Pre-processing

Data pre-processing involved statistical analysis of the data and removal of "bad data points" (Loke, 2004), characterized by unreasonably high and low (negative) values which can be caused by several factors, such as failure during survey of equipment used, for example electrode malfunction, poor electrode - ground coupling, etc.

ERTLab™ software comes with an option of statistical analysis of the acquired data by displaying data distribution curve (Figure 4.7 & 4.8). By plotting resistivity pseudo-sections, the outliers (bad data points) are displayed by black dots as shown in Figure (4.9), which need to be filtered/removed prior to inversion. Data filtering was applied for eliminating abnormal values of the apparent resistivity, voltage and the geometric factor *k*. The final pseudo-section of the filtered data is shown in Figure (4.10). The inversion-ready dataset was produced after filtering 7.8% of erroneous data points.

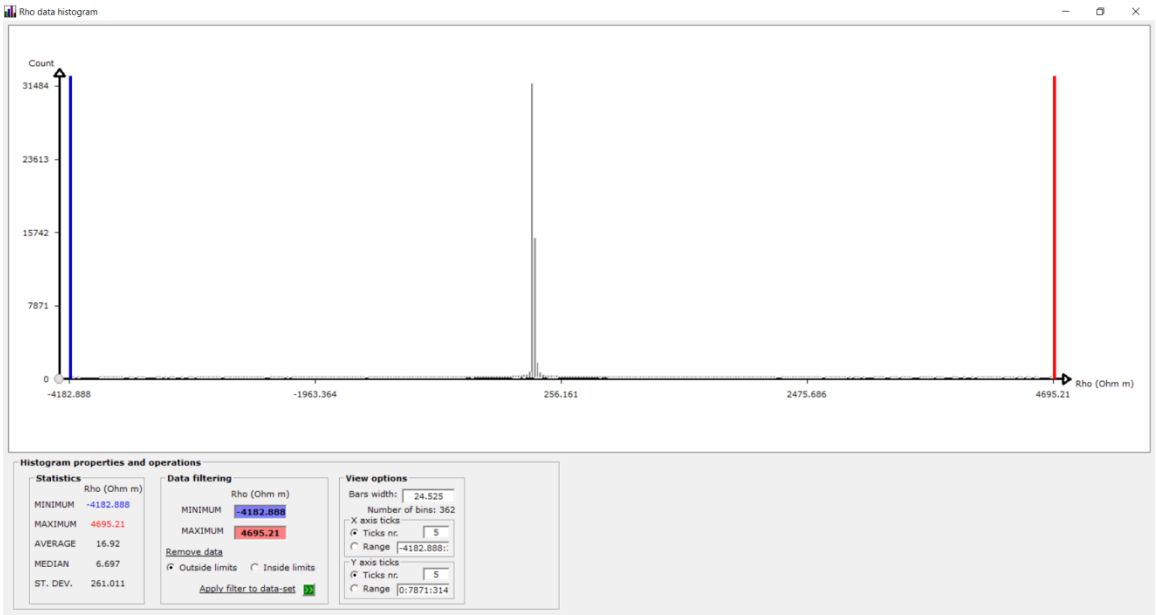


**Figure 4.7: Data distribution curve (histogram) of unfiltered apparent resistivity data.**

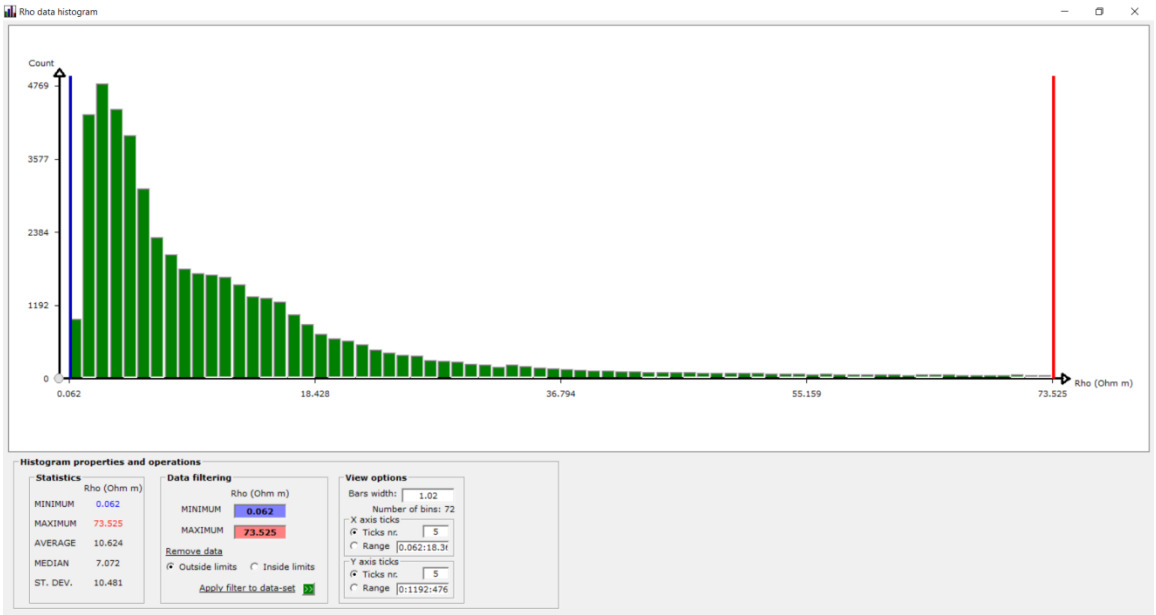


**Figure 4.8: Data distribution curve (global histogram) of filtered apparent resistivity data.**

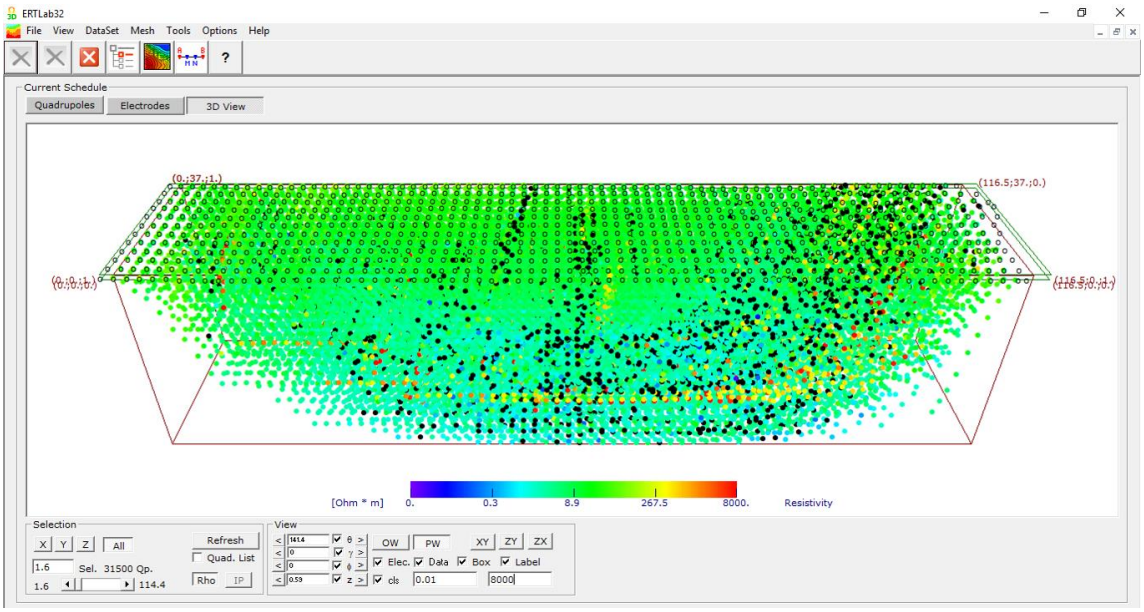


**Figure 4.9: Pseudo-section of the acquired unfiltered apparent resistivity data showing outliers (bad data points) represented by black dots.**

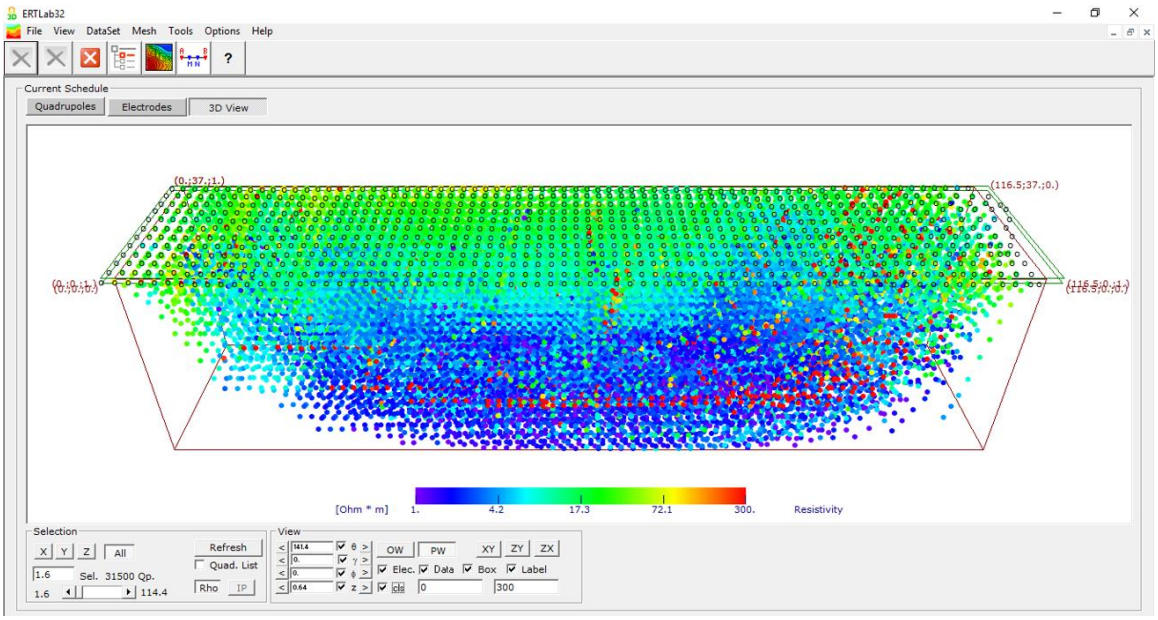


**Figure 4.5: Pseudo-section of the acquired filtered resistivity data after elimination of outliers (bad data points).**

### 4.2.2 Data Inversion

After data acquisition and pre-processing (data filtering), a full 2D and 3D inversion of resistivity data was performed to convert the apparent resistivity pseudo-sections into a true resistivity model representing continuous distribution of calculated electrical resistivity in the subsurface.

In order to calculate a true resistivity image from ERT data, it is necessary to carry out an inversion that produces a model (i.e. a spatially varying distribution of resistivity) that gives an acceptable fit to the data and satisfies the prescribed constraints (boundary conditions). The numerical procedure required three elements:

- A forward modeling algorithm (a 2D or 3D finite element formulation) used to compute the transfer impedances;
- An objective function which states the model fitting criteria (how well the model would reproduce the field measurements subject to a level of uncertainty in the data);
- A search algorithm which determines the way in which the optimum resistivity model is found.

Since the inverse problems related to potential waves and electromagnetic fields are nonlinear in nature, the solution requires an iterative approach (Daily and Owen 1991; LaBrecque et al. 1996). In such an approach, the ‘‘forward model’’ (simulation of electric field for a given resistivity distribution using a distinct domain) was iteratively solved while changing the subsurface electrical properties.

The software ERTLab™ (produced by Geostudi Astier srl, Multi-Phase Technologies LLC) implements this 3D inversion approach by utilizing Occam’s regularization proposed

by Constable et al. (1987) and further improved by Morelli and LaBrecque (1996), for the optimal control of signal to noise ratio. The Finite Element Method was used which allows great flexibility in discretization in cases of irregular electrode positioning. In addition, treatment of irregular topography and other boundary features is easily achieved. The iterative procedure requires an initial starting model; the best choice is usually a half-space of homogenous resistivity derived from the aforementioned (section 4.2.1) statistical analysis of apparent resistivity.

The inversion was performed from an initial guess-model with a homogenous resistivity of 10 Ohm.m (Figure 4.11) which represents the apparent resistivity value with the highest frequency in the global histogram (see Figure 4.8), with a reasonable sensitivity to investigate down to a depth of 20 m. The iterative inversion operation was carried out to the point at which the variance between consecutive root-mean square (RMS) errors was reduced to 5%. Since there were no apparent disturbances from external sources, this residual noise level was referred to measurement errors or to the effects of 3D morphology of the structure.

The complete progress of the inversion routine applied by ERTLab™ software is shown in the figure (4.12). At the top right corner is the dispersion plot, showing mismatch between the real data and simulated data. At the start of 1$^{st}$ iteration, we can see that the data shows maximum dispersion (since we started from a guess-model of uniform resistivity), which was concurrently minimized after each iteration. As shown in plot of 5$^{th}$ iteration, the data points are aligned to the axis, confirming that the error is minimized to the maximum and the simulated data matched well with the real data.

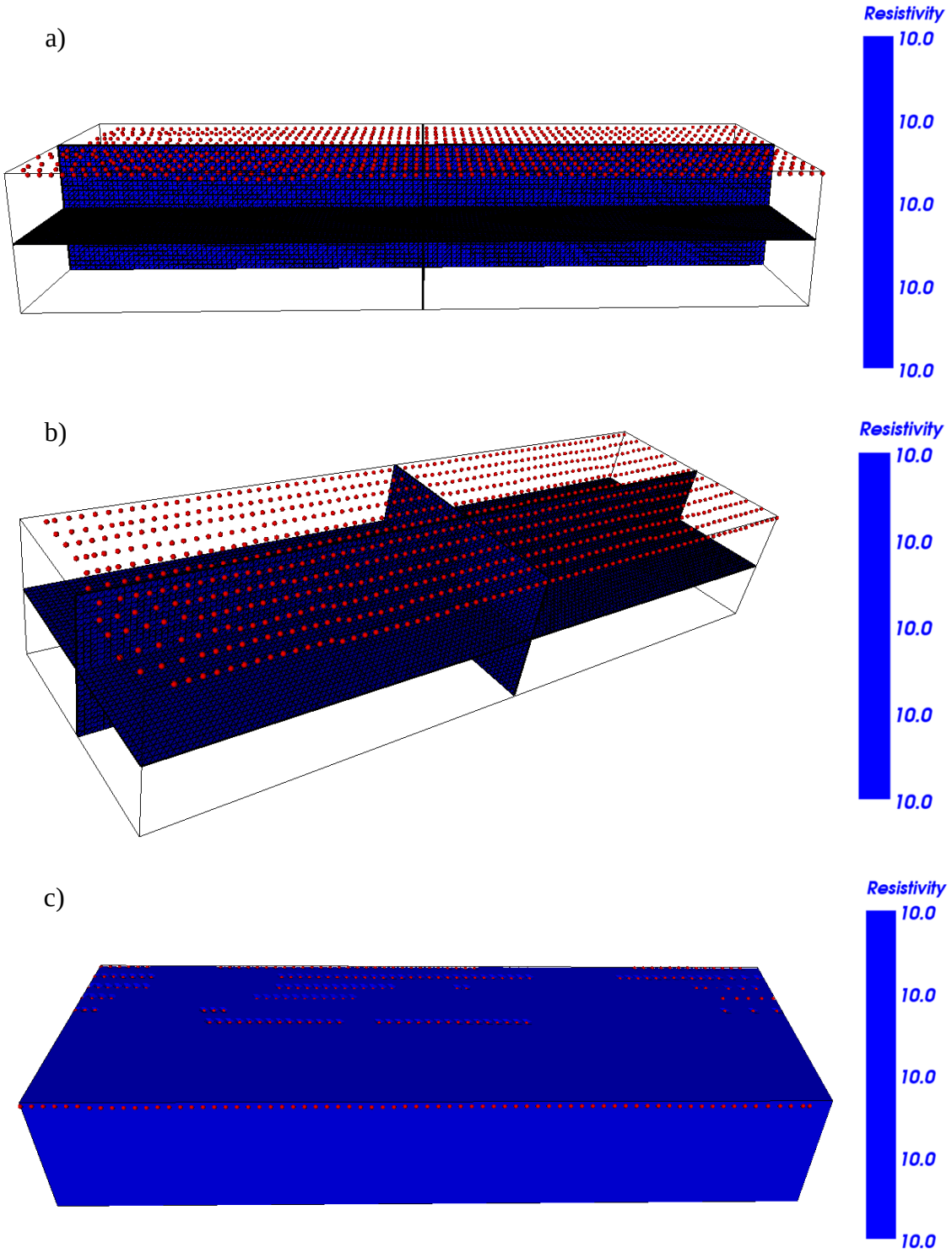


**Figure 4.11: (a & b) ERTLab™ utilizing Finite Element approach to model the subsoil by adopting mesh of hexahedrons to correctly incorporate terrain topography. (c) Starting (guess) model with homogenous resistivity of 10 Ohm.m, based on the highest frequency in the global histogram.**

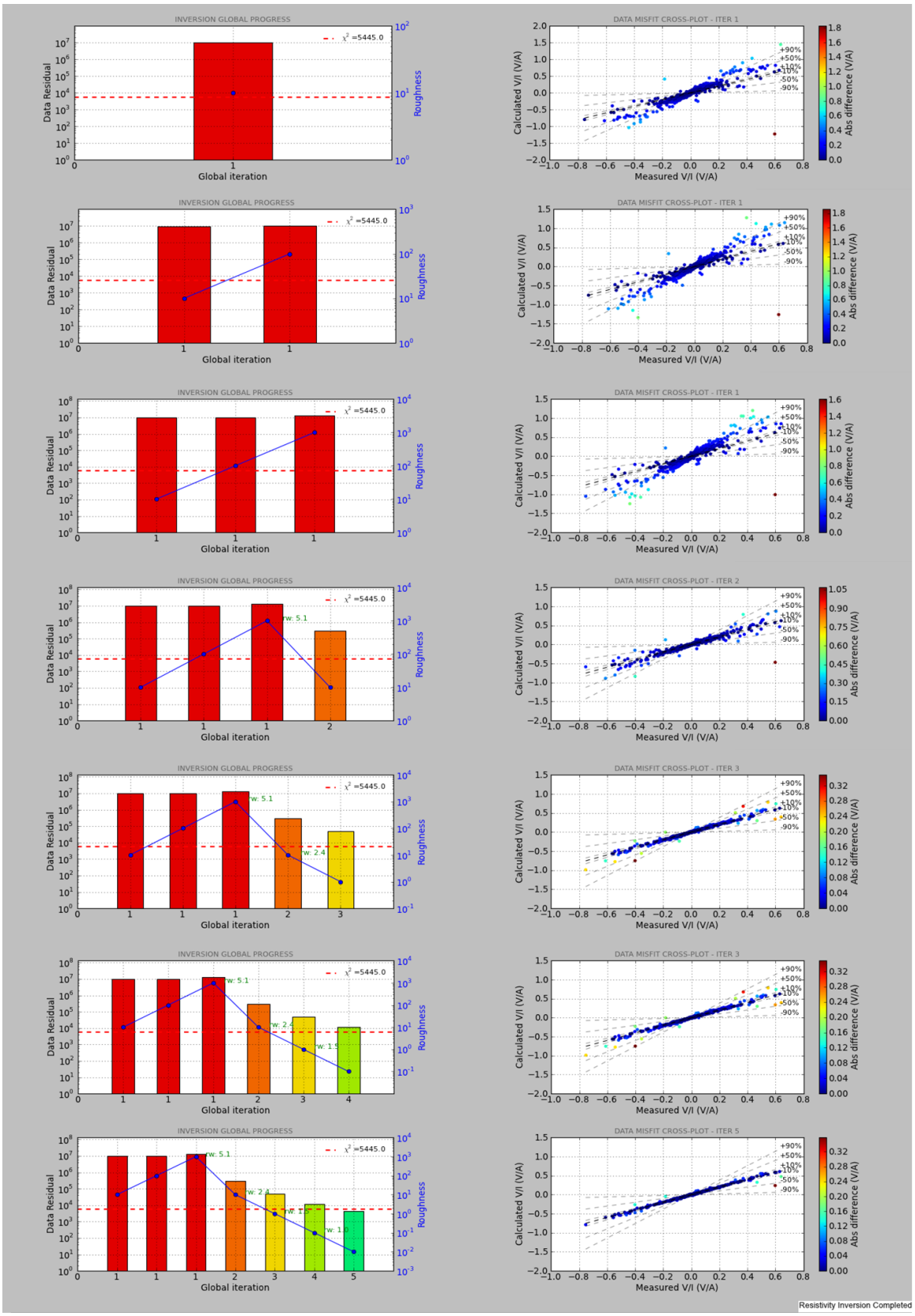


**Figure 4.12: Global progress of inversion operation.**

# CHAPTER 5

# DATA INTERPRETATION AND RESULTS

In this chapter, the 2D and 3D resistivity inversion results (i.e., resistivity tomograms) are presented and discussed. A geological interpretation is provided based on a joint correlation of tomograms (constructed using twelve parallel lines and two C-shaped loop datasets), topographic features and geotechnical information.

The apparent resistivity is a term used for the field measurement, since without interpretation; the resistivity measurement does not refer to any particular geologic layer. The resistivity data acquired at site produce apparent resistivity pseudosections, which need to be inverted to represent the actual geologic model of the subsurface; which gives information on the vertical distribution of layer thicknesses, depths and resistivity.

After data processing and inversion have been applied, the resulting images obtained were plotted in the following three different ways in order to optimize for a modelling and interpretation of the subsoil underneath the survey area down to 20 m depth:

- **XY depth-slices***: Plan views (depth slices) to allow for the visualization of the variation of electrical resistivity from surface down to -20 m below ground level, georeferenced with a recent aerial photograph;
- **XZ cross-sections***: To highlight the resistivity changes along sections "cut" through different sectors of the site, including a color legend and the indication of depth and the horizontal distance, together with the relative position of the section;

- **3D iso-resistivity volume***: 3D visualization of the whole investigated area allowing highlighting volumes having the same resistivity values. In this visualization, only subsoil volumes having the same electrical resistivity are visualized and the rest is blanked out.

Resistivity tomography is a valuable technique because it is non–invasive, and this type of spatially contiguous subsurface information is difficult, if not impossible, to obtain in any other way. Because of variability in resistivity of earth materials, interpretation of electrical resistivity tomography (ERT) data must be handled with caution. Factors such as temperature, porosity, conductivity, salinity, clay content, degree of fracturing, degree of consolidation, saturation and lithology generally affect the resistivity of earth materials.

When it comes to interpretation, the bulk resistivity information contained within the tomographic images is often ambiguous. For example, sandstone, limestone, dolomite, sand, and clay have resistivity values that can range from 1 ohm-m to $10^8$ ohm-m. The inherent ambiguities of resistivity tomogram interpretation must be kept in mind for any objective whatsoever. Incorporation of auxiliary data, such as drill core or geophysical logs, can greatly reduce the inherent uncertainty, although these data are often available at only one or a few discrete points.

Several cores were taken by an independent geotechnical engineering contractor during drilling at the site in January 2014. Borehole logs provided vital information like subsurface stratigraphy, depth of water table and type, nature and condition of the rock mass by conducting, Rock Quality Designation (RQD) and Standard Penetration Test

*See appendix A for complete graphical results

(SPT). Constraining resistivity data with borehole log data quite considerably reduces such ambiguities and non-uniqueness of the inverse problem, yielding true and acceptable earth model. Therefore, in order to prevent over-interpretation and deal with the non-unique nature of the inverse problem, the ERT results were correlated with the geotechnical engineering data from borehole logs and with aerial photographs to establish a correlation between resistivity tomograms and topographic features at the site.

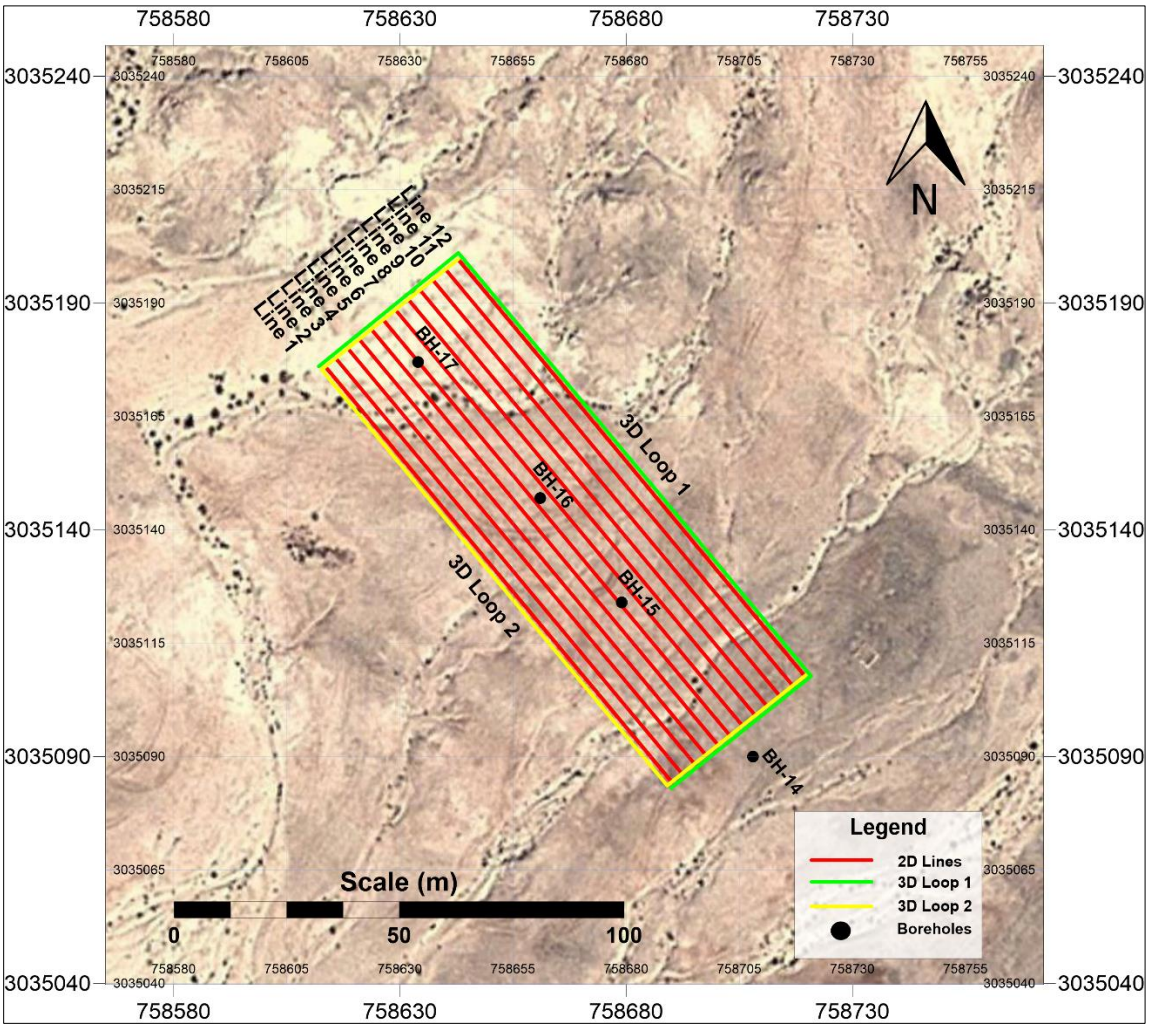


**Figure 5.1: Plan view of the area of investigation along with borehole locations.**

The site lies at a distance of around 300 m from the Red Sea shoreline, at almost 15 m above mean sea level. Several boreholes were drilled at the project site down to depth of 10 to 15 m. As shown in Figure 5.1, three boreholes BH-15, BH-16 and B-17 lie within the area of investigation. According of borehole logs, the area is characterized by the presence of highly fractured and highly weathered coralline limestone overlain by a silty sand layer of varying thickness. Figures 5.2 and 5.3 summarize the borehole logs of BH-14, BH-15, BH-16 and BH-17. Actual borehole logs can be found in Appendix B.

## 5.1 Correlation of ERT Results with RQD Values

Borehole log data has been incorporated in this study for the necessary preliminary calibration of the resistivity results. Several boreholes were drilled at the project site down to a depth of 10 to 15 m. Three boreholes BH-15, BH-16 and B-17 lie within the area of investigation, while BH-14 lies in a close proximity (Figure 5.1). According to geological description of borehole logs (Fig. 5.2 and 5.3), the area is characterized by the presence of thick layer of highly fractured and highly weathered coralline limestone overlain by thin silty sand layer of marginally varying thickness.

During the borehole drilling, RQD tests were conducted for coralline limestone layer at every 1.5 m. The stratigraphy shown by the drilling is quite the same up to 10.0 m depth, however a certain variation in the RQD values exists among BH-16 and others (BH-14, BH-15 and BH-17). In BH-14, BH-15 and BH-17 the RQD values range between 0% and 12%, with a mean value of 5%, while in BH-16 the RQD values range between 19% and 31%, with a mean value of 22% for the depth column of 10 to 15 m - all suggesting the rock quality as poor to very poor. This difference in rock quality in terms of slightly higher

RQD value is clearly reflected on 2D XZ cross-section at BH-16 (Figure 5.4); marked by higher resistivity of 80 to 120 Ohm.m from 1.5 m to 4.5 m depth.

The stratigraphy shown by the borehole logs indicates shallow and very thin (less than 1.0 m) silty sand layer. Thus, the resistivity variation below 1.0 m depth can be attributed to the physical characteristics of coralline limestone, such as degree of fracturing, sediment fill, as well as the effect of ground water. There are possibly more compact volumes inside this geological formation down to 5 m depth that are marked by a higher resistivity values.

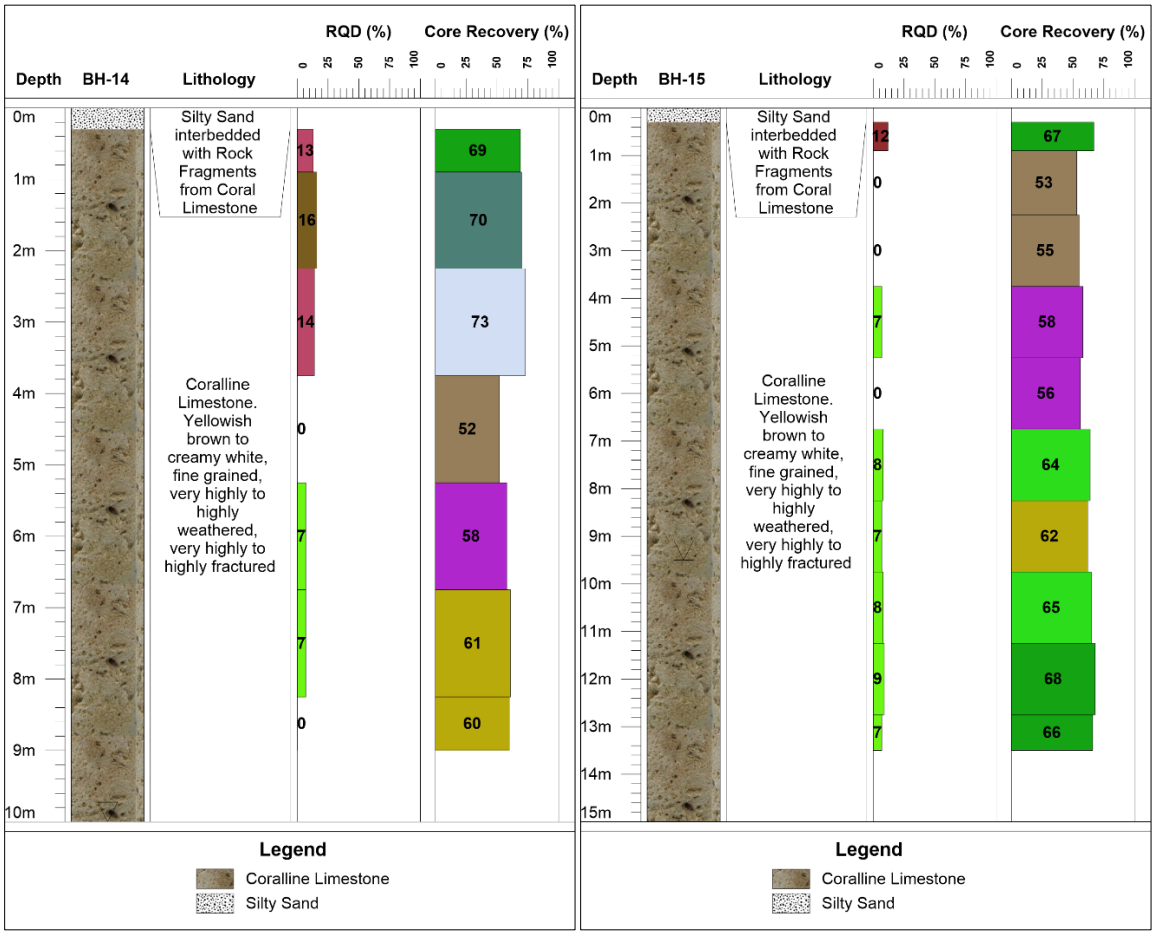


**Figure 5.2: Borehole logs of BH-14 and BH 15**

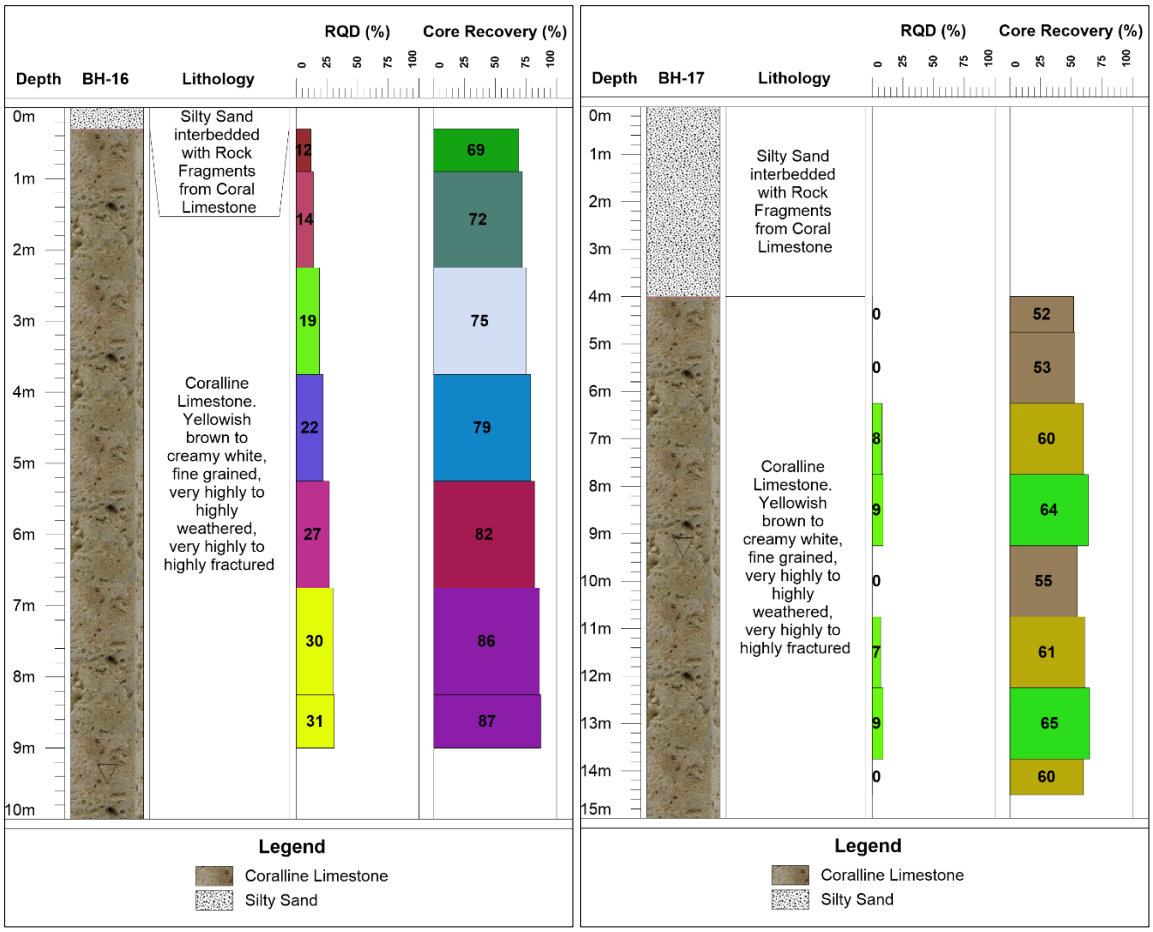


**Figure 5.3: Borehole logs of BH-16 and BH 1**

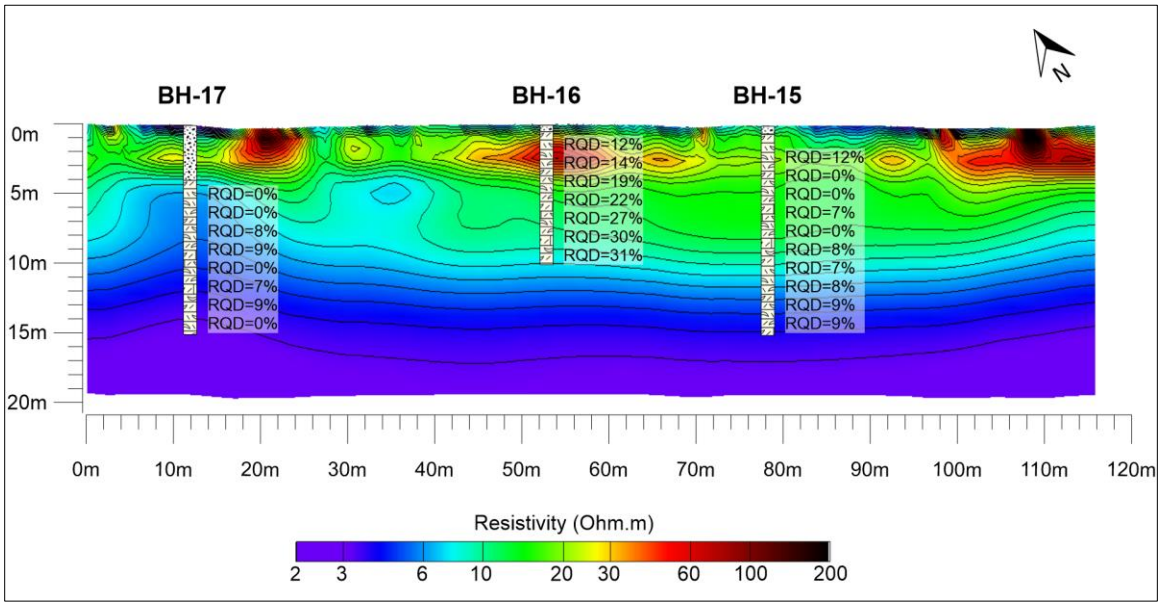


**Figure 5.4: 2D resistivity tomogram overlapped with RQD values from borehole logs**

Groundwater table was detected at 9.5 m during geotechnical investigation using a well-sounder. Electrical conductivity of ground water could not be checked physically at the site, however the site being located almost 200 m away from the Red Sea shoreline suggests the ground water to be highly saline to brackish. It is evident from the 2D & 3D tomograms (Figure 5.4 and 5.5) that the water table is well defined by the presence of a low resistivity layer (< 3 Ohm.m) just starting around 10.0 m depth.

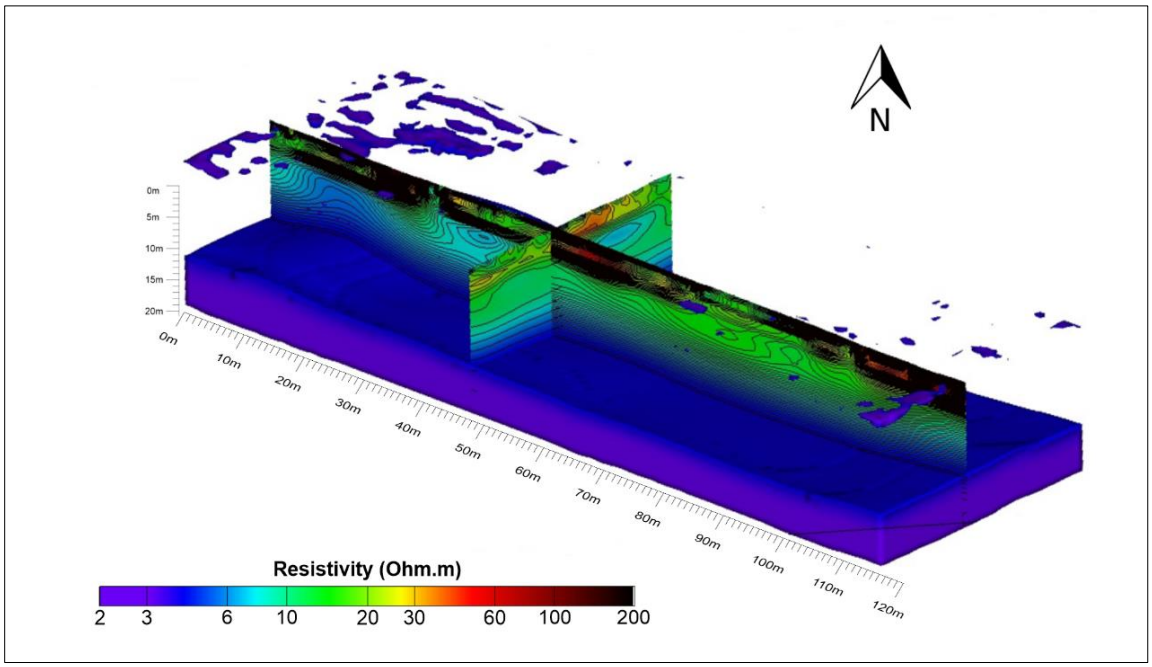


**Figure 5.5: 3D resistivity tomogram - Low resistivity volume < 3.0 Ohm.m showing the water table**

Inspecting the XZ resistivity cross-sections (Figure 5.6), there is a conspicuous **lift** on the north-western (left) side starting at around 7.0 m depth, marked by lines AA', BB'. As displayed in the borehole log of BH-17 (Figure 5.3), the mean RQD value of 4% suggests that such occurrence of uplift in the low resistivity volume can be attributed to the high permeation of water by capillary effect through highly fractured/weathered rock. Such occurrence is potentially considered as a negative factor for the stability of the ground.

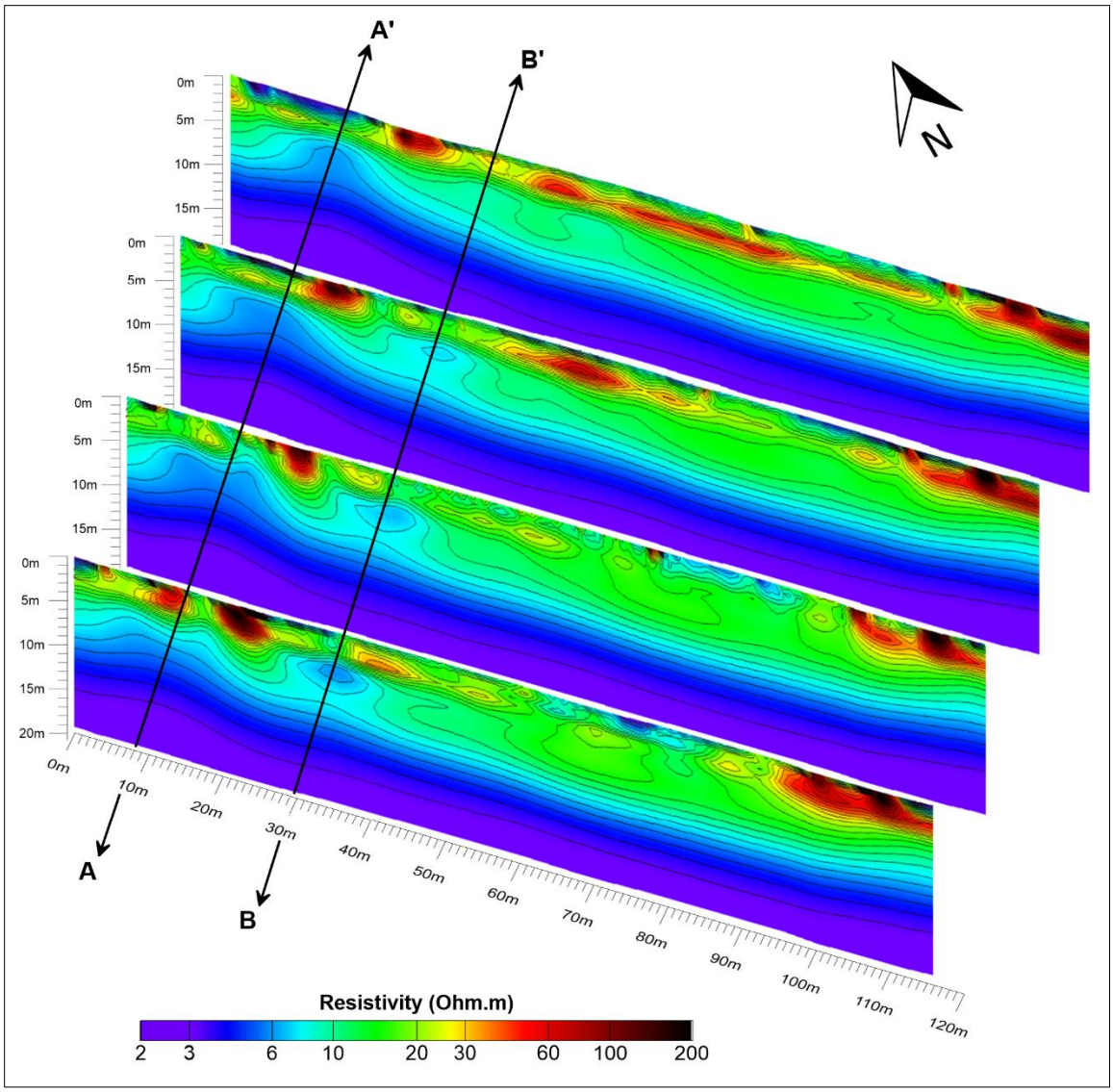


**Figure5.6: XZ cross-sections cut through 3D tomogram. A lift in the low resistivity volume at north-western side can be attributed to high water permeation or high degree of fracturing.**

## 5.2 Correlation of ERT Results with Topographic Features

After 3D inversion, a true 3D resistivity model was generated representing continuous distribution of calculated electrical resistivity in the subsurface. The 3D tomogram showed peculiar patterns on the surface (Figure 5.7); therefore XY-depth slices were generated for

(every 1.0 m, up to 19.0 m depth) and georeferenced using Surfer software in order to make accurate correlation with the actual site topography.

The shallow layer, starting from surface to 2.0 m depth, shows some spots of high resistivity anomalies (up to 200 ohm.m) with a curvilinear shape. By overlapping the resistivity maps to the aerial images (Figure 5.8 -5.10), it is possible to recognize a strong correlation between these anomalies and variations of the shallow geology. The aerial image suggests the presence of wadi river beds (dry river beds) and its shape has a significant correspondence with the resistive anomalies. A river or a wadi bed can be characterized by the presence of a higher sand percentage which is reflected by an electrical resistivity increase. The high resistivity volumes distribution in Figure 5.4 and 5.6 show that these are "confined" from the surface down to 5.0 m depth.

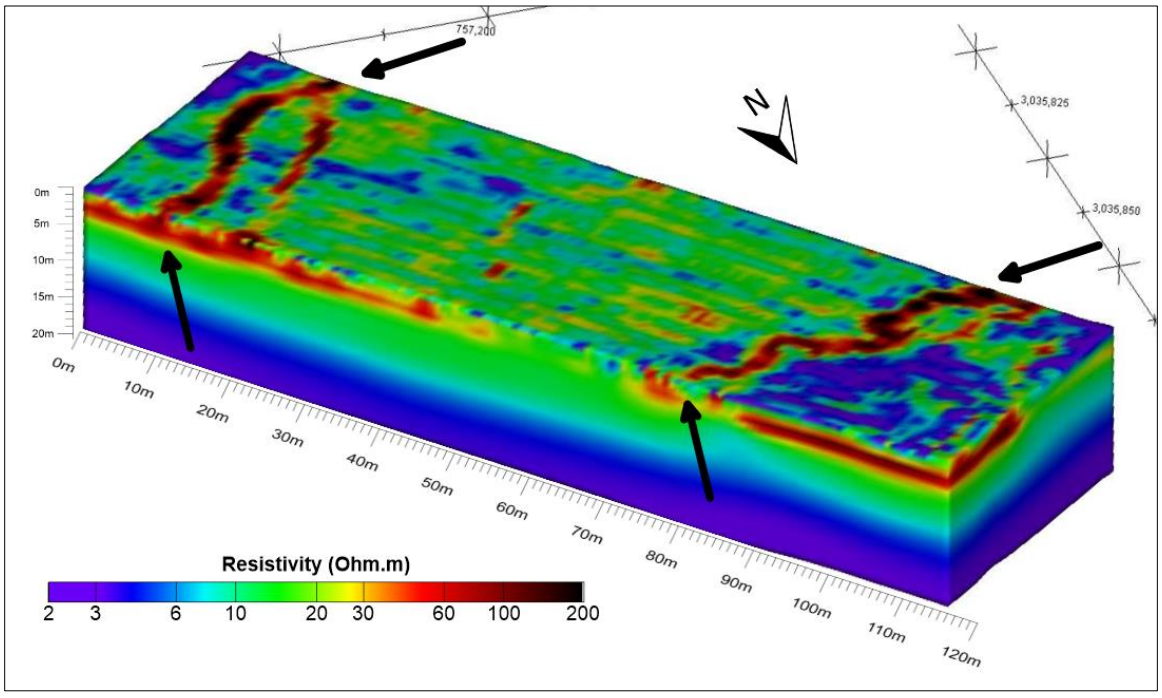


**Figure 5.7: 3D tomogram showing high resistivity volumes with distinct patterns on the surface.**

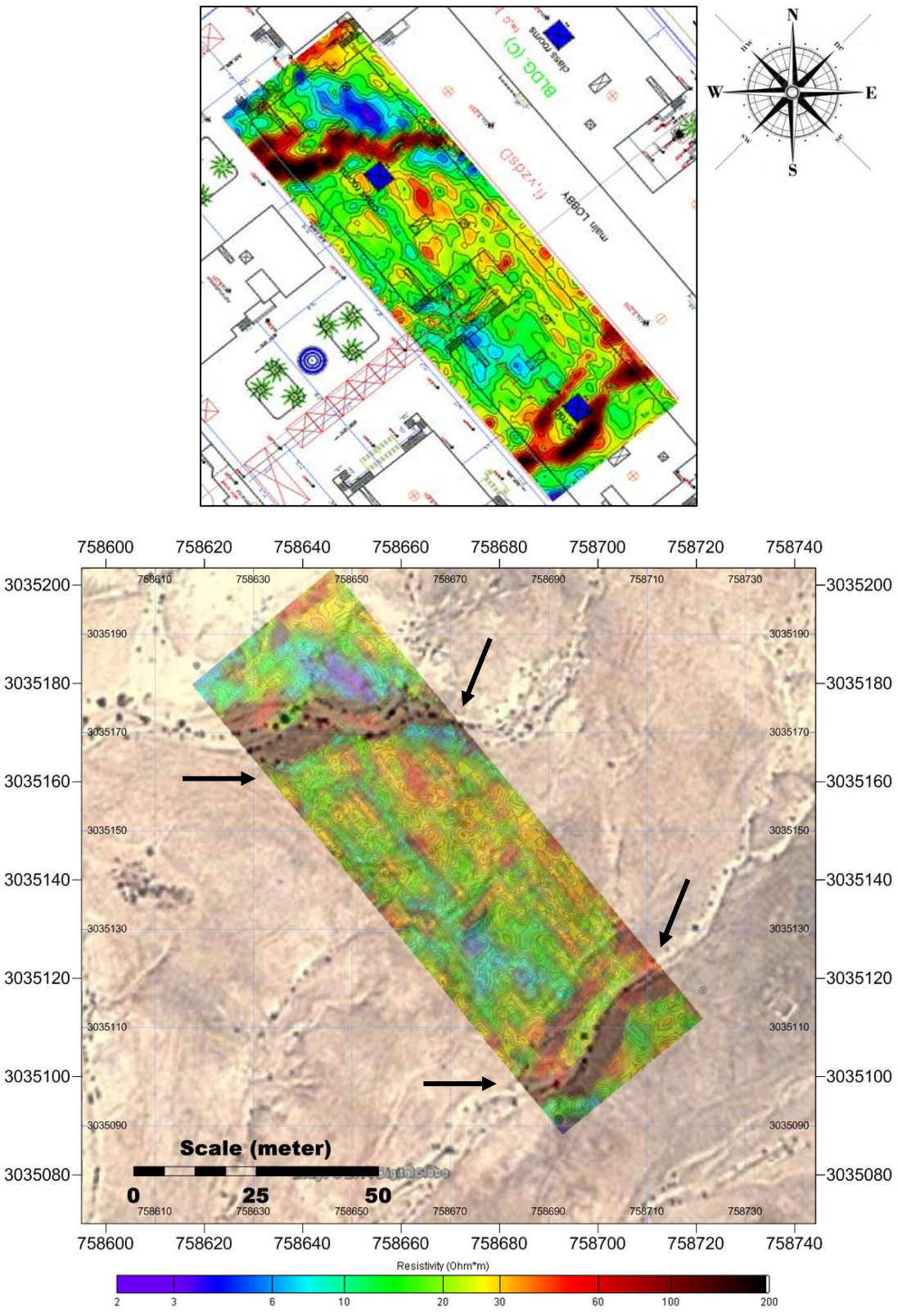


**Figure 5.8: Overlap of the XY resistivity depth-slice (z = 1 m). The arrows indicate shallow ground features that could be related to the presence of wadi beds (dry river beds)**

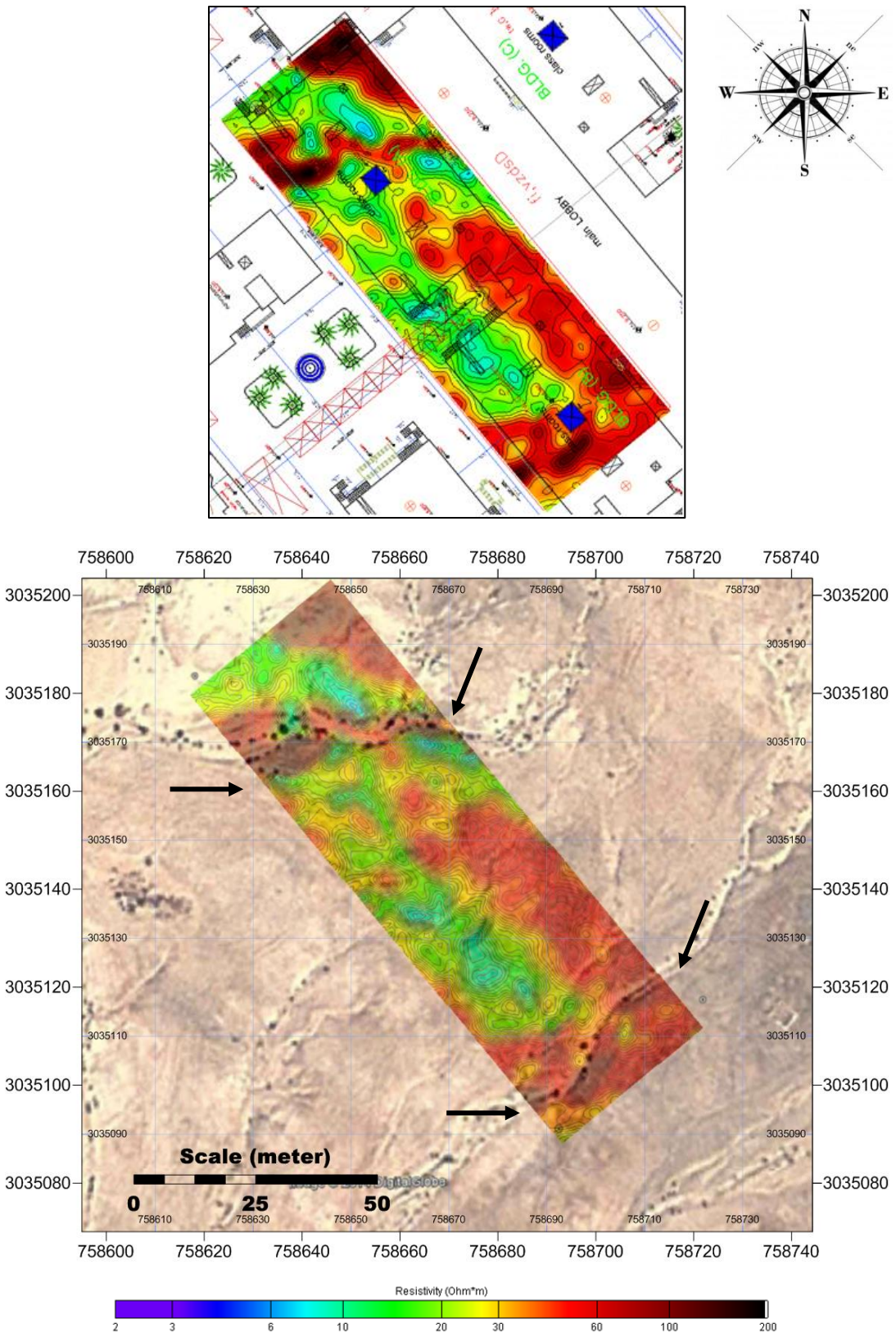


**Figure 5.9: Overlap of the XY resistivity depth-slice (z = 2 m). The arrows indicate shallow ground features that could be related to the presence of wadi beds (dry river beds)**

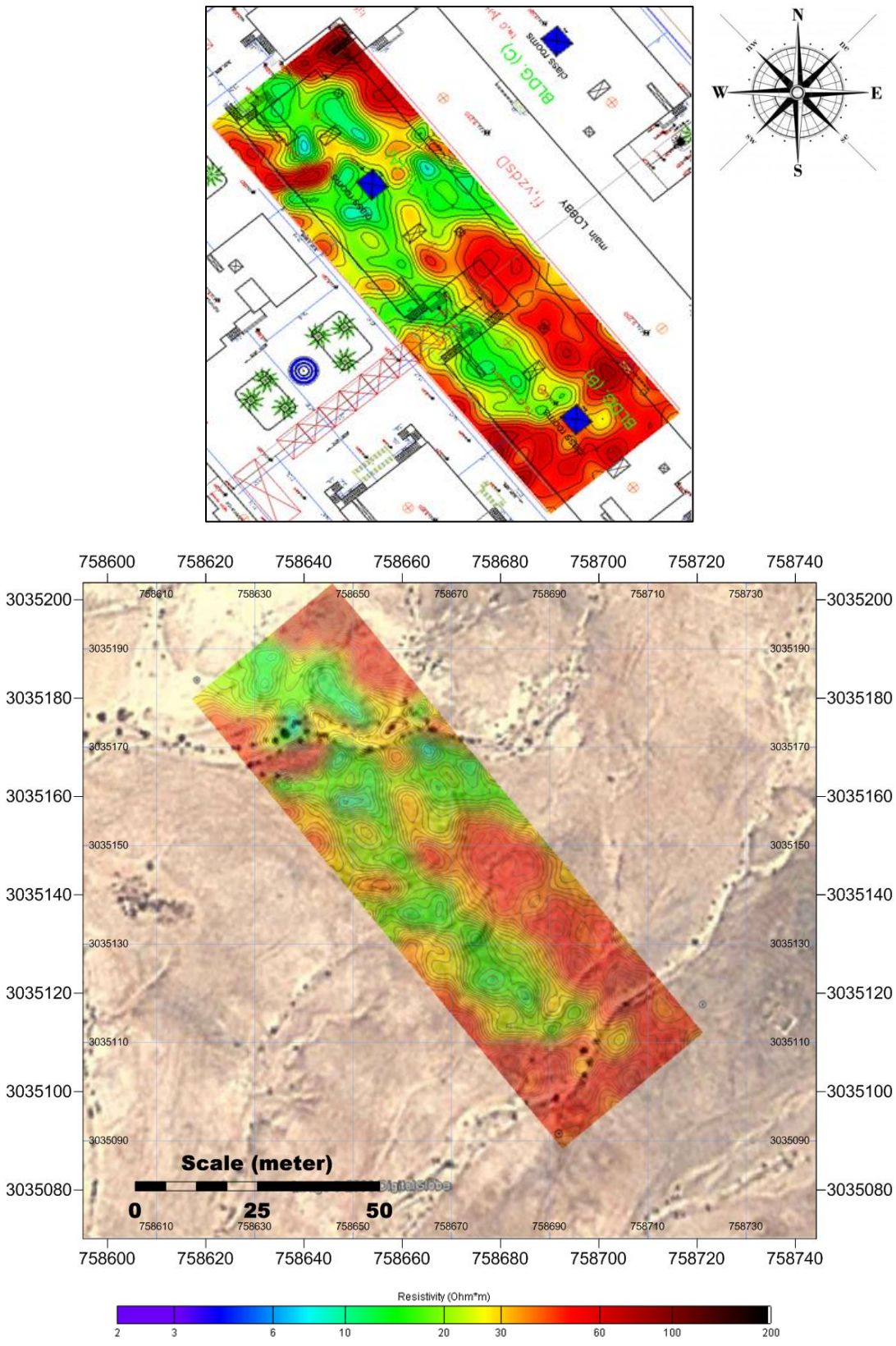


**Figure 5.10: Overlap of the XY resistivity depth-slice (z = 3 m). The arrows indicate shallow ground features that could be related to the presence of wadi beds (dry river beds).**

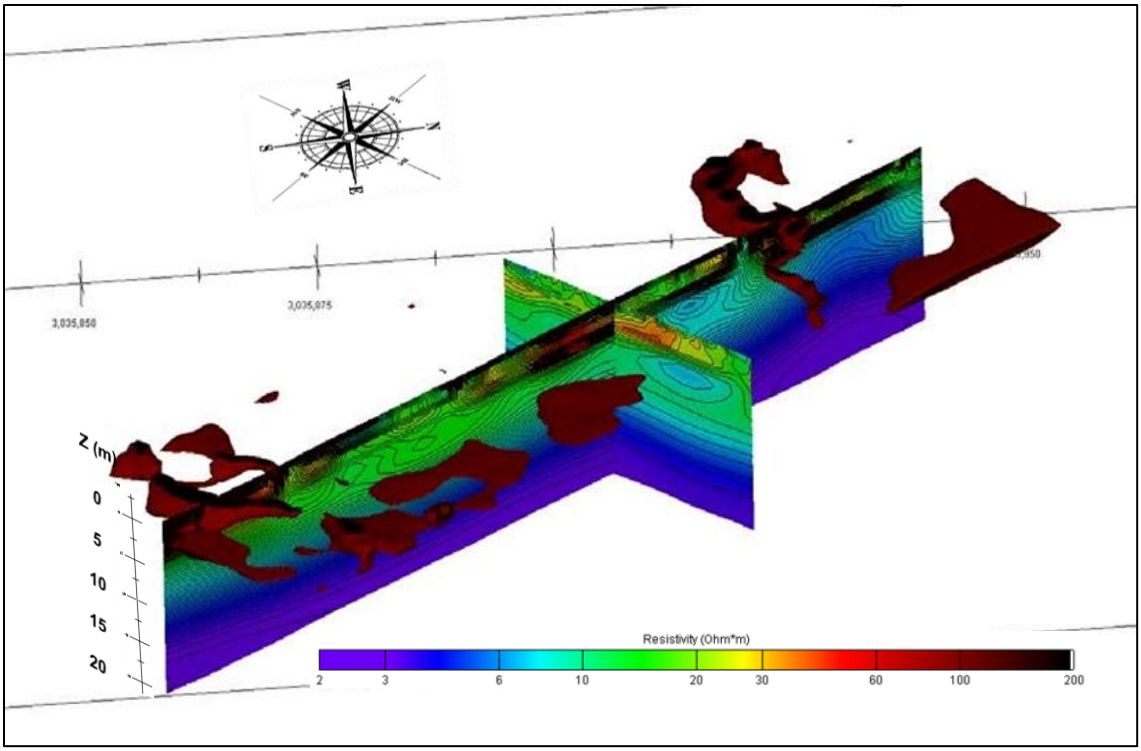


**Figure 5.11: 3D iso-resistivity volume > 70 ohm.m showing shallow resistive anomalies**

# CHAPTER 6

# CONCLUSIONS AND RECOMMENDATIONS

## 6.1 Conclusions

The results from the joint inversion of 2D and 3D data show a very good correlation between the high conductivity layer starting from 10 m depth and the groundwater table level. The overlap of resistivity map over the aerial photo, allows marking a good correspondence between the position and shape of high resistivity anomalies and some topographic variations. The topography itself suggests the presence of an old wadi bed, where it is easy to find a sand bank that increases the ground resistivity value (Figure 5.7, 5.8).

The RQD information derived from drilled boreholes show that geotechnical characteristics of the coral limestone are very poor in the whole area, but looking at the resistivity sections a concern arises regarding the presence of a conductive anomaly starting from 7.0 m depth, that cannot be correlated to the presence of water in the north-western side of the survey area, in correspondence of the Borehole BH-17.

Shallow resistivity values variations (Figure 5.4, 5.6) can be attributed to relatively more compact coral limestone presence. The information obtained from the analysis of the borehole stratigraphy and geotechnical tests indicate that even if the geological formation is the same in the study area, there are strong lateral variations of the mechanical properties.

There are possibly more compact volumes inside this geological formation that are marked by a greater resistivity.

The low resistivity volumes are due to high permeation of water or to higher rocks fracturing. Normally, the presence of cavities or voids is revealed by very high resistivity values (several thousands of Ohm.m). These values are not present in the data analysis, as the resistivity values did not exceed 200 Ohm*m; hence reinforcing our findings.

The topography of the survey area and the analysis of aerial photographs suggest the presence of at least two wadi beds crossing the surveyed (Figure 5.8). It is not a coincidence that the high resistive shallow volumes are exactly around and above these sectors. A more detailed geological knowledge of the area, as in every geophysical survey data analysis, is always desirable to fully understand the behavior of the investigated subsoil.

## 6.2 Recommendations

This study has uncovered several potential directions for future research. Latest developments in engineering geophysics provide a large set of techniques for non-invasive and in situ data recording for high-resolution parameterization.

Such problems can be further studied using combinations (e.g., products, ratios, etc.) of resistivity and shear-wave tomography to enhance the near-surface anomalies imaged by both techniques, while retaining the effectiveness of seismic and electrical methods and reducing the possibility of ambiguous results.

Electrical and seismic data can be combined to enhance various types of anomalies. For example, the division of resistivity into shear-wave velocity $V_s$ (from the surface-wave inversion) can be used to strengthen the contrast of the alluvium/consolidated rock contact.

Similarly, a void is usually reflected by a high resistivity anomaly and displays low shear-wave velocity ($V_s$), the ratio of resistivity to $V_s$ will enhance anomalies due to voids and suppress those arriving from other features.

Thus, combined surface-wave and electrical resistivity surveys can be effective in situations where the need for increased anomaly strength and/or decreased ambiguity in interpretation are worth the additional field work and processing time.

On the technology/engineering side, any development that reduces field time spent stringing cable would increase the cost effectiveness of using multiple methods. For example, developing a single cable for both the electrodes and geophones would be very useful. Carrying this idea further, allowing the ground spike on a geophone casing to serve as an electrode would also decrease deployment and take-down time.

# REFERENCES


Abu-Shariah, M.I.I., "Determination of cave geometry by using a geoelectrical resistivity inverse model." *Engineering Geology* 105, 239-244, 2009.

Anderson N. L., Apel D. B. and Ismail A., "Assessment of karst activity at highway construction sites using the Electrical Resistivity method." *unpublished report for MoDOT*, 2006.

Anon, "Engineering Geophysics - Report of the Geological Society Engineering Group Working Party." *Q. J. Eng. Geol.*, 21, 207–271,1988.

Anon, "Code of practice for site investigations, BS 5930:1999." *British Standards Institution*, London, 1999.

Anon, "Code of practice for investigation of potentially contaminated sites BS 10175:2001." *British Standards Institution*, London, 2001.

Barker, R. D., "The offset system of electrical resistivity sounding and its use with a multicore cable." *Geophysical Prospecting*, 29, 128–143, 1981.

Barker, R.D., "Depth of investigation of collinear symmetrical four-electrode arrays." *Geophysics*, 54, 1031-1037, 1989.

Cardarelli, E., Di Filippo, G., Tuccinardi, E., "Electrical resistivity tomography to detect buried cavities in Rome: a case study." *Near Surface Geophysics* 4, 387–392, 2006.

Cardimona, S., "Electrical Resistivity Technique for Subsurface Investigation." 2011. http://citeseerx.ist.psu.edu/viewdoc/download?doi=10.1.1.135.2978&rep=rep.

Chambers, J., Ogilvy, R., Meldrum, P., and Nissen, J., "3D resistivity imaging of buried oil- and tar-contaminated waste deposits." *European Journal Environmental and Engineering Geophysics*, 4, no. 1, 3–14, 1999.

Coggon, J. H., "Electromagnetic and electrical modeling by the finite element method." *Geophysics*, 36, no. 1, 132–155, 1971.

Constable, S. C., Parker, R. L., and Constable, C. G., "Occam's inversion: A practical algorithm for generating smooth models from electromagnetic sounding data." *Geophysics*, 52, no. 3, 289–300, 1987.

Cook K. L., Van Nostrand R. G., "Interpretation of resistivity data over filled sinks." *Geophysical Prospecting*, 21, 716–723, 1954.

Dabas, M., Tabbagh, A., and Tabbagh, J., "3-D inversion in subsurface electrical surveying I-Theory." *Geophysical Journal International*, 119, 975–990, 1994.

Dahlin, T., and Bernstone, C., "A roll-along technique for 3D resistivity data acquisition with multi-electrode arrays." *Proceedings of the Symposium on the Application of Geophysics to Engineering and Environmental Problems (SAGEEP)*, Vol. 2, Reno, Nevada, EEGS, 927–935, 1997.

Dahlin, T., "On the automation of 2D resistivity surveying for engineering and environmental applications." *Ph.D. thesis, Lund University*, 1993.

Dahlin, T., "2D resistivity surveying for environmental and engineering applications.": *First Break*, 14, no. 7, 275–283, 1996.

Daily, W. and Owen, E. "Cross-borehole resistivity tomography." *Geophysics* 56:1228–1235, 1991.

Das, U. C., and Parasnis, D. S., "Resistivity and induced polarization responses of arbitrarily shaped 3D bodies in a two-layered earth." *Geophysics Prospecting*, 35, 98–109, 1987.

Davies FB "Explanatory notes on the geologic map of Al Wajh quadrangle, Sheet 26 B." *Ministry of Petroleum and Mineral Resources, Deputy Ministry for Mineral Resources*, Jeddah, Saudi Arabia, p 27, 1985

Davies, FB, Grainger DJ "Explanatory notes on the geologic map of Al Muwaylih quadrangle, Sheet 27A." *Ministry of Petroleum and Mineral Resources, Deputy Ministry for Mineral Resources,* Jeddah, Saudi Arabia, p 31, 1985.

deGroot-Hedlin, C., and Constable, C., "Occam's inversion to generate smooth, two-dimensional models from magnetotelluric data." *Geophysics*, 55, no. 12, 1613–1624, 1990.

Dey, A., and Morrison, H. F., "Resistivity modelling for arbitrary shaped two-dimensional structures." *Geophysical Prospecting*, 27, 106–136, 1979.

Dobrin, M. B., and Savit, C. H., "Introduction to Geophysical Prospecting." *McGraw-Hill*, 1988.

Dutta N., Bose R., Saikia B., "Detection of solution channels in limestone by electrical resistivity method." *Geophysical Prospecting*, 18, 405–414, 1970.

Edwards, R. N., Lee, H., and Nabighian, M. N., "On the theory of magnetometric resistivity (MMR) methods." *Geophysics*, 43, no. 6, 1176–1203, 1978.

Edwards, R. N., "The magnetometric resistivity method and its application to the mapping of a fault." *Canadian Journal of Earth Sciences*, 11, 1136–1156, 1974.

Edwards, L. S., "A modified pseudosection for resistivity and IP." *Geophysics*, 42, no. 5, 1020–1036, 1977.

El Mahmoudi, A. et al., "2D Electrical Tomography for Mapping of Aquifers at the New Campus of King Faisl University, Al Hassa, KSA". *International Journal of Water Resources and Arid Environments* 1(6): 397-410, 2011.

Ellis, R. G., and Oldenburg, D. W., "The pole pole 3-D dc-resistivity inverse problem - a conjugate gradient approach." *Geophysical Journal International*, 119, 187–194, 1994.

Gautman, P., Pant, S. R. and Ando, H., "Mapping of Subsurface Karst Structure with Gamma Ray and Electrical Resistivity Profiles: a Case Study from Pokhara Valley, Central Nepal." *Journal of Applied Geophysics* 45, 2, 97-110, 2000.

Gibson, P. J., Lyle, P. and George, D. M., "Application of Resistivity and Magnetometry Geophysical Techniques for Near-Surface Investigations in Karstic Terranes in Ireland." *Journal of Cave and Karst Studies*, 66, 2, 35-38, 2004.

Greenfield R. J., "Review of geophysical approaches to the detection of karst." *Bull. Assoc. Engineering Geology*, 16, 393–408, 1979.

Habberjam, G. M., "Apparent resistivity observations and the use of square array techniques." *Geoexploration Monographs*, Series 1, No. 9. Gebr¨uder Borntraeger, Berlin, Stuttgart, 1979.

Hiltunen, D. R., and Roth, M. J. S., "Investigation of Bridge Foundation Sites in Karst Terrains via Multi-Electrode Electrical Resistivity." 2011. http://www.dot.state.fl.us/statematerialsoffice/geotechnical/conference/materials/hiltunen-roth.pdf.

Hughes, G.W., Johnson, R.S., "Lithostratigraphy of the Red Sea region." *GeoArabia* 10:49–126, 2005.

Hutchinson, D. J., Phillips C., Cascante G., "Risk considerations for crown pillar stability assessment for mine closure planning." *Journal of Geotechnical and Geological. Engineering.*, 20, 41–64, 2002.

Hamzah, U., Yaacup, R., Samsudin, A. R., Ayub, M. S., "Electrical Resistivity Imaging of the Groundwater Aquifer at Banting, Selangor, Malaysia." *Journal of Environmental Geology*; Volume 49, pp1156-1162, April 2006.

Garman K. M. and Purcell S., "Three-Dimensional Electrical Resistivity Surveys to Identify Buried Karst Features Affecting Road projects." 2011. http://www.dot.state.fl.us/statematerialsoffice/geotechnical/conference/materials/garman-purcell.pdf.

LaBrecque D. J., Miletto M., Daily W., Ramirez A., Owen E., "The effects of noise on Occam's inversionof resistivity tomography data." *Geophysics* 61:538–548, 1996.

LaBrecque, D., Heath, G., Sharpe, R., Versteeg, R., "Autonomous monitoring of fluid movement using electrical resistivity tomography." *Engineering Geophysics* 9, 167–176, 2004.

Li, Y. G., and Oldenburg, D. W., "Inversion of 3D dc resistivity data using an approximate inverse mapping." *Geophysical Journal International*, 116, 527–537, 1994.

Lines L. R., and Treitel, S., 1984, "Tutorial: A review of least-squares inversion and its application to geophysical problems" *Geophysical Prospecting*, 32, 159–186, 1984.

Loke M. H., "Electrical Imaging Surveys for Environmental and Engineering Studies." http://www.terraip.co.jp/lokenote.pdf, Pp 445-478, 2011.

Loke M. H. and Barker R.D., "Practical techniques for 3D resistivity surveys and data inversion." *Geophysical prospecting*, 44, 499-523, 1996a.

Loke M. H. and Barker R.D, "Rapid least-squares inversion of apparent resistivity pseudosections by a quasi-Newton method." *Geophysical Prospecting*, 44, 131–152, 1996b.

Loke, M. H., "Electrical imaging surveys for environmental and engineering studies.", *Unpublished report*: www.geoelectrical.com, 1999.

McDowell, P. W., "Geophysics in engineering investigations." *Construction Industry Research and Information Association*, London, 2002.

Farooq et al., "Subsurface cavity detection in a karst environment using electrical resistivity (er): a case study from Yongweolri, South Korea." *Earth Science Research Journal* Vol 16, No 1: 75 – 82, June 2012.

Militzer, H., Rosler, R., Losch, W., "Theoretical and experimental investigations for cavity research with geoelectrical resistivity methods." *Geophysical Prospecting*, 27640–652, 1979.

Metwaly M. and AlFouzan F., "Application of 2D geoelectrical resistivity tomography for subsurface cavity detection in the eastern part of Saudi Arabia." *Geoscience Frontiers* (4): 469-476, 2013.

Mochales, T. et al., "Detection of underground cavities by combining gravity, magnetic and ground penetrating radar surveys: A case study from the Zaragoza area, NE Spain." *Environmrntal Geology* 53:1067–1077, 2008.

Morelli G., LaBrecque D.J., "Advances in ERT inverse modelling." *European Journal of Environmental and Engineering Geophysical Society*, 1(2), 171-186, 1996.

Mufti, I. R., "A practical approach to finite-difference resistivity modeling." *Geophysics*, 43, no. 5, 930–942, 1978.

Ogilvy, R. D., Meldrum, P. I., and Chambers, J. E., "Imaging of industrial waste deposits and buried quarry geometry by 3-D resistivity tomography." *European Journal of Environmental and Engineering Geophysics*, 3, 103–114, 1999.

Ogilvy, R. D., Meldrum, P. I., Kuras, O., Beamish, D., and Chambers, J. E., "Detection of abandoned mine-shafts by 3D resistivity tomography: a parametric modelling study." *Proceedings of the 7th meeting of the Environmental and Engineering Geophysical Society* - European Section, Birmingham, 166–167, 2001.

Ogilvy, R. D., et al., "The Use of 3D Electrical Resistivity Tomography to Characterise Waste and Leachate Distribution within a Closed Landfill, Thriplow, UK" *Journal of Environmental and Engineering Geophysics*, 7, no. 1, 11–18, 2002.

Owen, T.E., "Detection and mapping of tunnels and caves." In: *Fitch, A.A. (Ed.), Developments in Geophysical Exploration Methods-5.* Applied Science Publishers Ltd, pp. 161–258, 1983.

Pelton, W. H., Rijo, L., and Swift, C. M., "Inversion of two-dimensional resistivity and induced polarisation data." *Geophysics*, 43, no. 4, 788–803, 1978.

Parasnis, D. S., "Reciprocity theorems in geoelectric and geoelectromagnetic work." *Geoexploration*, 25, 177–198, 1988.

Parasnis, D. S., "Principles of Applied Geophysics." *Chapman & Hall*, London, 5th edition, 1997.

Petrick, W. R., Sill, W. R. and Ward, S. H., "Three-dimensional resistivity inversion using alpha centres." *Geophysics*, 46, no. 8, 1148–1162, 1981.

Reynolds, J. M., "An Introduction to Applied and Environmental Geophysics." *John Wiley & Sons*, 1997.

Reynolds, J. M., "The role of geophysics in the investigation of contaminated land." *Proceedings of the Fifth International Conference, Re-Use of Contaminated Land and Landfills*, Brunel University, London, Engineering Technics Press, 131–137, July 1998.

Roy, A., and Apparao, A., "Depth of investigation in direct current methods." *Geophysics*, 36, no. 5, 943–959, 1971.

Sheriff, R. E., "Encyclopedic Dictionary of Exploration Geophysics." *Society of Exploration Geophysicists*, Tulsa, 3rd edition, 1991.

Smith, N. C., and Vozoff, K., "Two-dimensional dc resistivity inversion for dipole-dipole data." *IEEE Trans. Geosci.* Remote Sensing, 22, 21–28, 1984.

Smith, D. L., "Application of the pole–dipole resistivity technique to the detection of solution cavities beneath highways." *Geophysics*, 51, 833–837, 1986.

Sum, C. W., Othman, J., Loganathan, P., "Geotechnical problems in limestone terrain with emphasis on cavities and sinkholes." *Seminar Geologi dan Sekitarn*, UKM, Puri Pujangga, Bangi, pp. 102–117, 1996.

Telford, W. M., Geldart, L. P., and Sheriff, R. E., "Applied Geophysics" *Cambridge University Press*, 2nd edition, 1990.

Thomas, B., Roth M. J. S., "Evaluation of site characterization methods for Sinkholes in Pennsylvania and New Jersey." *Engineering Geology*, 52, 147–152, 1999.

Tripp, A. C., Hohmann, G. W., and Swift Jr., C. M., "Two-dimensional resistivity inversion." *Geophysics*, 49, 1708–1717, 1984.

U.S. Environmental Protection Agency, Use of Airborne, Surface, and Borehole Geophysical Techniques at Contaminated Sites: A Reference Guide: Publ.No. EPA/625/R-92/007, 1993.

Van Schoor, M., "Detecting of sinkholes using 2D electrical resistivity imaging." *Journal of Applied Geophysics* 50, 4, 393-399, 2002.

Vazquez-Lopez, R., Motti, E., "Prospecting in the sedimentary formations of the Red Sea coastal plain between Yanbu al Bahr and Maqna, 1968–1979." *Saudi Arabian Deputy Ministry for Mineral Resources Technical Record*, BRGM-10-1, 1981.

Zhang, J., Mackie, R. L., and Madden, T. R., "3D resistivity forward modeling and inversion using conjugate gradients." *Geophysics*, 60, 1313–1325, 1995.

Zhou, W., B. F. Beck and A. L. Adams, "Effective Electrode Array in Mapping Karst Hazards in Electrical Resistivity Tomography." *Journal of Environmental Geology*; Volume 32, Number 8; pp 922-928, November, 2002.

Zhou, W., B. F. Beck, and J.B. Stevenson, "Reliability of Dipole-Dipole Electrical Resistivity Tomography for Defining Depth to Bedrock in Covered Karst Terrains."

*Journal of Environmental Geology*; Volume 39, Number 7; pp 760-766, May, 2000.

Zhou, W., Beck, B.F., Adams, A.L., "Effective electrode array in mapping karst hazards in electrical resistivity tomography." *Environmental Geology* 42, 922-928, 2002.

Zhou, B., Greenhalgh S.A., "Finite element three-dimensional direct current resistivity modelling: accuracy and efficiency considerations." *Geophysical Journal International*, 145, 679-688, 2001.

# APPENDIX A

# ERT RESULTS

After data processing and inversion, the resulting images obtained were plotted in the following three different ways in order optimize for a modelling and interpretation of the subsoil underneath the survey area down to 20 m depth:

- **XZ cross-sections**: To highlight the resistivity changes along sections "cut" through different sectors of the site, including a color legend and the indication of depth and the horizontal distance, together with the relative position of the section;
- **3D iso-resistivity volume**: 3D visualization of the whole investigated area allowing highlighting volumes having the same resistivity values. In this visualization only subsoil volumes having the same electrical resistivity are visualized and the rest is blanked out. (See appendix A for complete results).
- **XY depth-slices**: Plan views (depth slices) to allow for the visualization of the variation of electrical resistivity from surface down to -19 m below ground level, georeferenced with a recent aerial photograph;

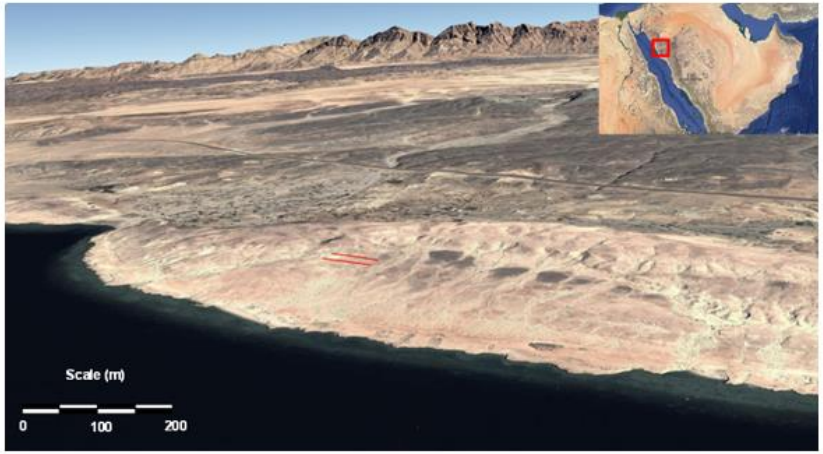



**Area of Investigation**

# XZ cross-sections

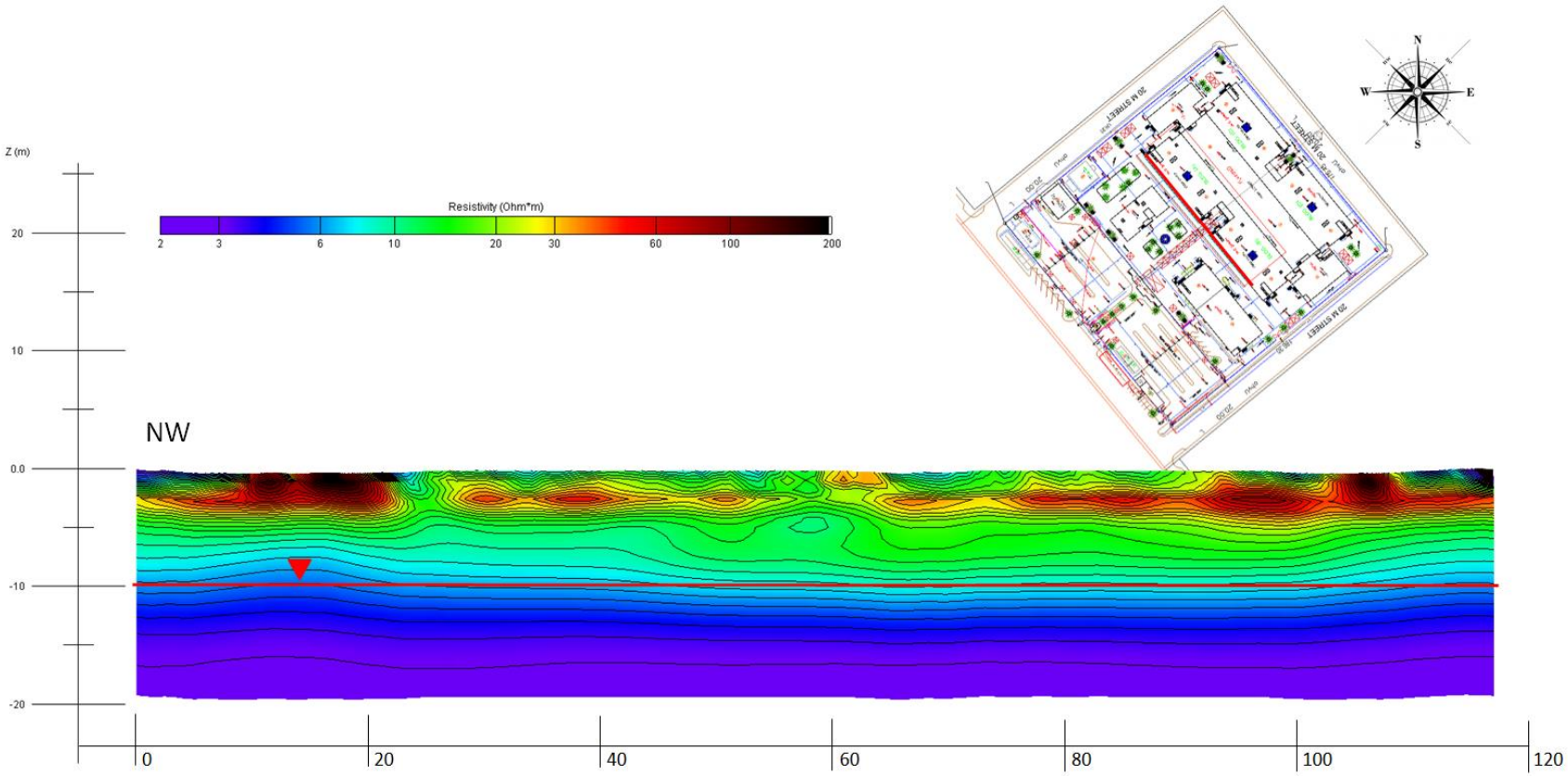


**Figure A6: XZ 2D cross-section 1 with corresponding location at the site indicated by red line.**

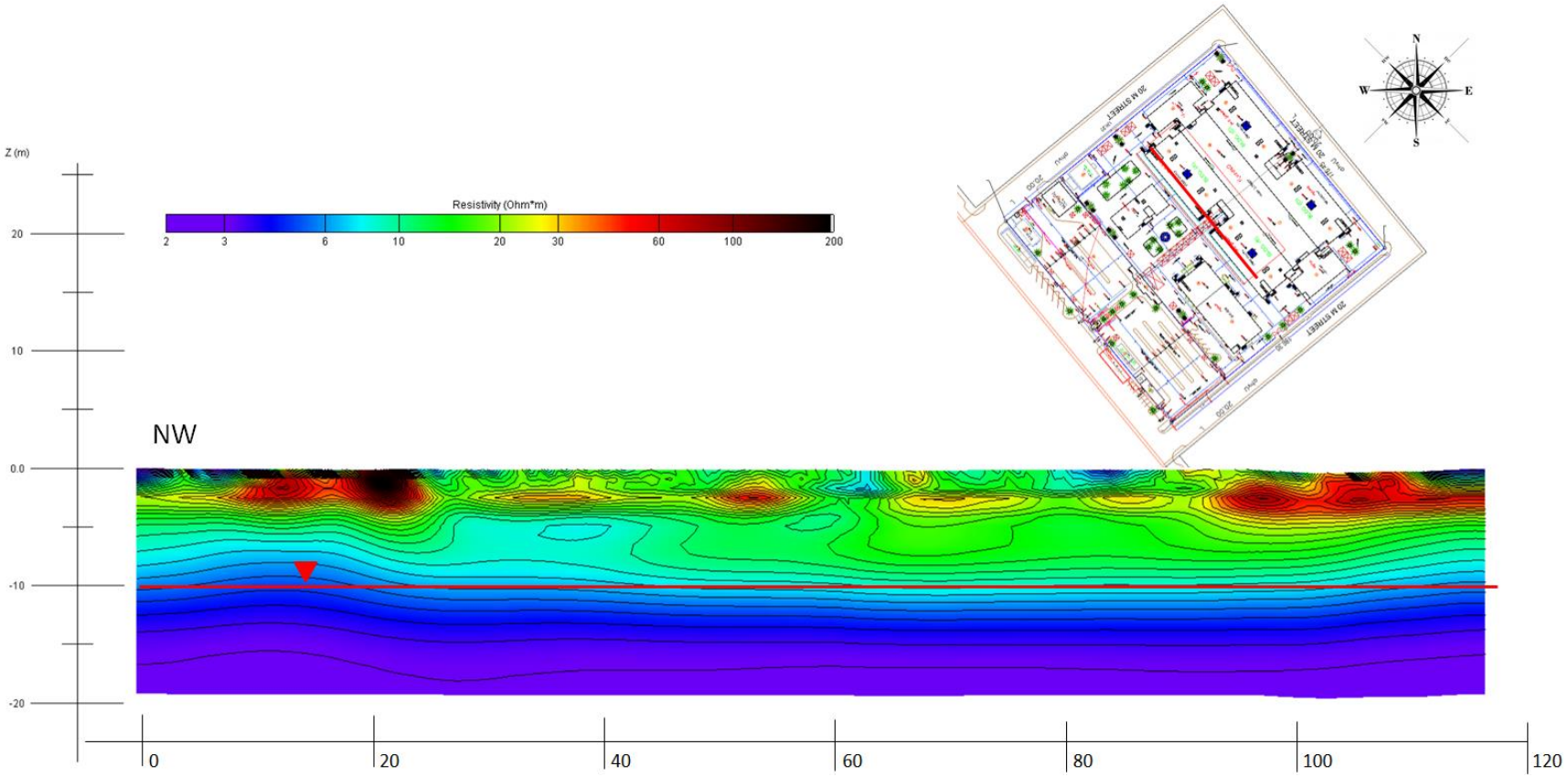


**Figure A7: XZ 2D cross-section 2 with corresponding location at the site indicated by red line.**

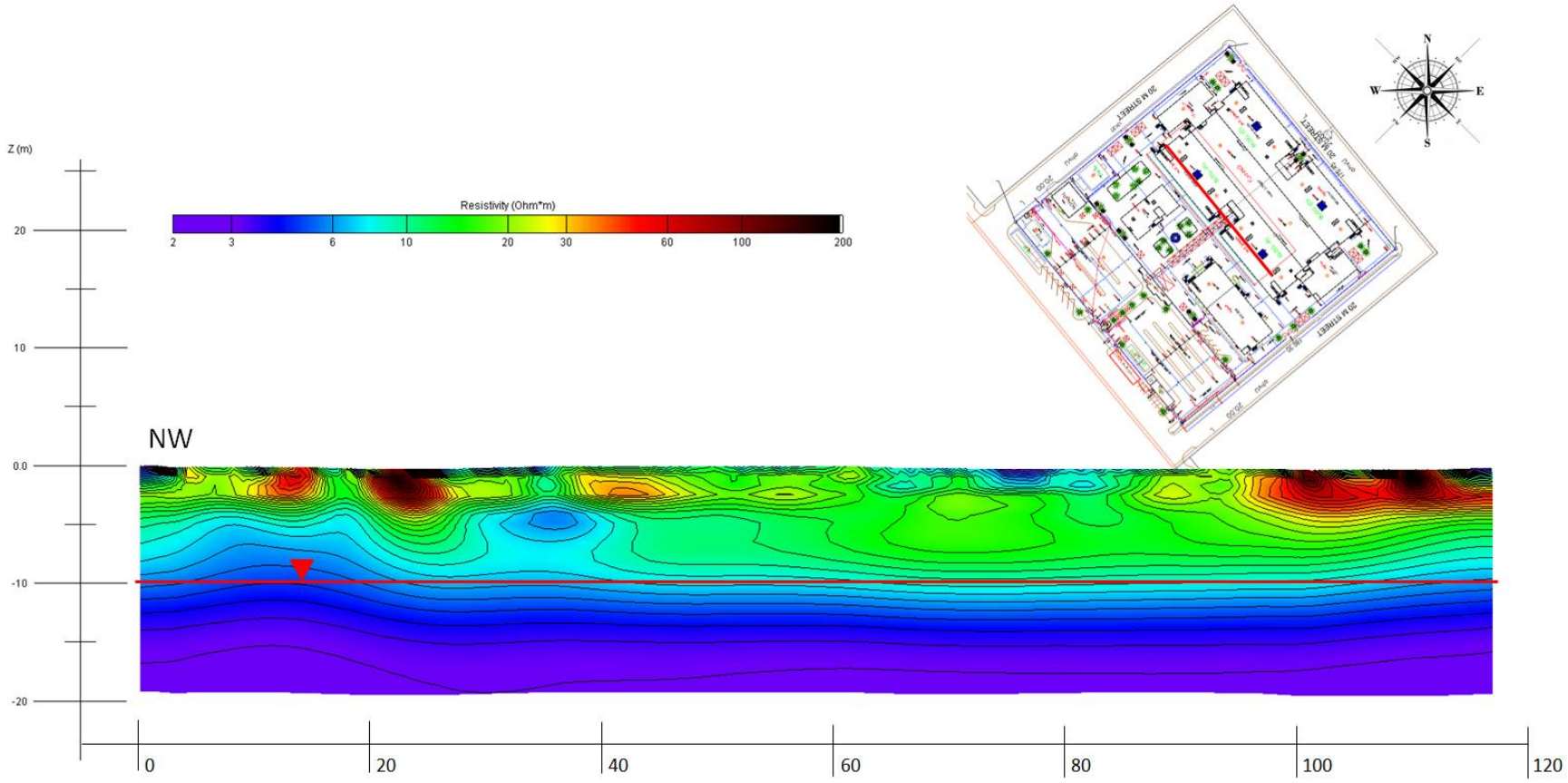


**Figure A8: XZ 2D cross-section 3 with corresponding location at the site indicated by red line.**

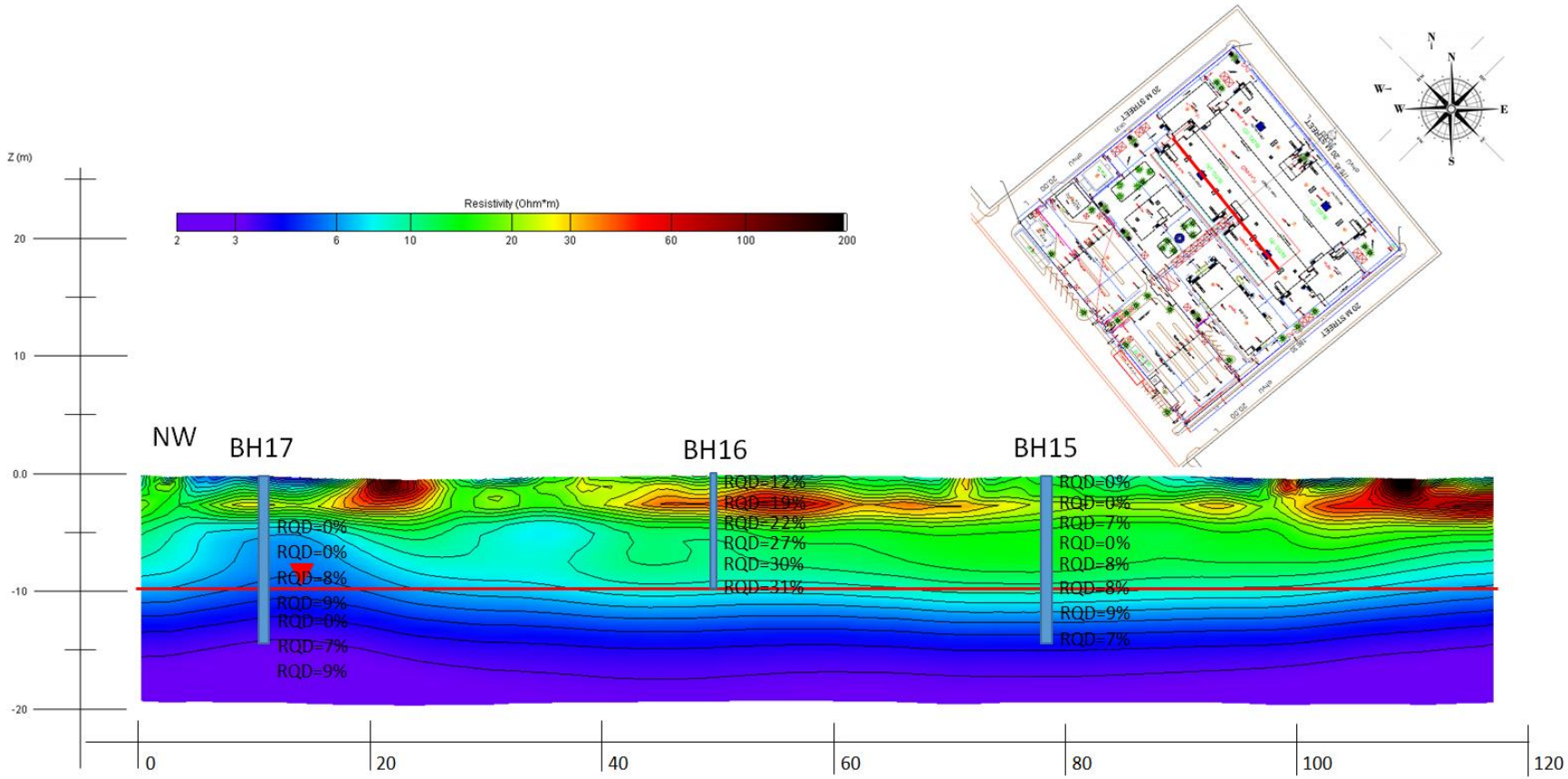


**Figure A9: XZ 2D cross-section overlapped with RQD values from borehole logs.**

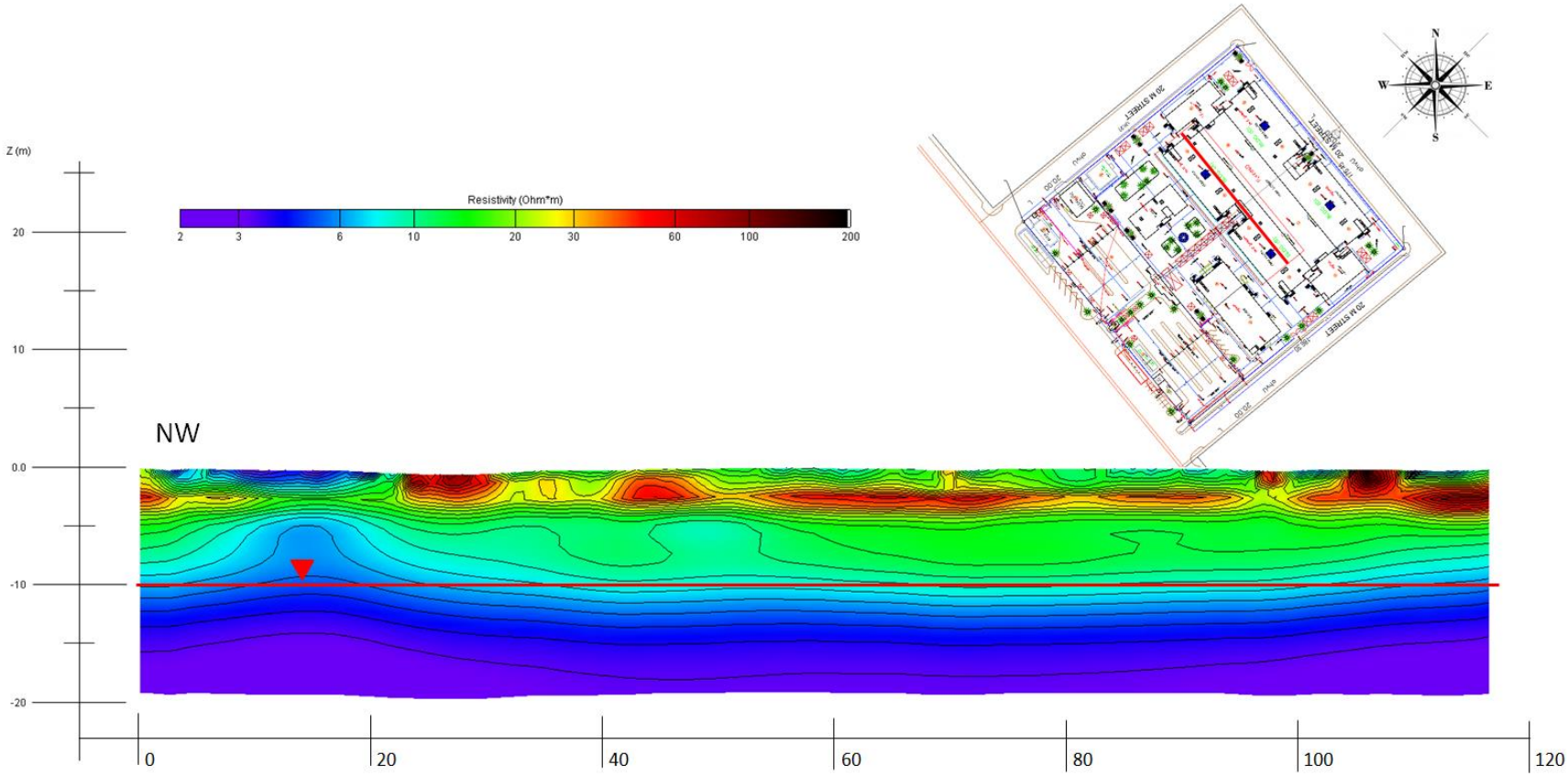


**Figure A10: XZ 2D cross-section 5 with corresponding location at the site indicated by red line.**

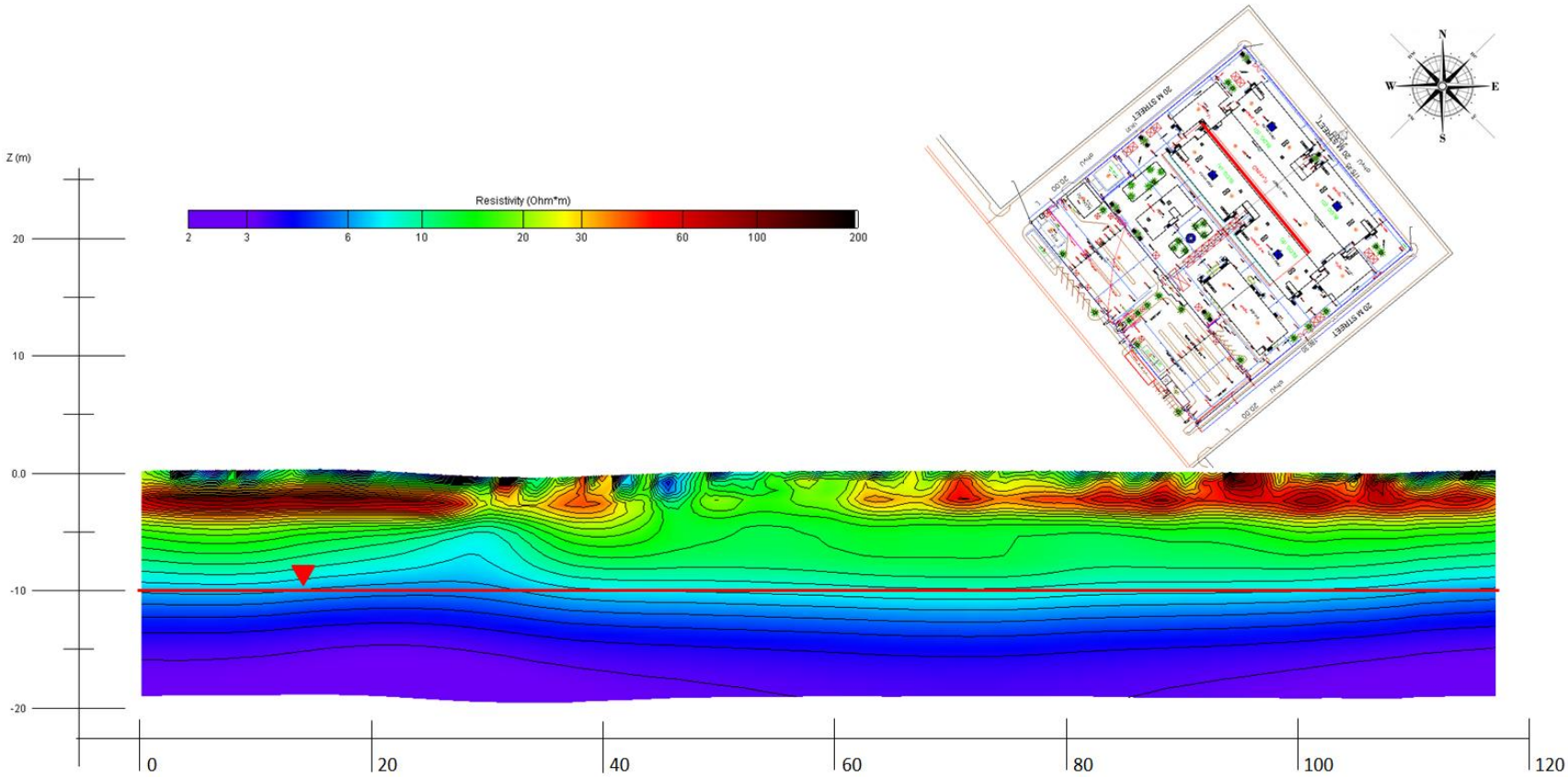


**Figure A11: XZ 2D cross-section 6 with corresponding location at the site indicated by red line.**

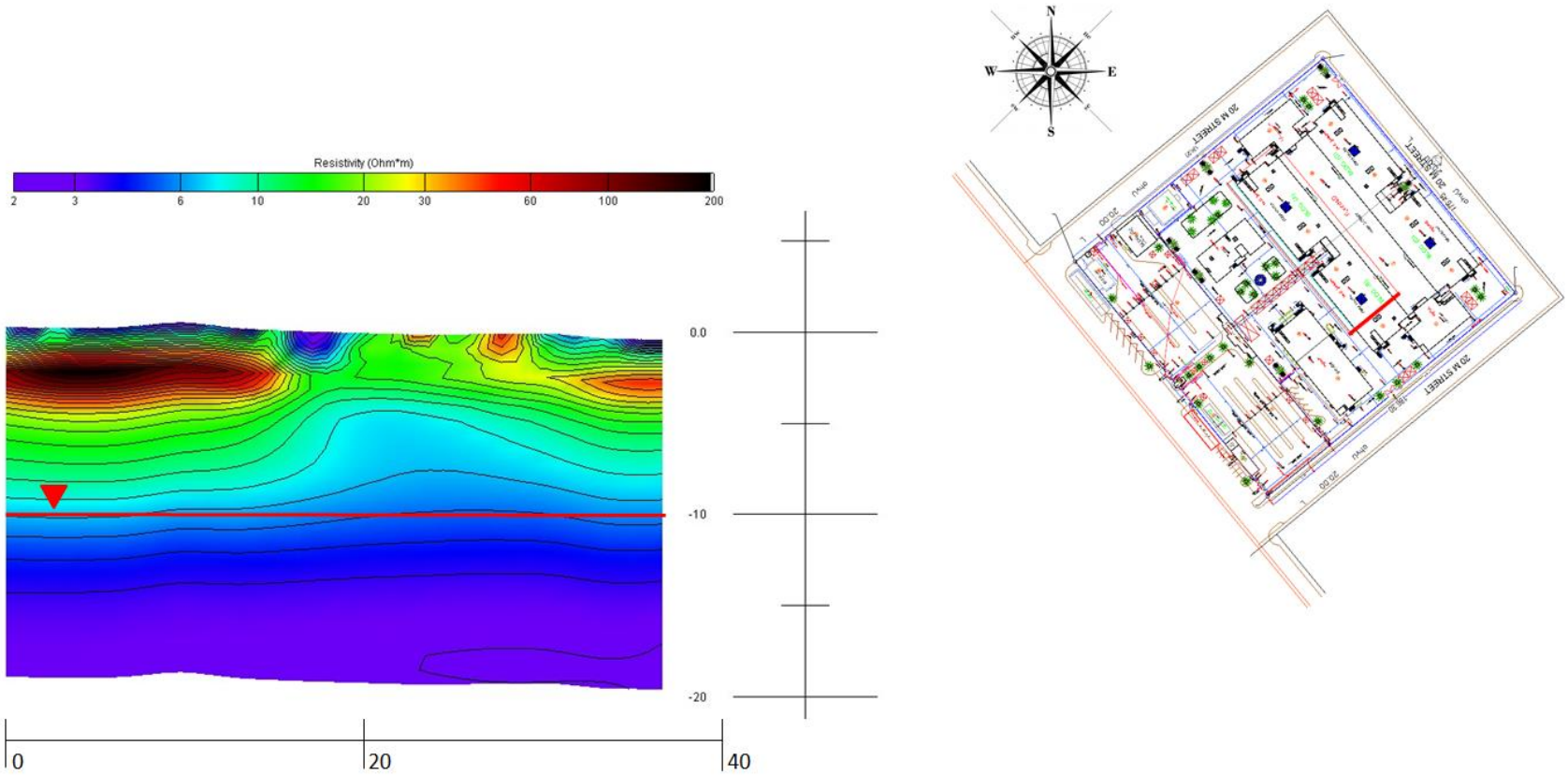


**Figure A12: XZ 2D cross-section 7 with corresponding location at the site indicated by red line.**

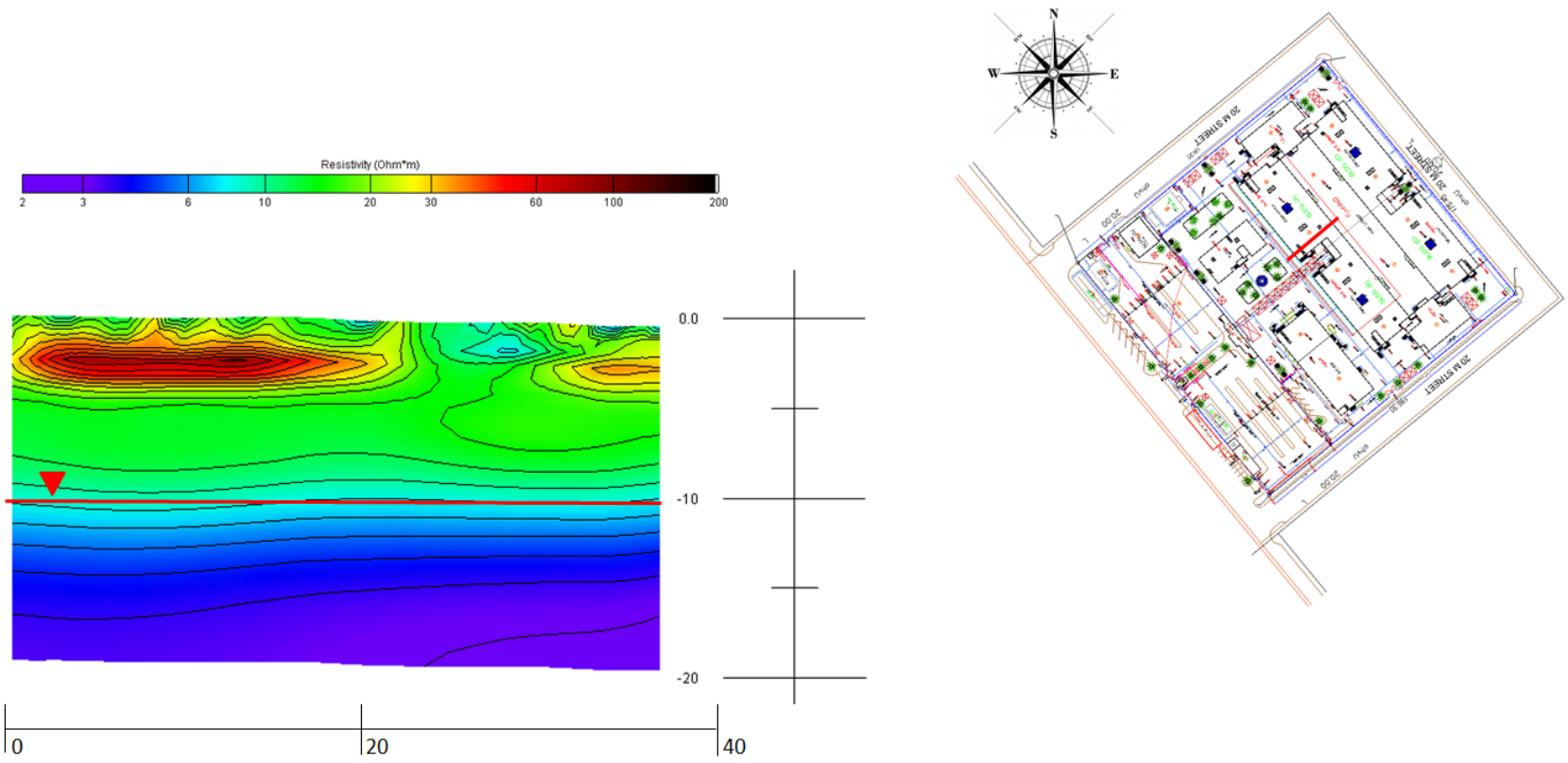


**Figure A13: XZ 2D cross-section 8 with corresponding location at the site indicated by red line.**

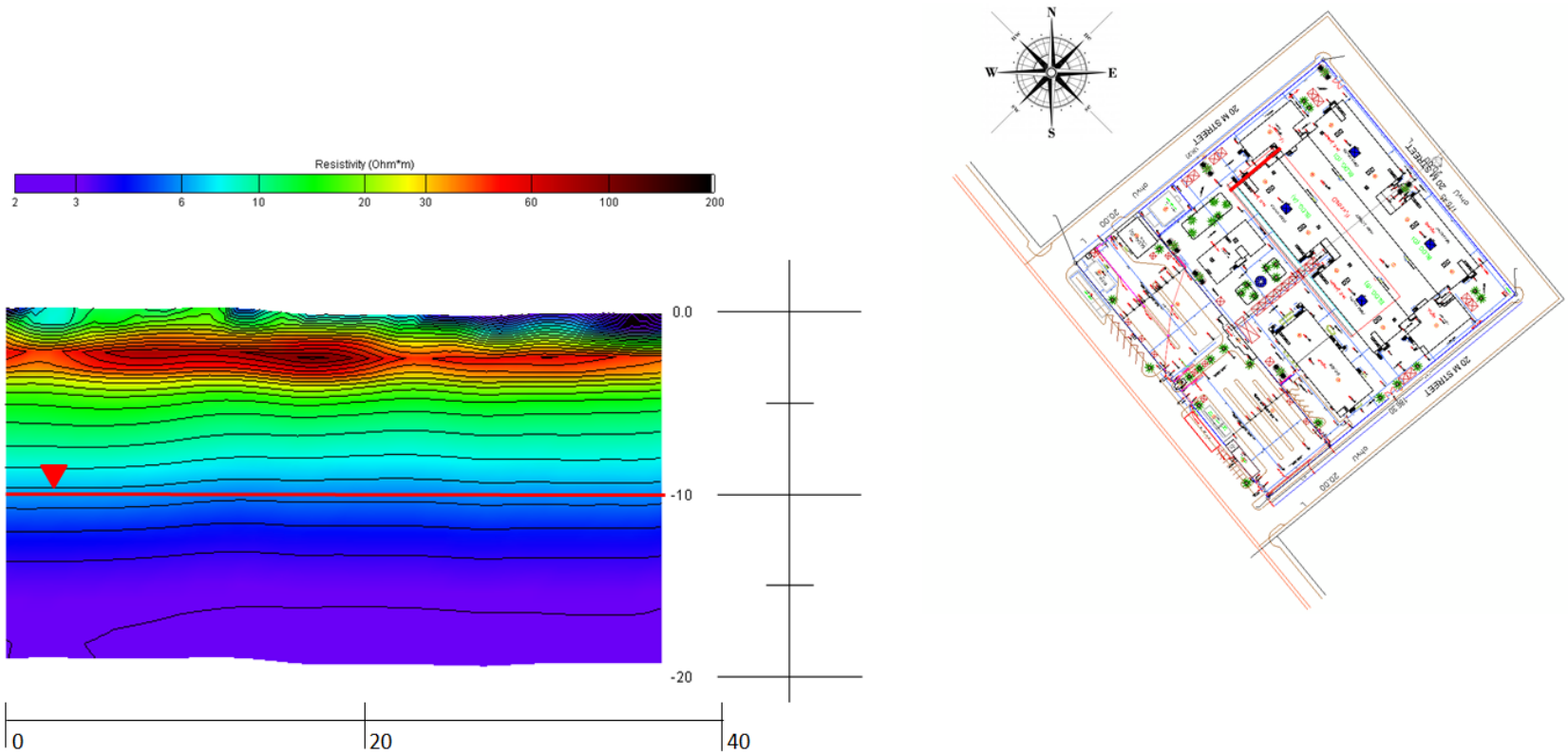


**Figure A14: XZ 2D cross-section 7 with corresponding location at the site indicated by red line.**

# 3D Iso-Resistivity Volumes

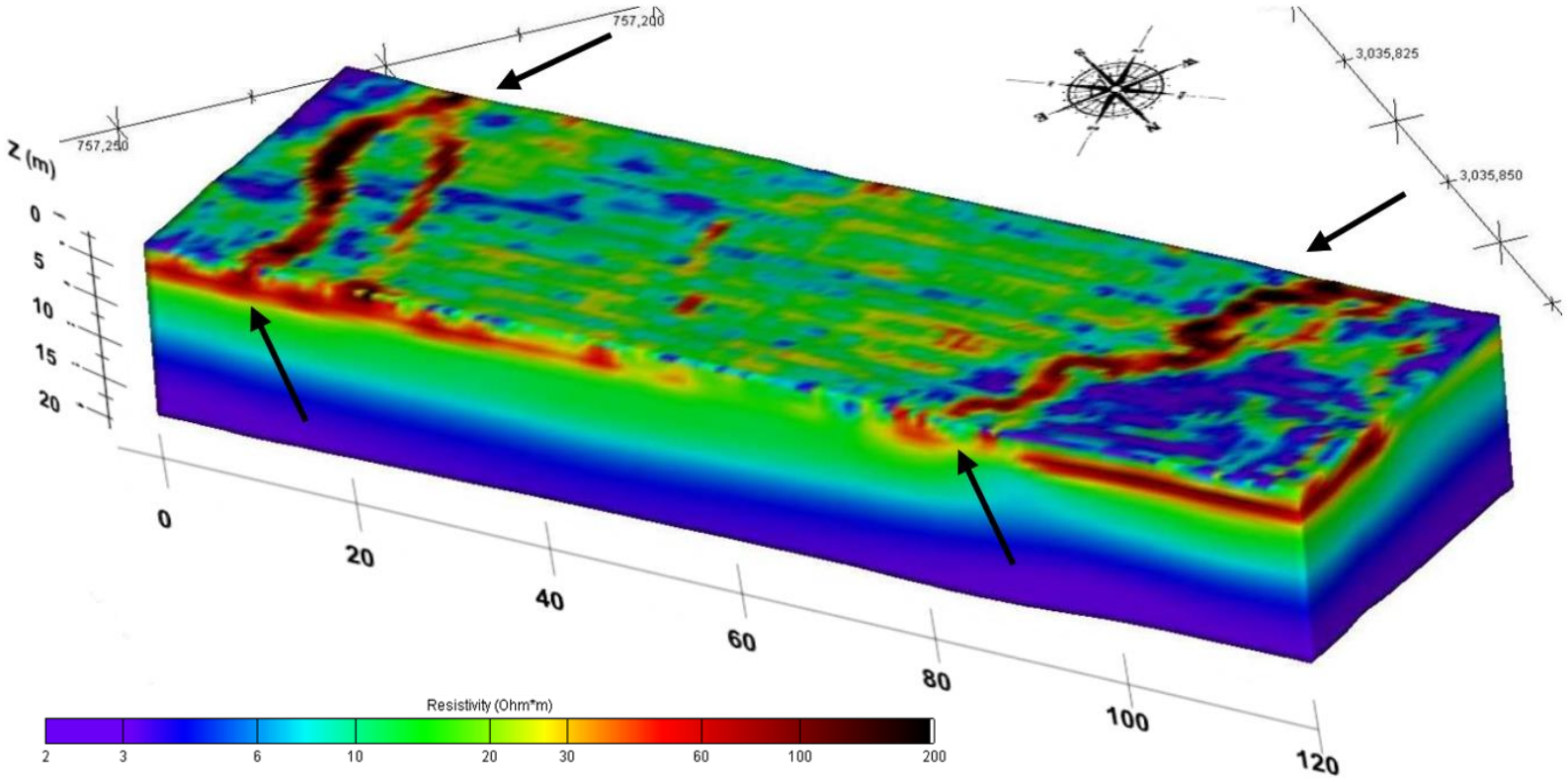


**Figure A15: 3D iso-resistivity volume – perspective view showing groundwater table and high resistivity anomalies at shallow depth.**

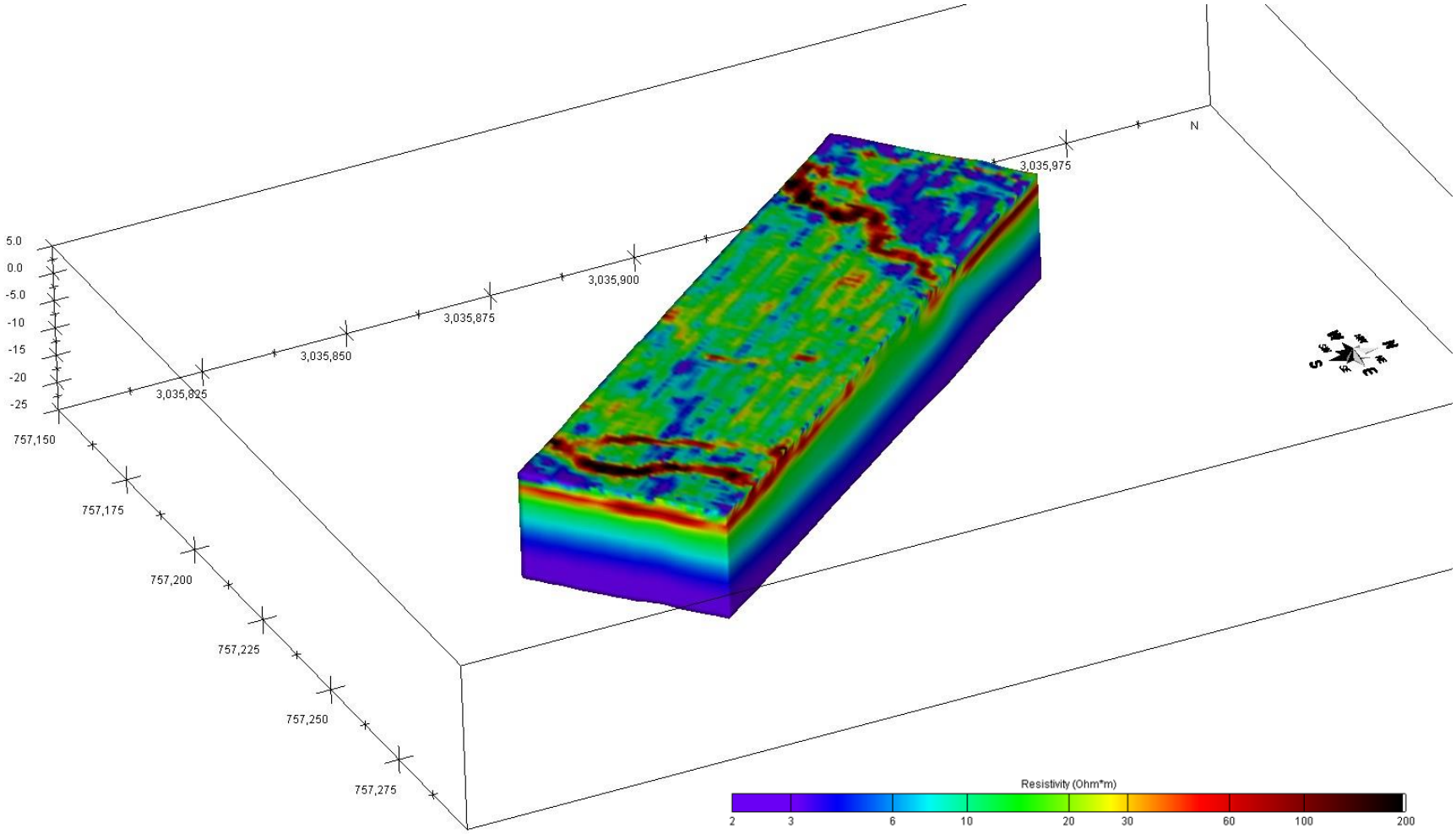


**Figure A16: 3D iso-resistivity volume – perspective view showing groundwater table and high resistivity anomalies at shallow depth.**

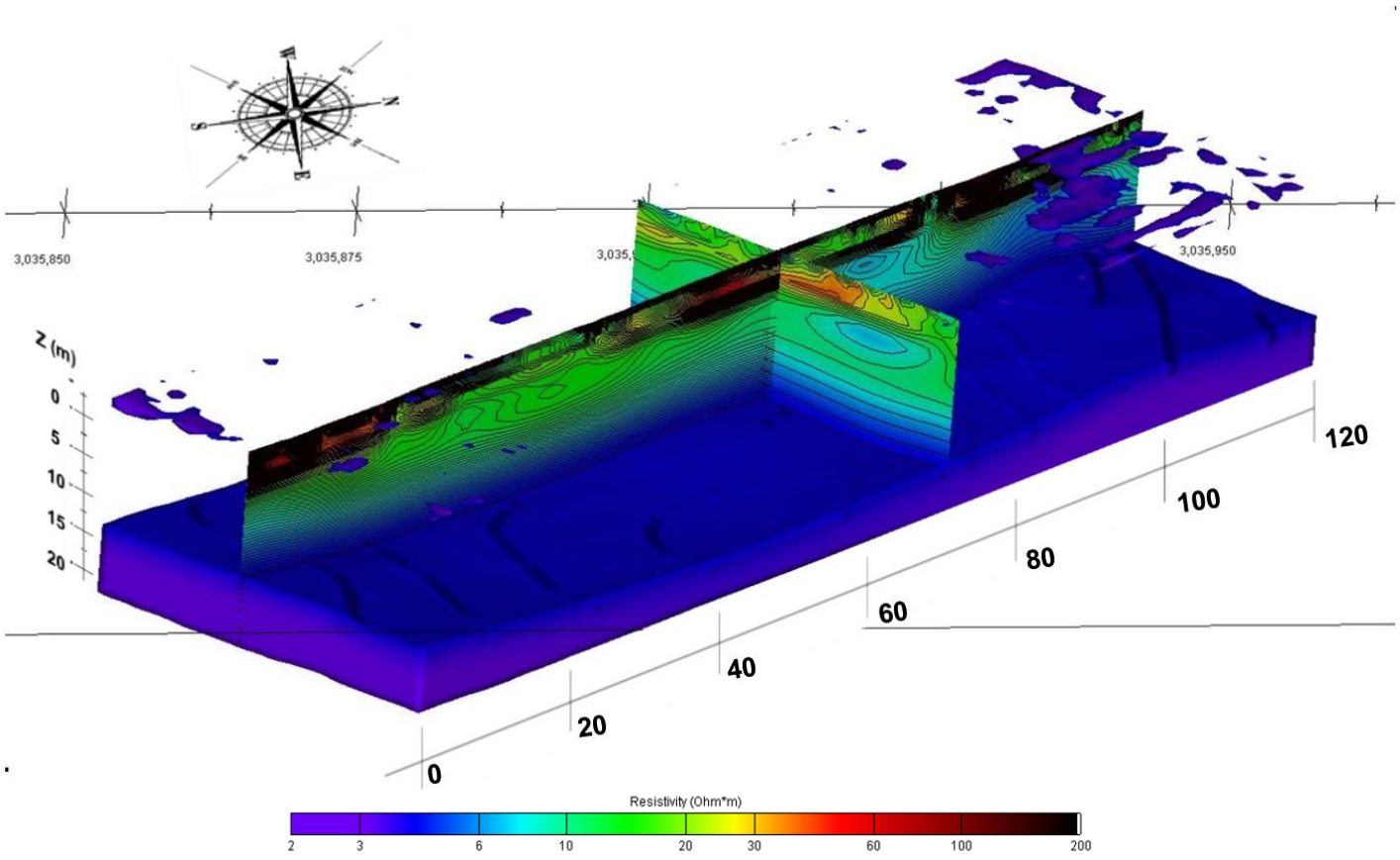


**Figure A17: 3D perspective view - iso-resistivity volume < 3 Ohm.m showing groundwater table.**

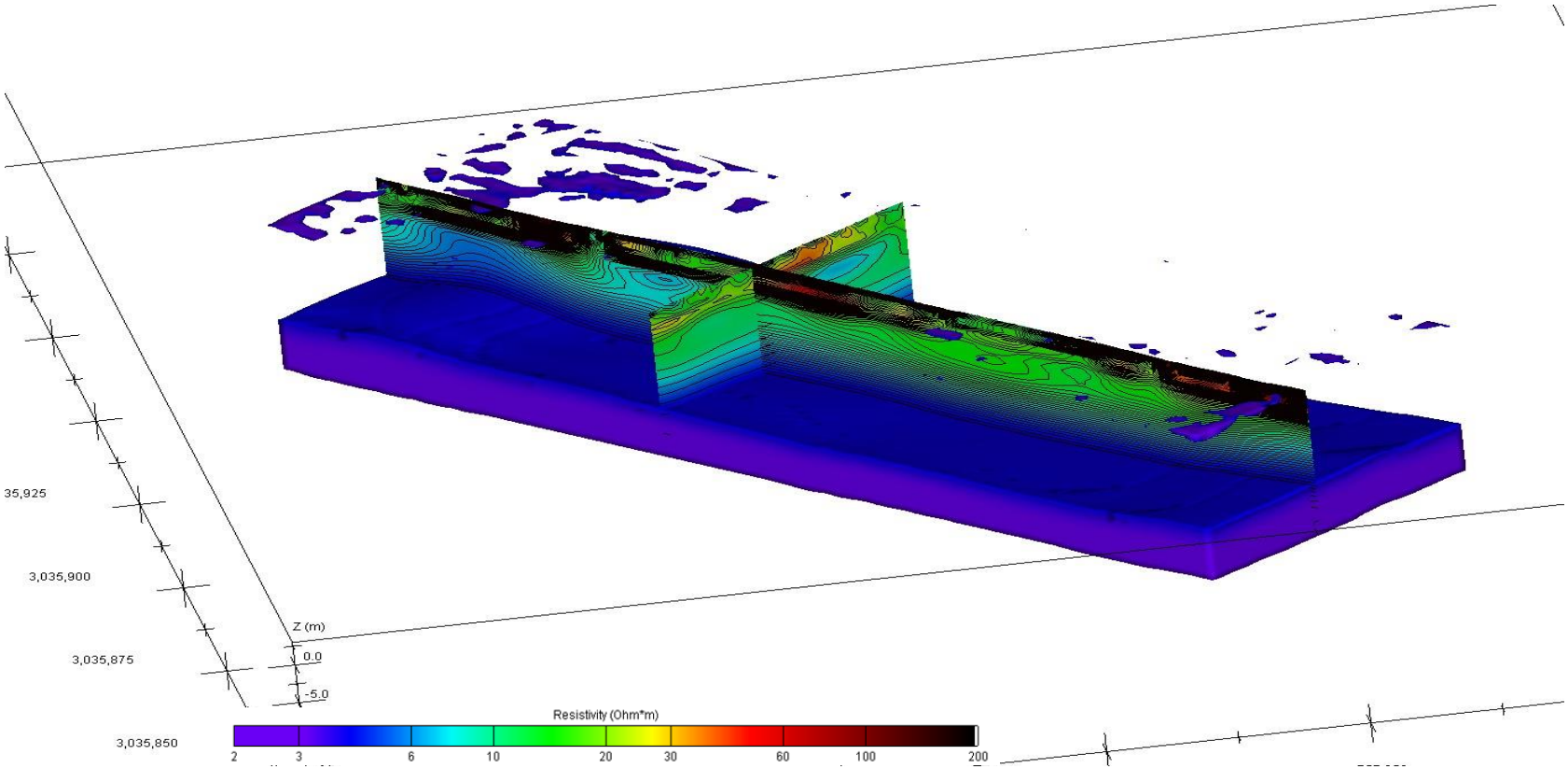


**Figure A18: 3D perspective view - iso-resistivity volume < 3 Ohm.m showing groundwater table.**

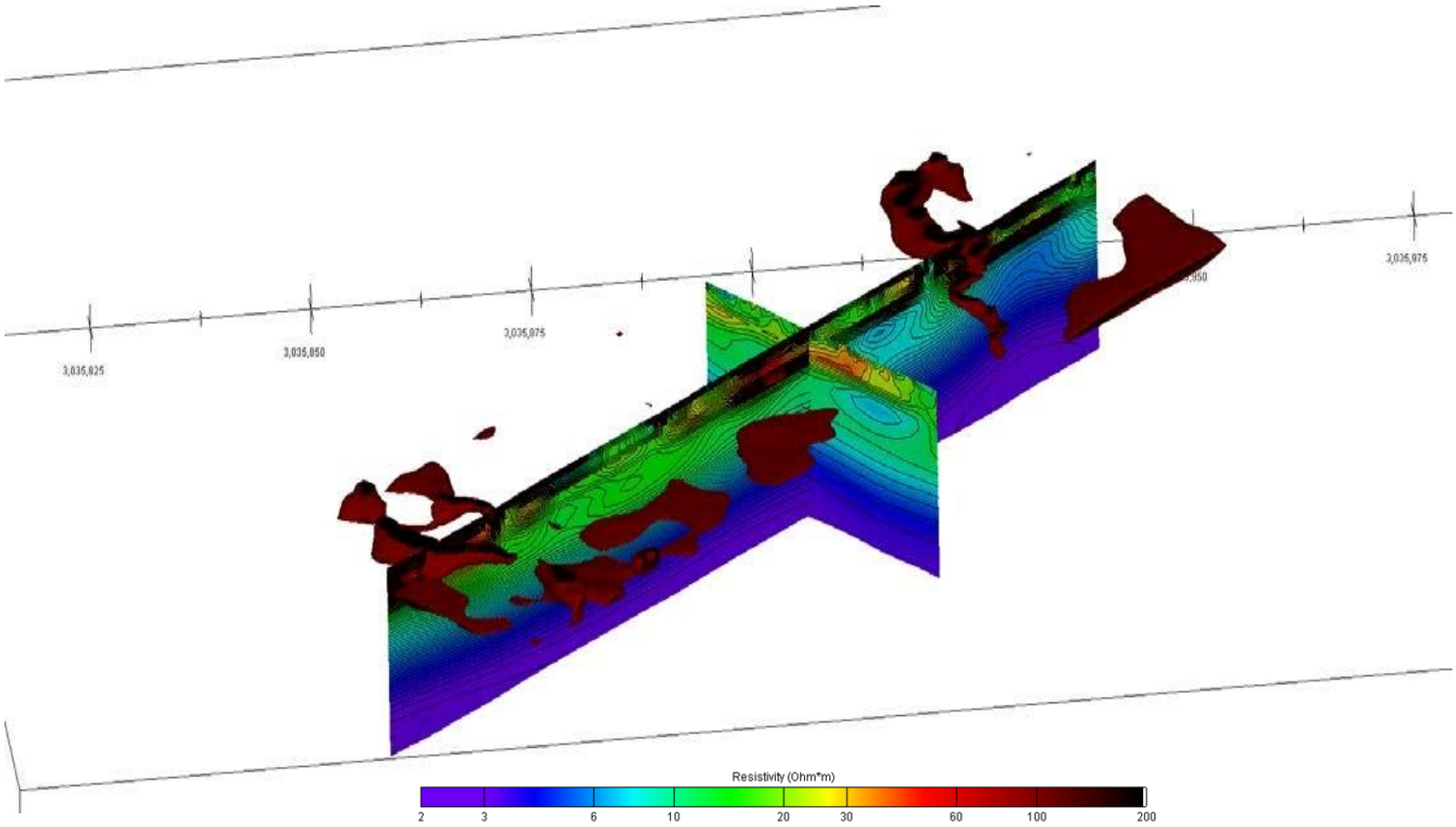


**Figure A19: 3D perspective view - iso-resistivity volume > 70 Ohm.m shallow resistivity anomalies**

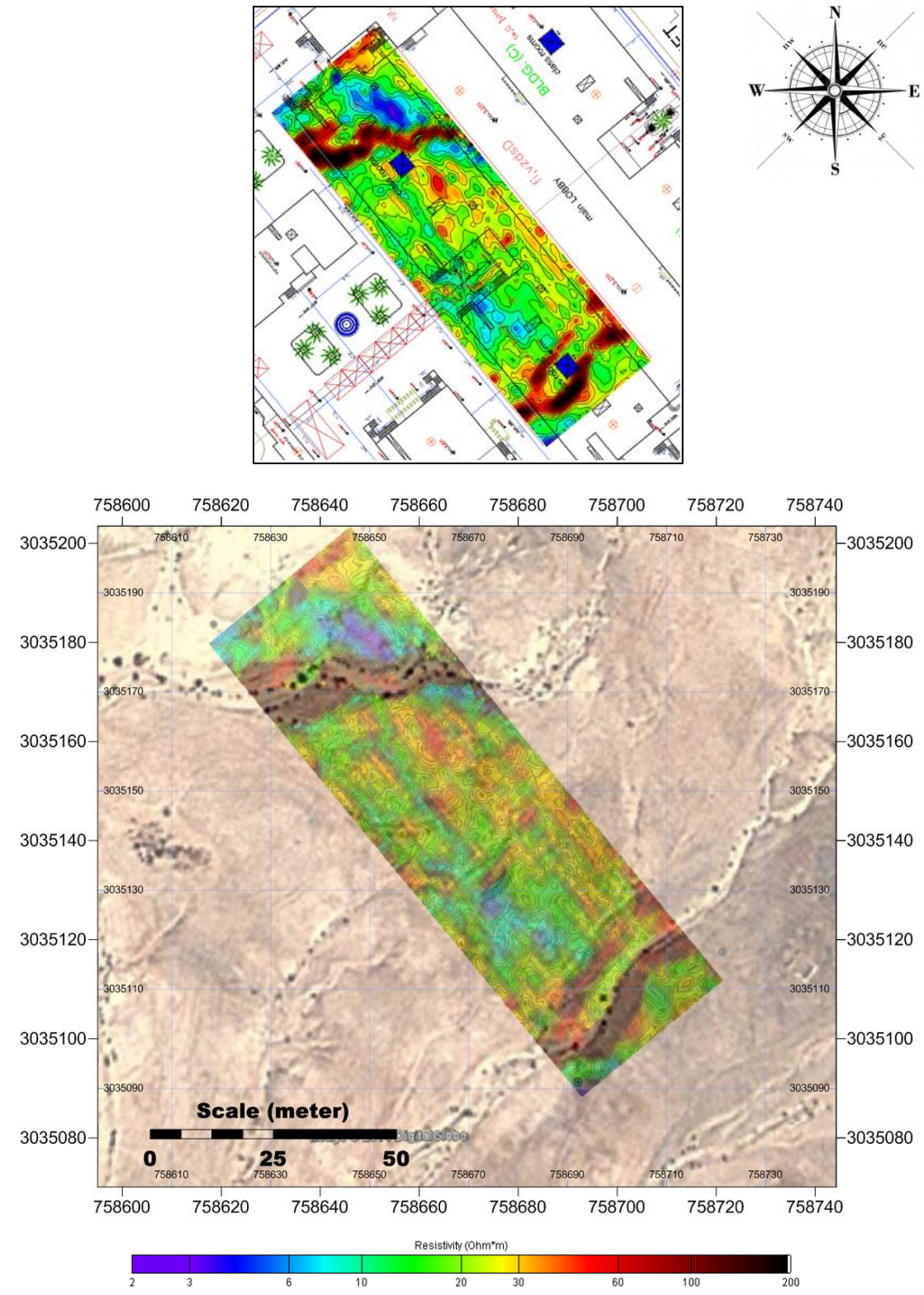


**Figure A20: Overlap of the XY resistivity depth-slice (z = 1 m). The arrows indicate shallow ground features that could be related to the presence of wadi beds (dry river beds).**

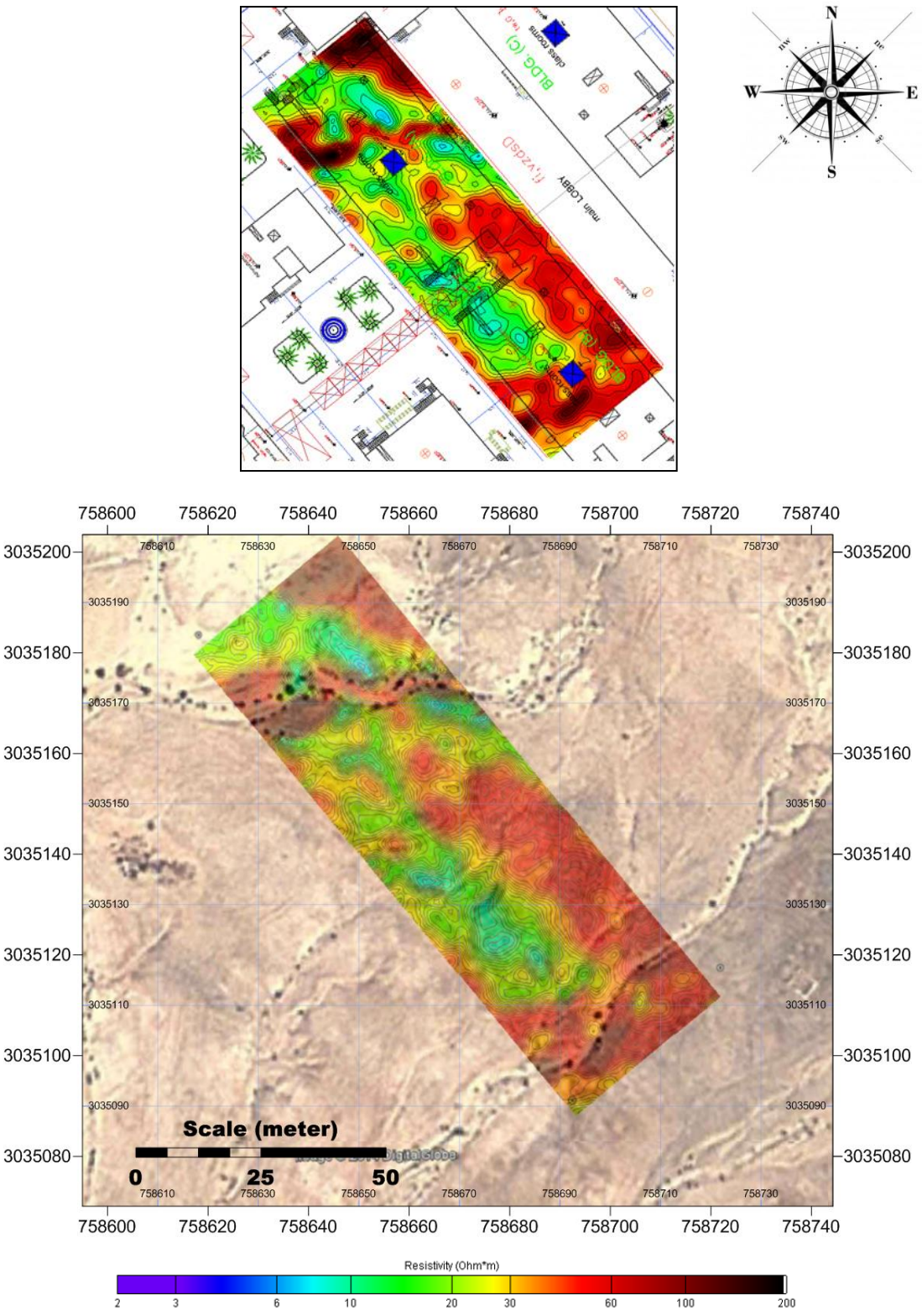


**Figure A21: Overlap of the XY resistivity depth-slice (z = 2 m). The arrows indicate shallow ground features that could be related to the presence of wadi beds (dry river beds).**

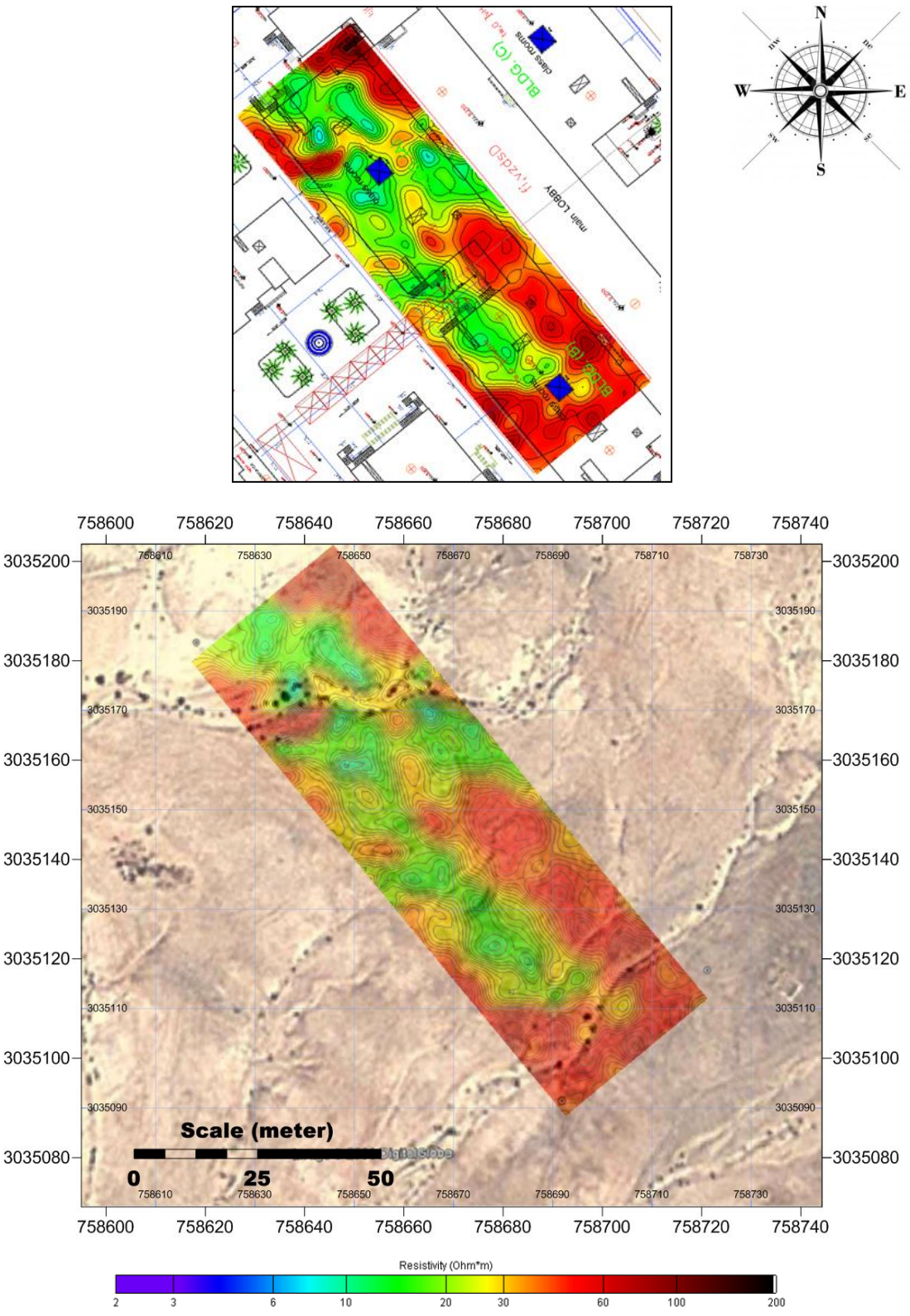


**Figure A22: Overlap of the XY resistivity depth-slice (z = 3 m). The arrows indicate shallow ground features that could be related to the presence of wadi beds (dry river beds).**

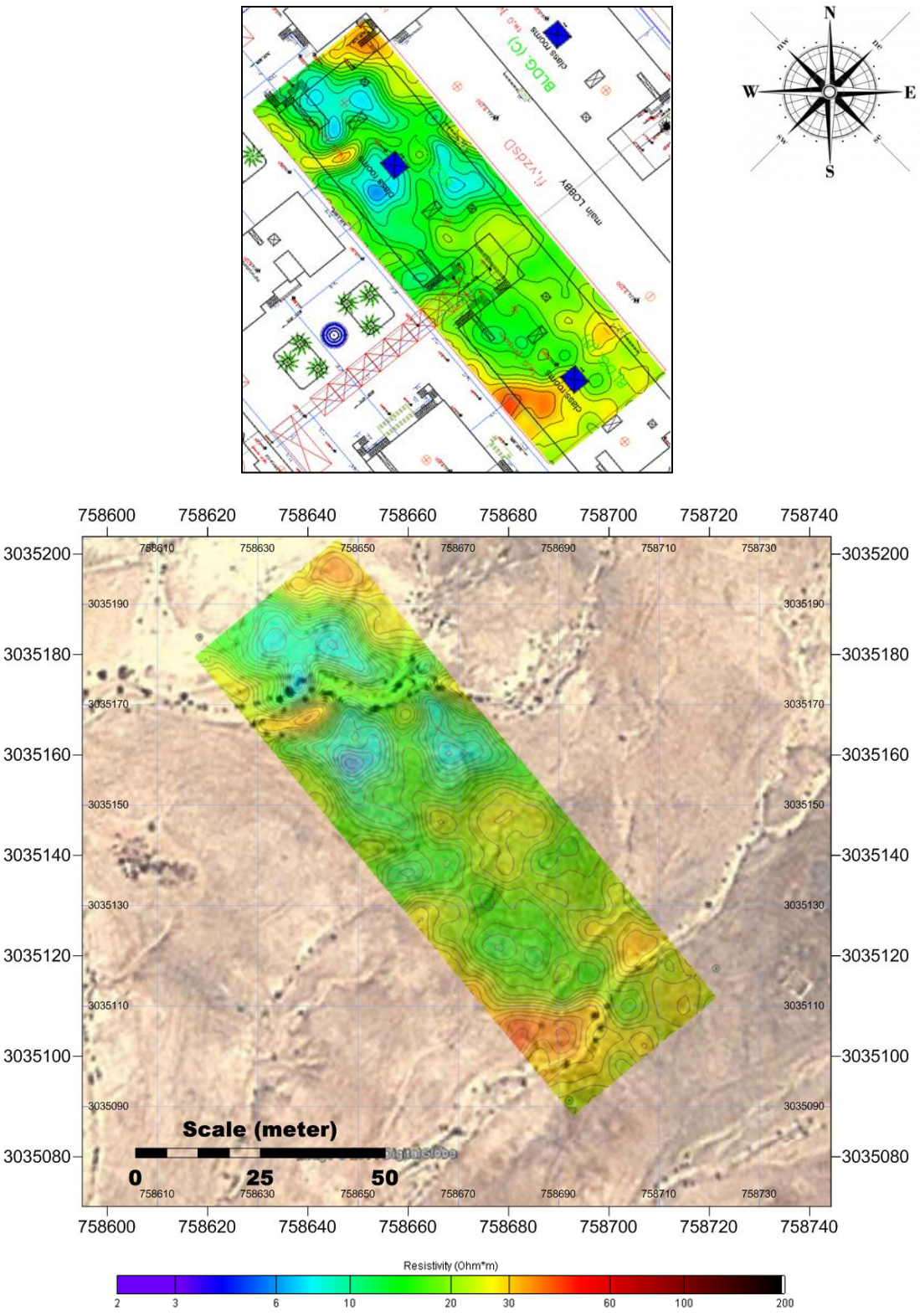


**Figure A23: Overlap of the XY resistivity depth-slice (z = 4m).**

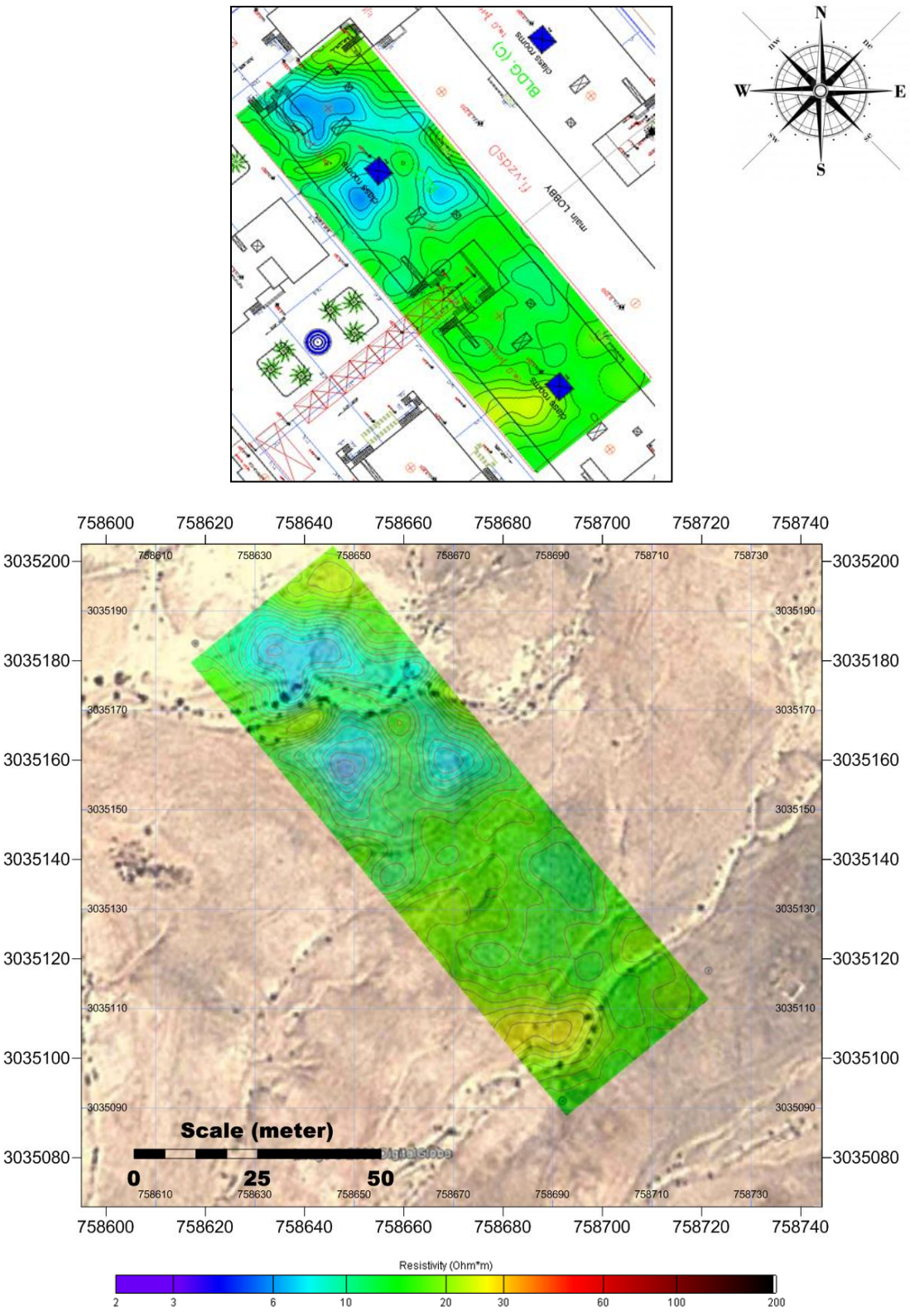


**Figure A24: Overlap of the XY resistivity depth-slice (z = 5m).**

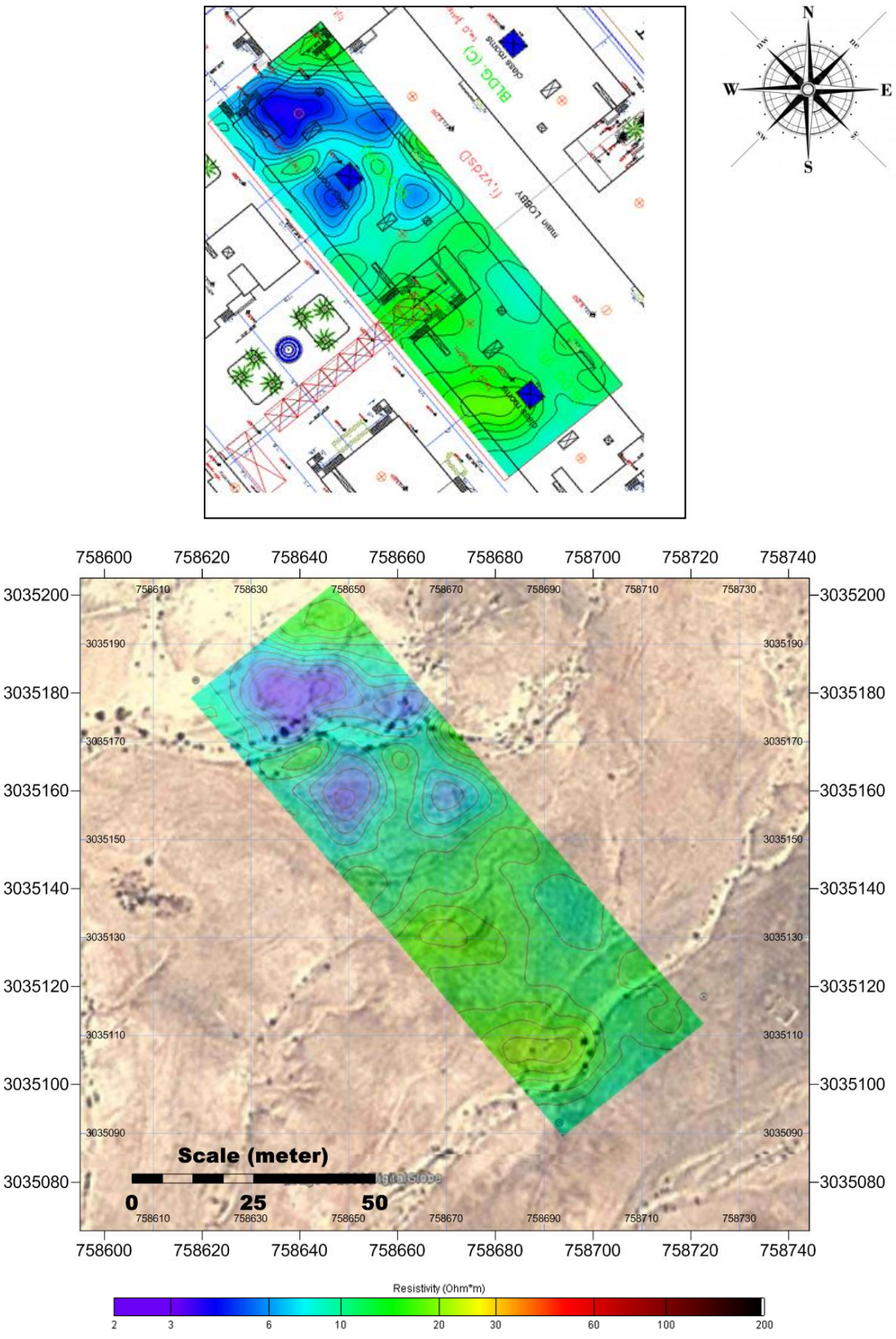


**Figure A25: Overlap of the XY resistivity depth-slice (z = 6 m).**

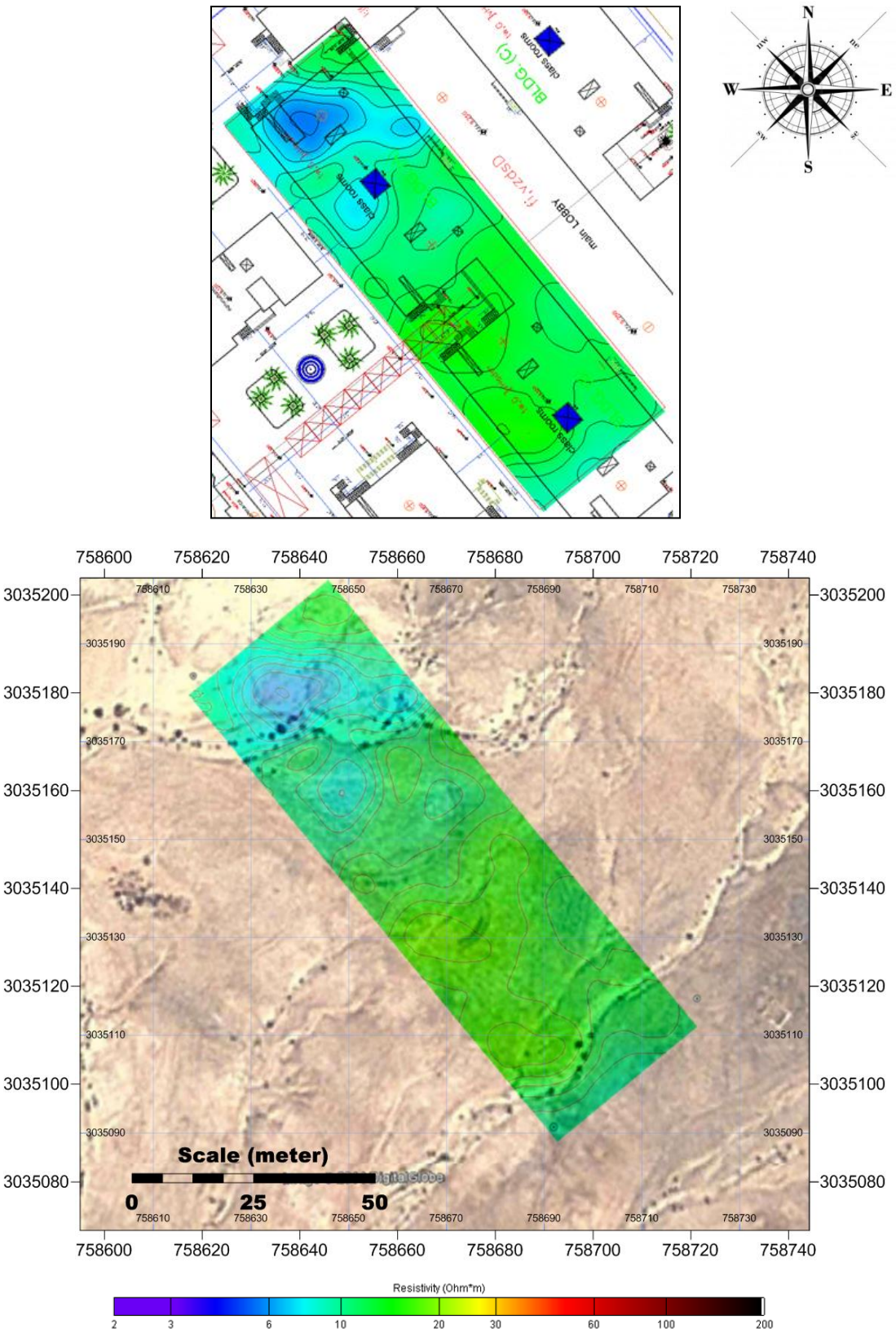


**Figure A26: Overlap of the XY resistivity depth-slice (z = 7 m).**

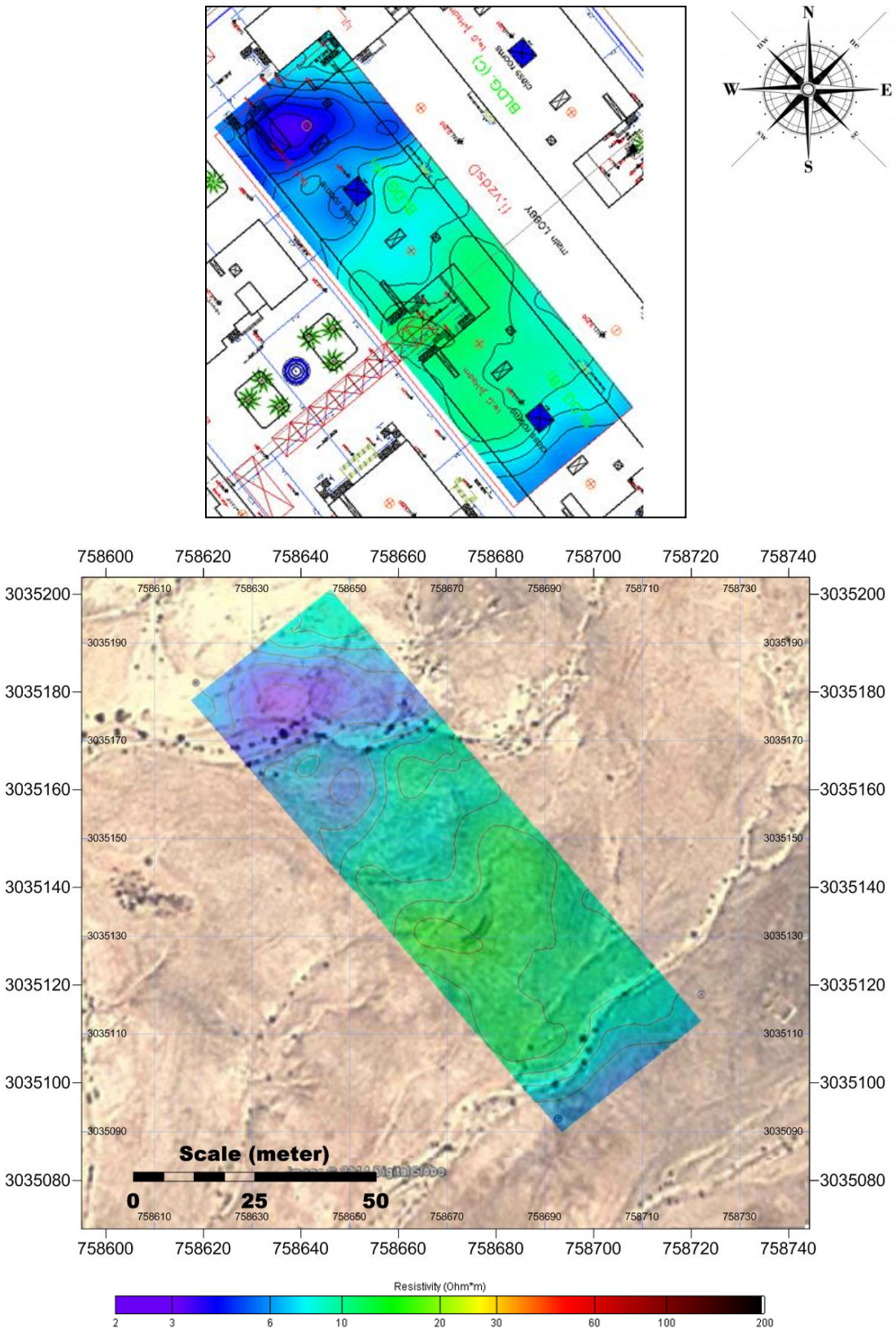


**Figure A27: Overlap of the XY resistivity depth-slice (z = 8 m).**

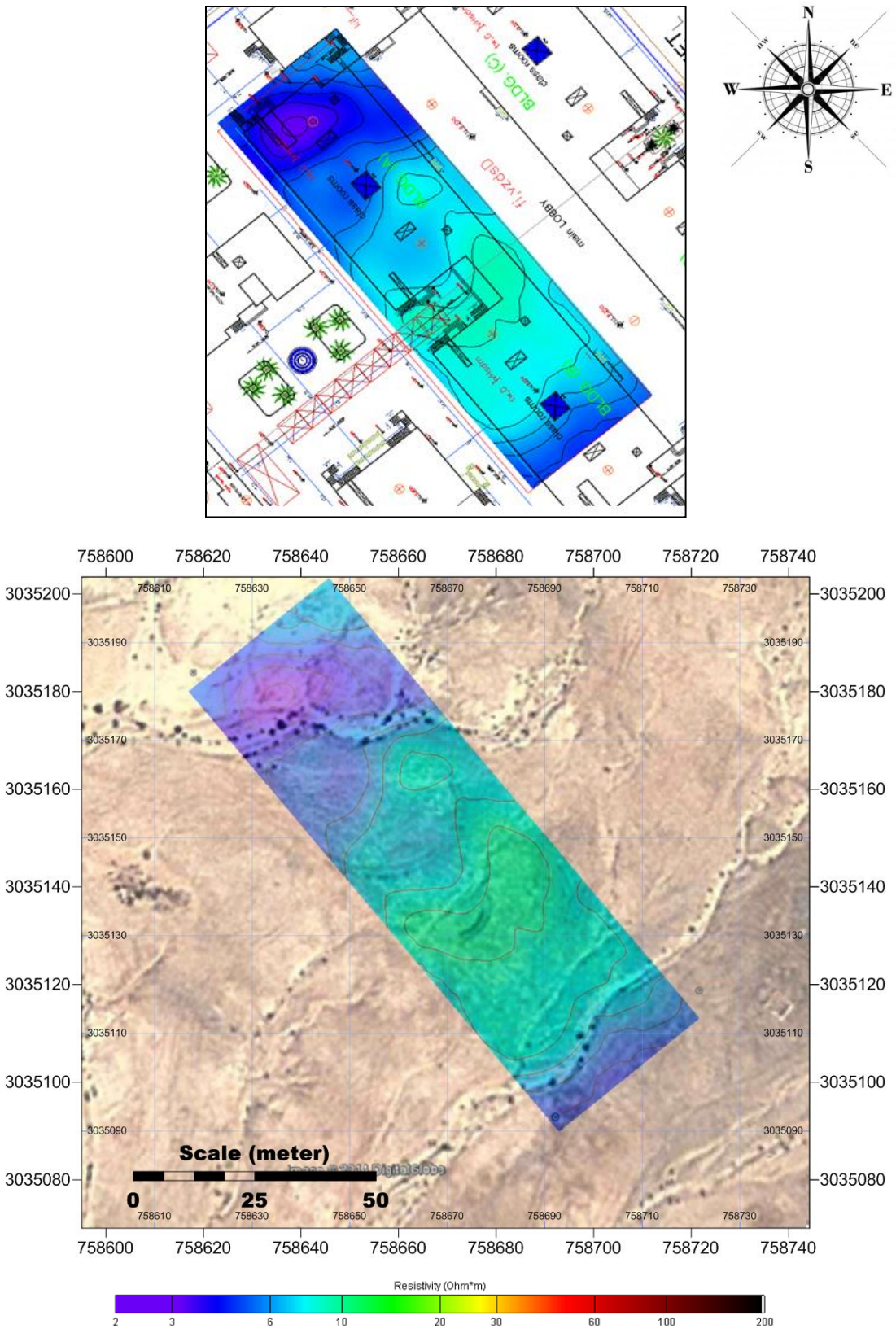


**Figure A28: Overlap of the XY resistivity depth-slice (z = 9 m).**

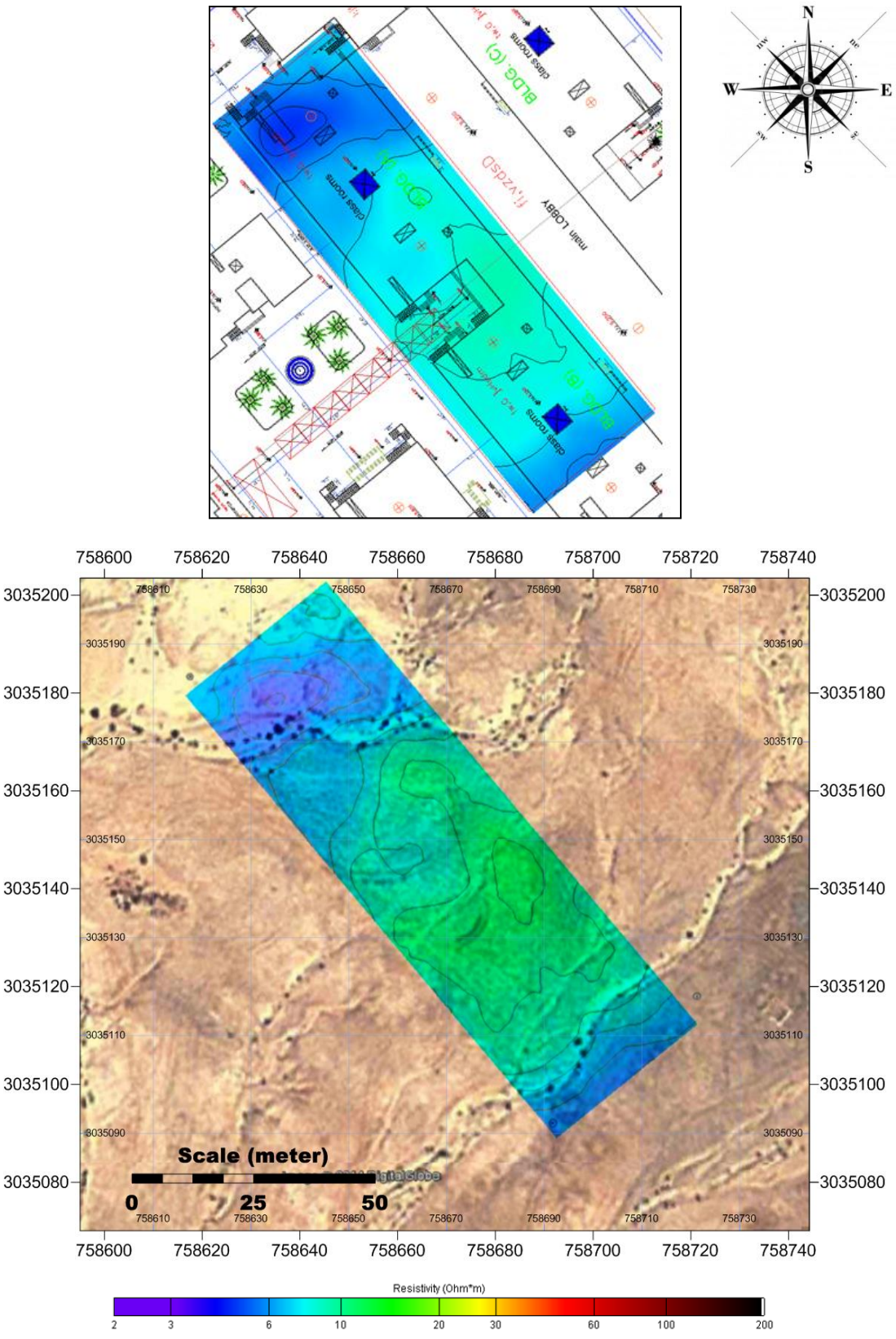


**Figure A29: Overlap of the XY resistivity depth-slice (z = 10 m).**

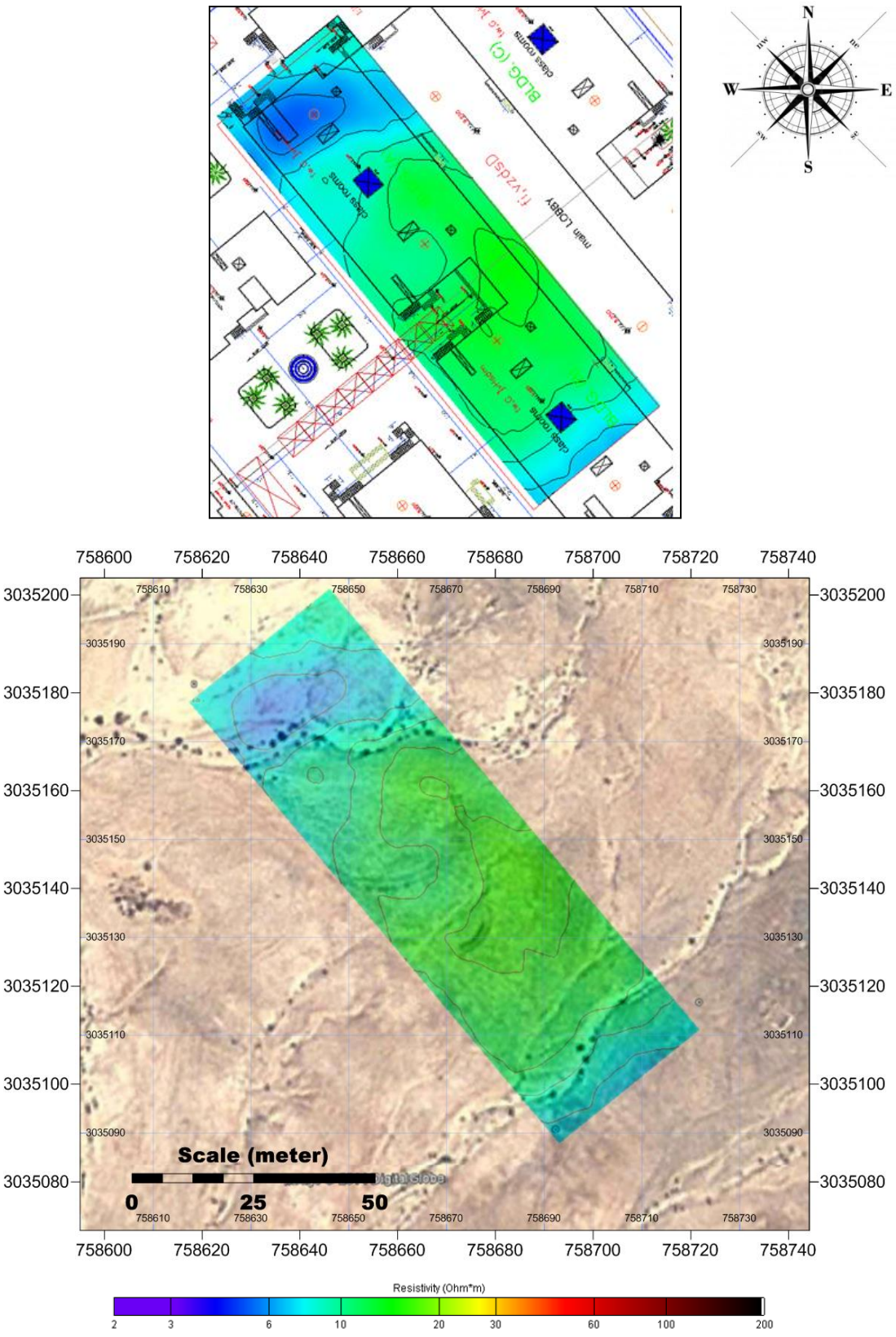


**Figure A30: Overlap of the XY resistivity depth-slice (z = 11 m).**

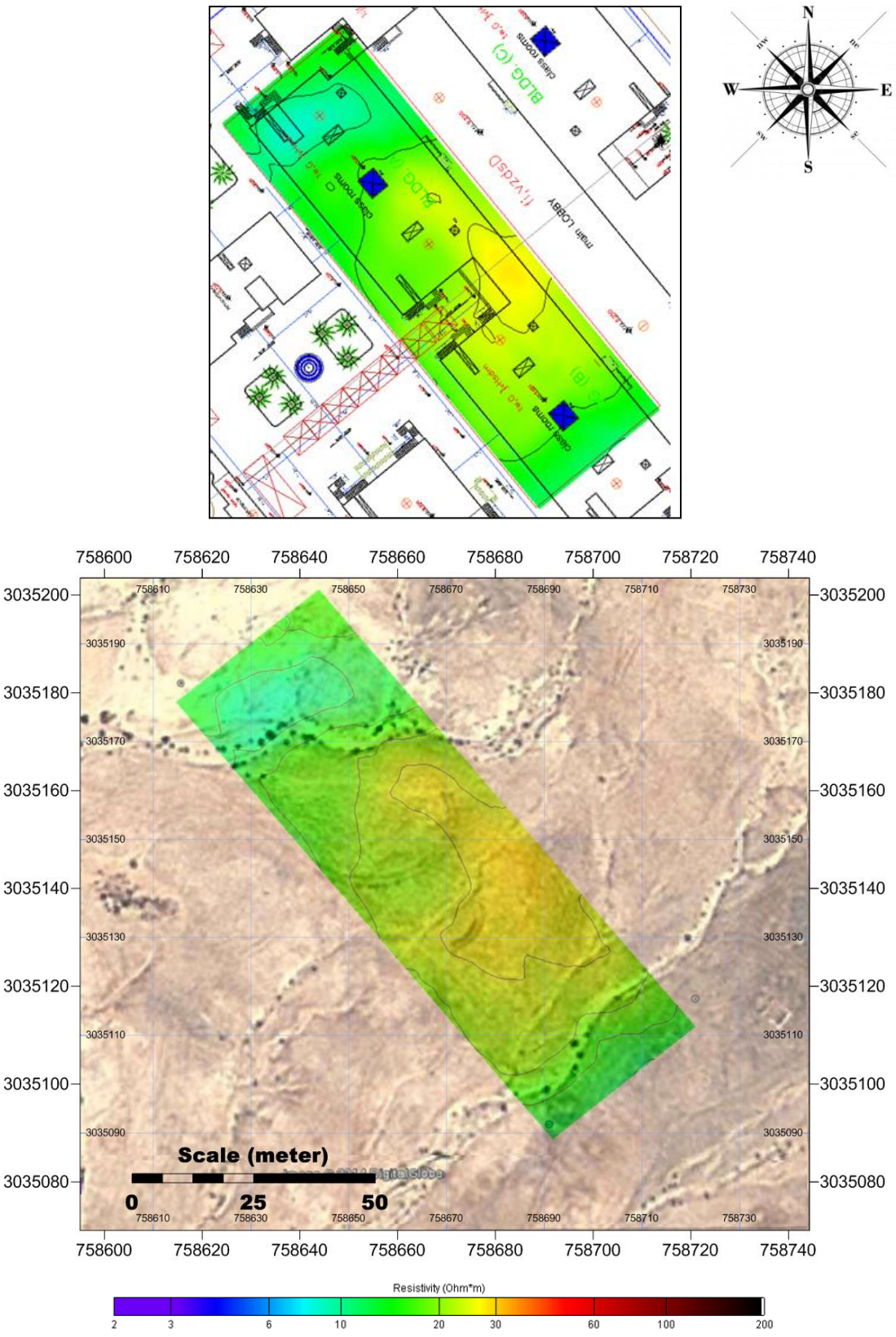


**Figure A31: Overlap of the XY resistivity depth-slice (z = 12 m).**

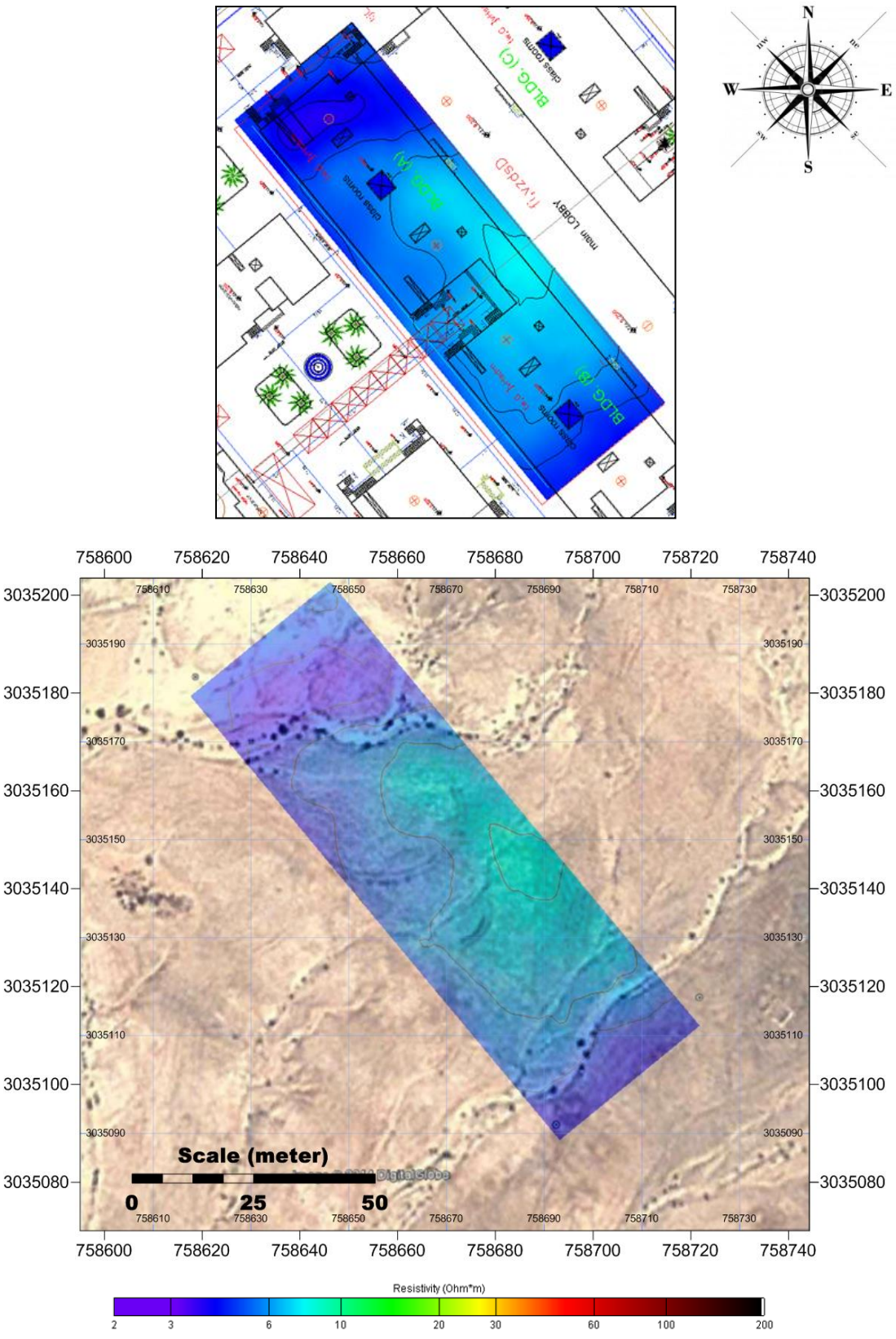


**Figure A32: Overlap of the XY resistivity depth-slice (z = 13 m).**

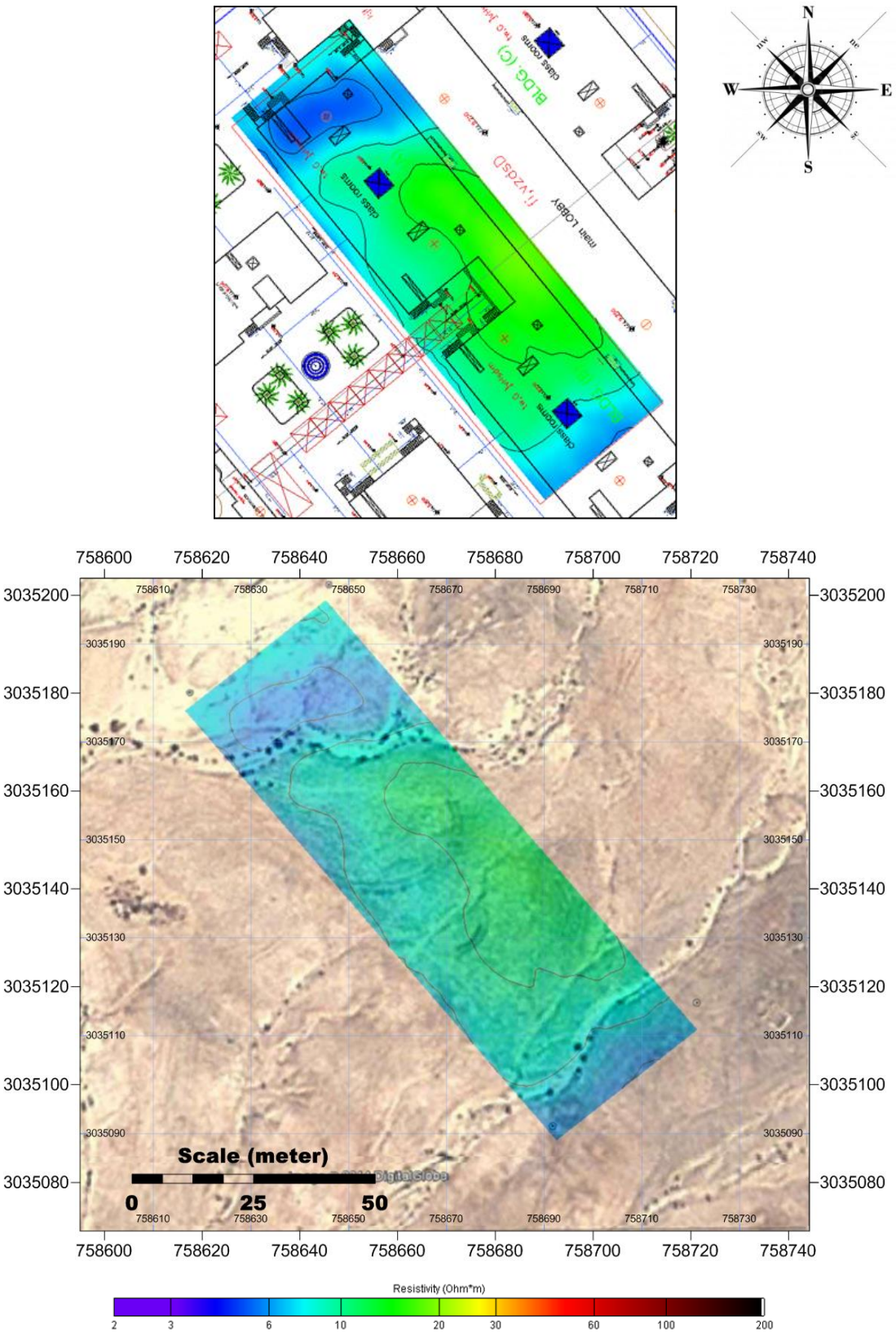


**Figure A33: Overlap of the XY resistivity depth-slice (z = 14 m).**

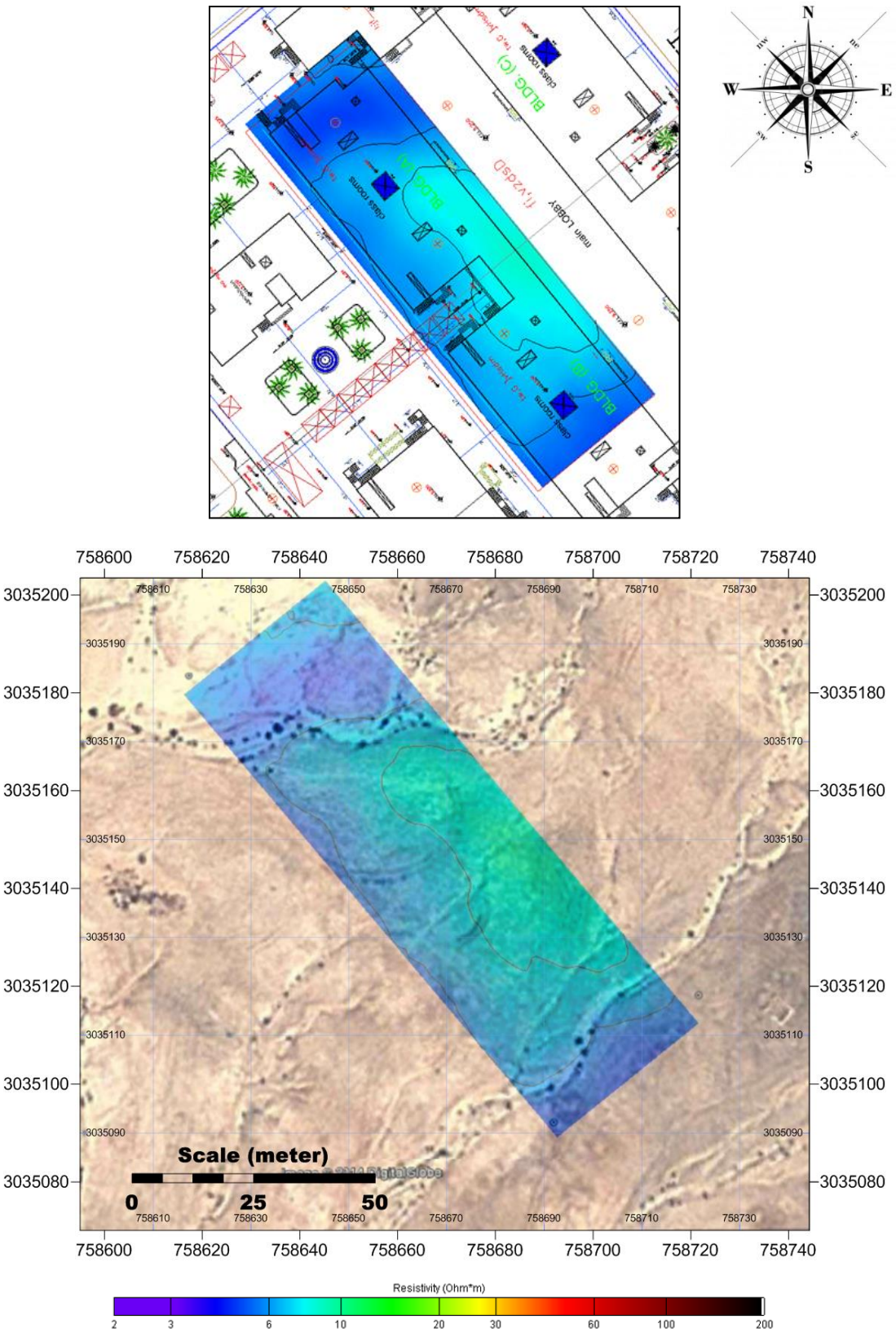


**Figure A34: Overlap of the XY resistivity depth-slice (z = 15 m).**

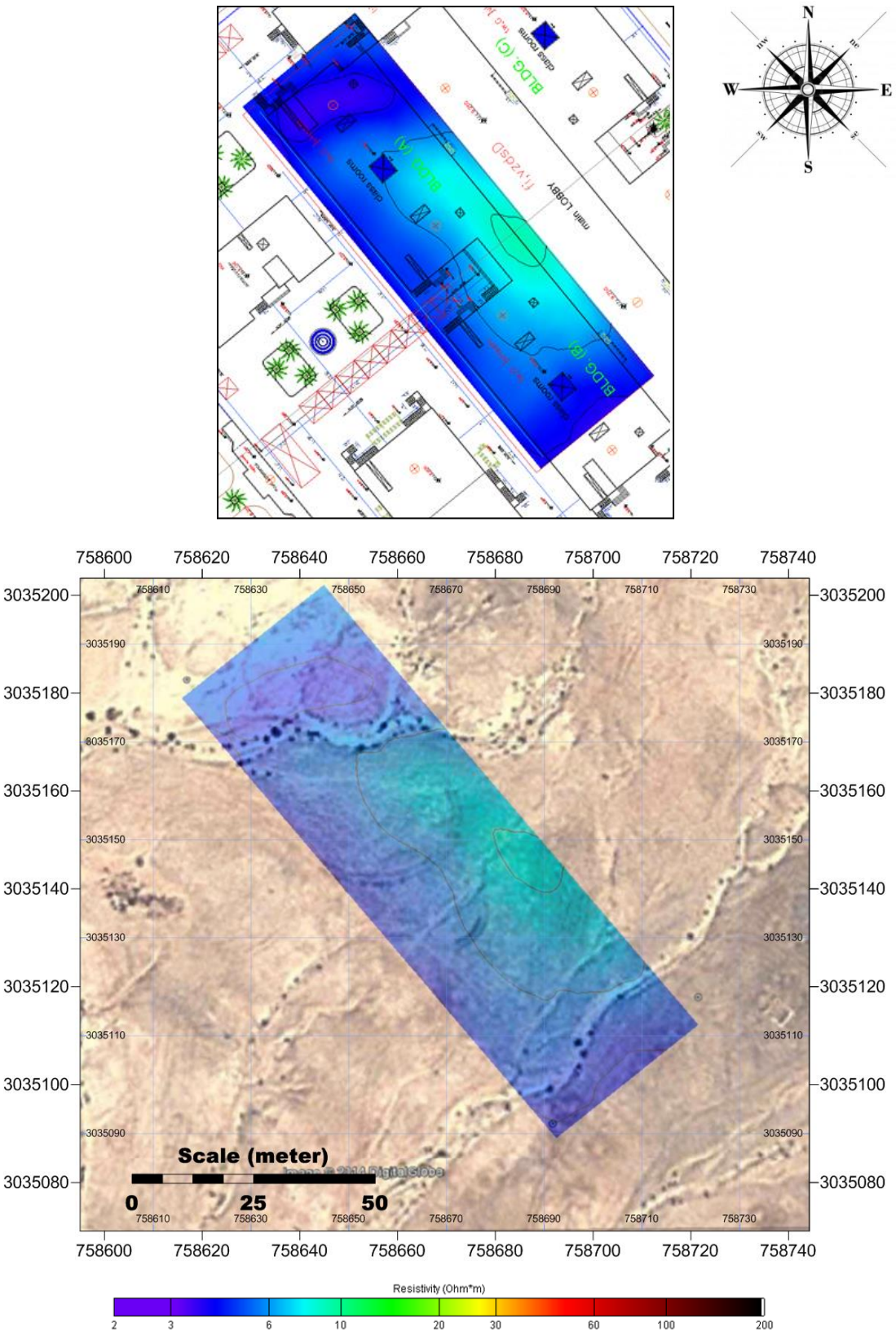


**Figure A35: Overlap of the XY resistivity depth-slice (z = 16 m).**

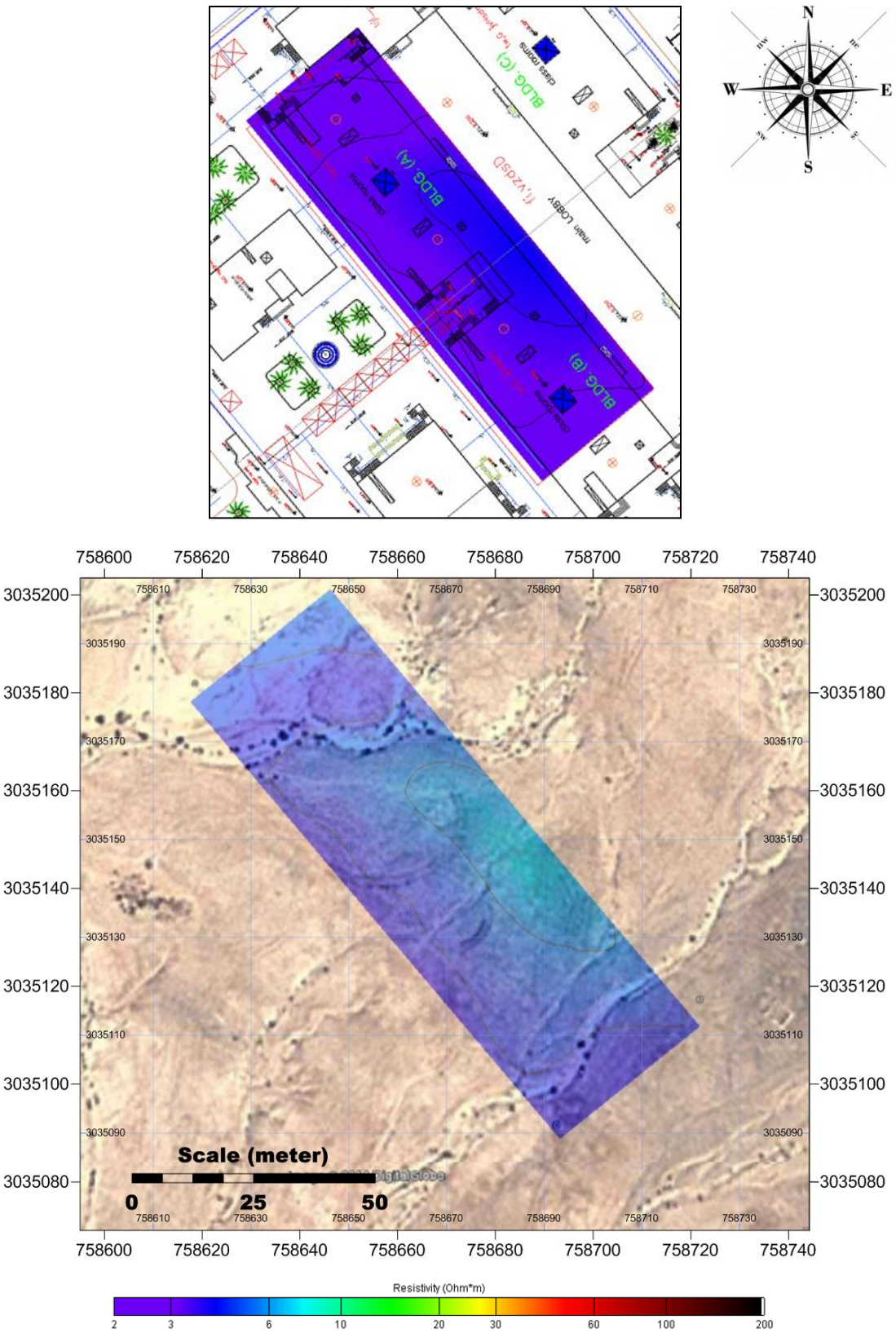


**Figure A36: Overlap of the XY resistivity depth-slice (z = 17 m).**

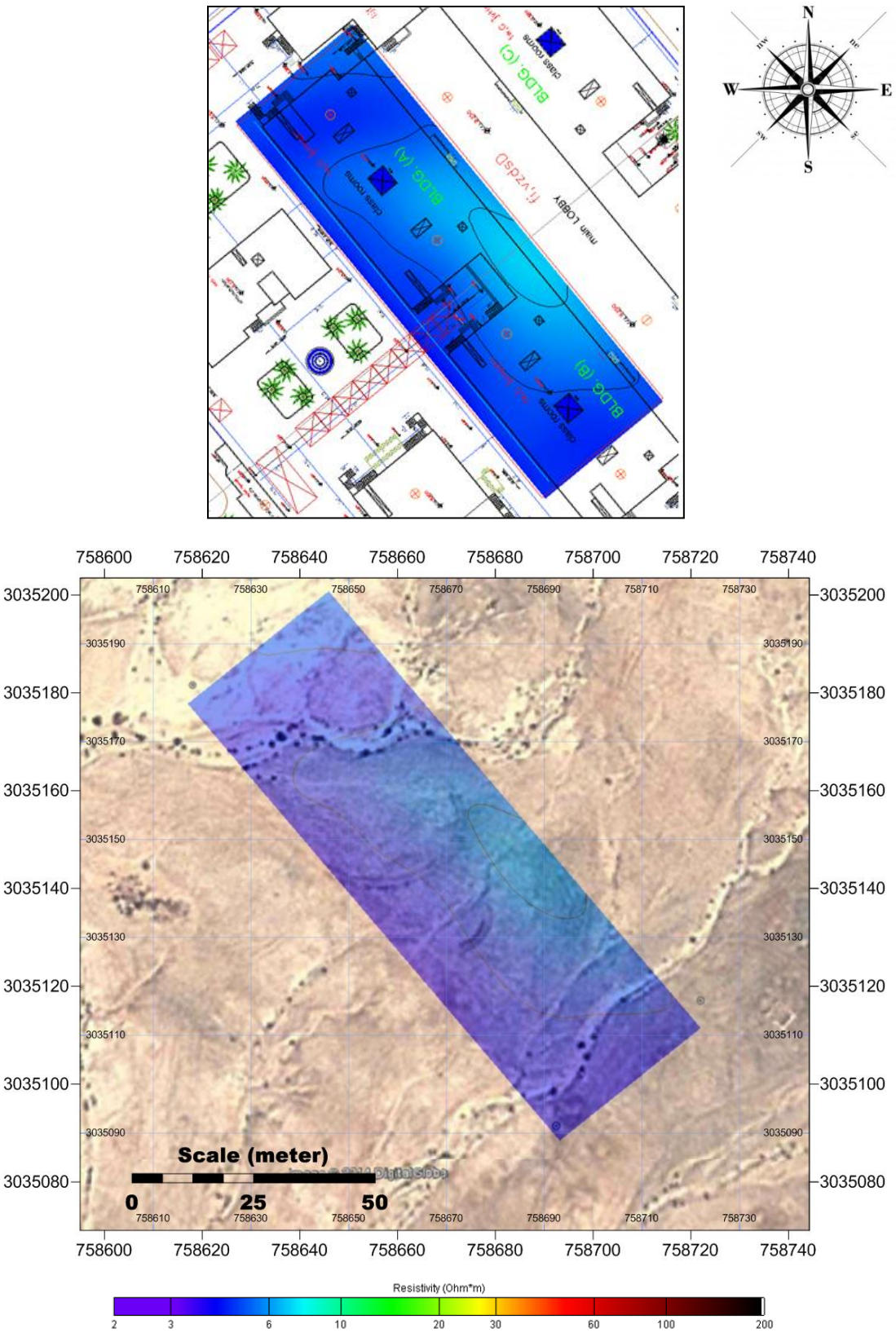


**Figure A37: Overlap of the XY resistivity depth-slice (z = 18 m).**

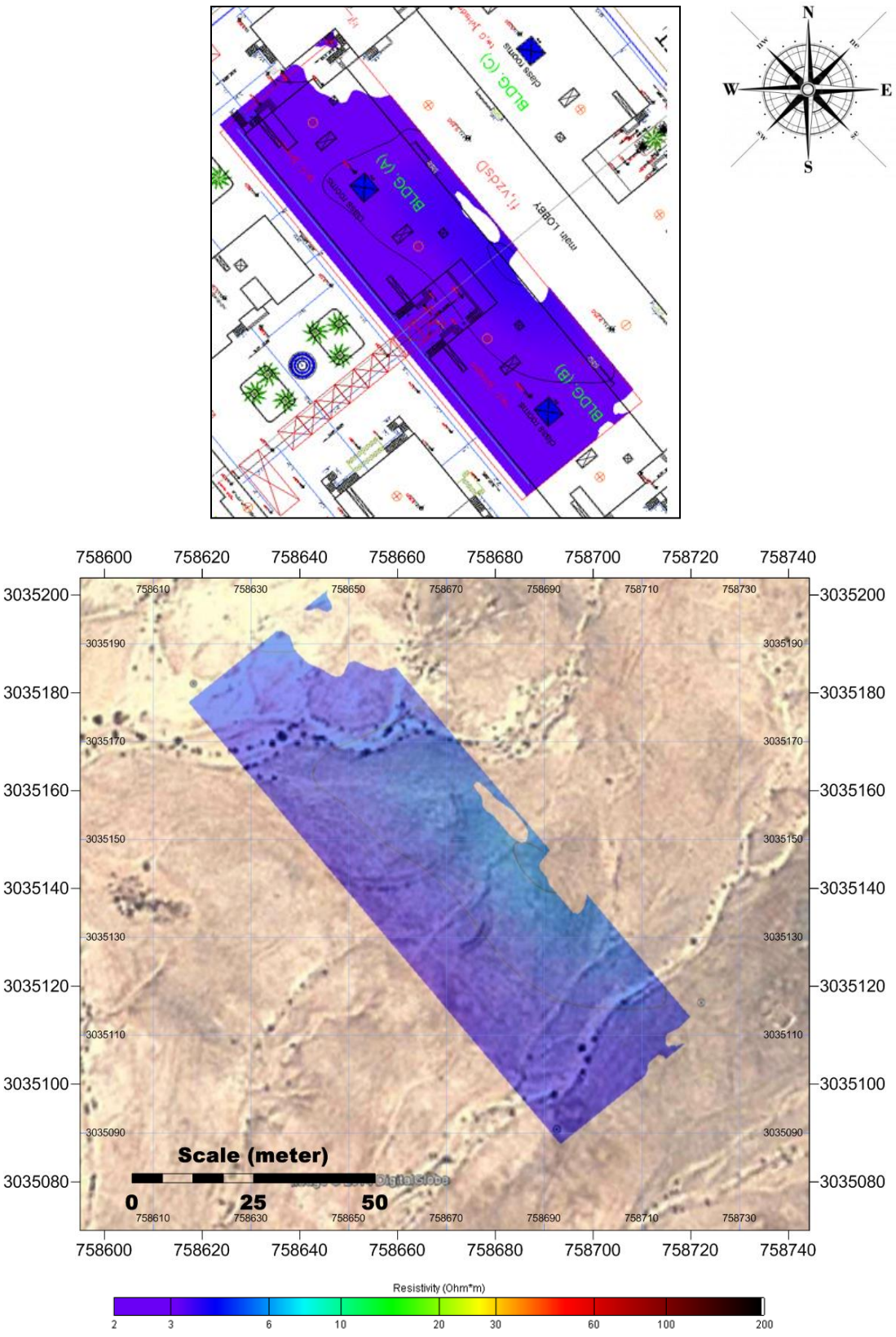


**Figure A38: Overlap of the XY resistivity depth-slice (z = 19 m).**

# APPENDIX B

# BOREHOLE LOGS

# TEST BORING LOG

**BORING NO.: B-14**

**PROJECT** : URGENT BUILDING IN TABUK UNI. IN DUBA.
**CLIENT** : [redacted]
**LOCATION** : DUBA, TABUK AREA, K.S.A.
**PROJECT NO.** : T/SM-2407 **ELEVATION** : 0.0
**G.W.D.** : **NORTH** :
**G.W.L.** : **EAST** :

**DATE STARTED** : 27-01-2014
**DATE FINISHED** : 27-01-2014
**DRILL RIG** : B-53
**DRILLER** : M. R.
**GEOLOGIST** : [redacted]
**TOTAL DEPTH** : 10.0M

| ELEV/ DEPTH | SOIL SYMBOLS, SAMPLERS AND TEST DATA | USCS | Description | SPT (N) | W.C. (%) | L L (%) | P I (%) | REC. (%) | SAMPLE NO. | CURVE (S.P.T.) 20 40 60 80 |
|---|---|---|---|---|---|---|---|---|---|---|
| 0 | 50 / 10 | SM | Silty Sand interbeded with Rock Fragments from Coral Limestone. Brown, very dense, dry. | 100 | 1.2 | 20 | 2 | 69 | B-14-1 BOX-14-1 | |
| -1 | | | Coral Limestone. Yellowish brown to creamy white, fine grained, very highly weathered, very highly fractured. R.Q.D. = 13.0 % | | | | | | | |
| -2 | | | R.Q.D. = 16.0 % | | | | | 70 | BOX-14-2 | |
| -3 | | | R.Q.D. = 14.0 % | | | | | 73 | BOX-14-3 | |
| -4 | | | R.Q.D. = 0.0 % | | | | | 52 | BOX-14-4 | |
| -5 | | | R.Q.D. = 7.0 % | | | | | 58 | BOX-14-5 | |
| -6 | | | R.Q.D. = 7.0 % | | | | | 61 | BOX-14-6 | |
| -7 | | | R.Q.D. = 0.0 % | | | | | 60 | BOX-14-7 | |
| -8 | | | | | | | | | | |
| -9 | | | | | | | | | | |

*Drilling performed by tricon bits.*
*Coring in rock performed by Double tube core barrels.*

Figure [redacted]

# TEST BORING LOG

**BORING NO.: B-15**

| | | | |
|---|---|---|---|
| **PROJECT** | : URGENT BUILDING IN TABUK UNI. IN DUBA. | **DATE STARTED** | : 27-01-2014 |
| **CLIENT** | : [redacted] | **DATE FINISHED** | : 27-01-2014 |
| **LOCATION** | : DUBA, TABUK AREA, K.S.A. | **DRILL RIG** | : B-53 |
| **PROJECT NO.** | : T/SM-2407 **ELEVATION** : 0.0 | **DRILLER** | : M. R. |
| **G.W.D.** | : **NORTH** : | **GEOLOGIST** | : [redacted] |
| **G.W.L.** | : **EAST** : | **TOTAL DEPTH** | : 15.0M |

| ELEV/ DEPTH | SOIL SYMBOLS, SAMPLERS AND TEST DATA | USCS | Description | SPT (N) | W.C. (%) | L L (%) | P I (%) | REC. (%) | SAMPLE NO. | CURVE (S.P.T.) 20 40 60 80 |
|---|---|---|---|---|---|---|---|---|---|---|
| 0 | 50 / 10 | SM | Silty Sand interbeded with Rock Fragments from Coral Limestone. Brown, very dense, dry. | 100 | 1.4 | 19 | 2 | 67 | B-15-1 BOX-15-1 | |
| -1 | | | Coral Limestone. Yellowish brown to creamy white, fine grained, very highly to highly weathered, very highly to highly fractured. R.Q.D. = 12.0 % | | | | | | | |
| -2 | | | R.Q.D. = 0.0 % | | | | | 53 | BOX-15-2 | |
| -3 | | | R.Q.D. = 0.0 % | | | | | 55 | BOX-15-3 | |
| -4 | | | | | | | | | | |
| -5 | | | R.Q.D. = 7.0 % | | | | | 58 | BOX-15-4 | |
| -6 | | | R.Q.D. = 0.0 % | | | | | 56 | BOX-15-5 | |
| -7 | | | | | | | | | | |
| -8 | | | R.Q.D. = 8.0 % | | | | | 64 | BOX-15-6 | |
| -9 | | | R.Q.D. = 7.0 % | | | | | 62 | BOX-15-7 | |

*Drilling performed by tricon bits.*
*Coring in rock performed by Double tube core barrels.*

Figure [redacted]

# TEST BORING LOG

**BORING NO.: B-15**

| | | | |
|---|---|---|---|
| **PROJECT** | : URGENT BUILDING IN TABUK UNI. IN DUBA. | **DATE STARTED** | : 27-01-2014 |
| **CLIENT** | : [redacted] | **DATE FINISHED** | : 27-01-2014 |
| **LOCATION** | : DUBA, TABUK AREA, K.S.A. | **DRILL RIG** | : B-53 |
| **PROJECT NO.** | : T/SM-2407 **ELEVATION** : 0.0 | **DRILLIER** | : M. R. |
| **G.W.D.** | : **NORTH** : | **GEOLOGIST** | : [redacted] |
| **G.W.L.** | : **EAST** : | **TOTAL DEPTH** | : 15.0M |

| ELEV/ DEPTH | SOIL SYMBOLS, SAMPLERS AND TEST DATA | USCS | Description | SPT (N) | W.C. (%) | L L (%) | P I (%) | REC. (%) | SAMPLE NO. | CURVE (S.P.T.) 20 40 60 80 |
|---|---|---|---|---|---|---|---|---|---|---|
| -10 — 10 | | | R.Q.D. = 8.0 % | | | | | 65 | BOX-15-8 | |
| -11 — 11 | | | | | | | | | | |
| -12 — 12 | | | R.Q.D. = 9.0 % | | | | | 68 | BOX-15-9 | |
| -13 — 13 | | | | | | | | | | |
| -14 — 14 | | | R.Q.D. = 7.0 % | | | | | 66 | BOX-15-10 | |
| -15 — 15 | | | END OF BORING. | | | | | | | |
| -16 — 16 | | | | | | | | | | |
| -17 — 17 | | | | | | | | | | |
| -18 — 18 | | | | | | | | | | |
| -19 — 19 | | | | | | | | | | |

Figure [redacted]

# TEST BORING LOG

**BORING NO.: B-16**

**PROJECT** : URGENT BUILDING IN TABUK UNI. IN DUBA.
**CLIENT** : [redacted]
**LOCATION** : DUBA, TABUK AREA, K.S.A.
**PROJECT NO.** : T/SM-2407 **ELEVATION** : 0.0
**G.W.D.** : **NORTH** :
**G.W.L.** : **EAST** :

**DATE STARTED** : 27-01-2014
**DATE FINISHED** : 27-01-2014
**DRILL RIG** : B-53
**DRILLER** : M. R.
**GEOLOGIST** : [redacted]
**TOTAL DEPTH** : 10.0M

| ELEV/ DEPTH | SOIL SYMBOLS, SAMPLERS AND TEST DATA | USCS | Description | SPT (N) | W.C. (%) | L L (%) | P I (%) | REC. (%) | SAMPLE NO. | CURVE (S.P.T.) 20 40 60 80 |
|---|---|---|---|---|---|---|---|---|---|---|
| 0 | 36 / 15<br>50 / 5 | SM | Silty Sand interbeded with Rock Fragments from Coral Limestone. Brown, very dense, dry. | 100 | 1.0 | 17 | 1 | | B-16-1 | |
| | | | Coral Limestone. Yellowish brown to creamy white, fine grained, very highly to highly weathered, very highly to highly fractured. R.Q.D. = 12.0 % | | | | | 69 | BOX-16-1 | |
| -1 | | | R.Q.D. = 14.0 % | | | | | 72 | BOX-16-2 | |
| -2 | | | | | | | | | | |
| -3 | | | R.Q.D. = 19.0 % | | | | | 75 | BOX-16-3 | |
| -4 | | | | | | | | | | |
| -5 | | | R.Q.D. = 22.0 % | | | | | 79 | BOX-16-4 | |
| -6 | | | R.Q.D. = 27.0 % | | | | | 82 | BOX-16-5 | |
| -7 | | | | | | | | | | |
| -8 | | | R.Q.D. = 30 % | | | | | 86 | BOX-16-6 | |
| -9 | | | R.Q.D. = 31.0 % | | | | | 87 | BOX-16-7 | |

*Drilling performed by tricon bits.*
*Coring in rock performed by Double tube core barrels.*

Figure [redacted]

# TEST BORING LOG

**BORING NO.: B-17**

**PROJECT** : URGENT BUILDING IN TABUK UNI. IN DUBA.
**CLIENT** : [redacted]
**LOCATION** : DUBA, TABUK AREA, K.S.A.
**PROJECT NO.** : T/SM-2407 **ELEVATION** : 0.0
**G.W.D.** : **NORTH** :
**G.W.L.** : **EAST** :

**DATE STARTED** : 28-01-2014
**DATE FINISHED** : 28-01-2014
**DRILL RIG** : B-53
**DRILLER** : M. R.
**GEOLOGIST** : [redacted]
**TOTAL DEPTH** : 15.0M

| ELEV/ DEPTH | SOIL SYMBOLS, SAMPLERS AND TEST DATA | USCS | Description | SPT (N) | W.C. (%) | L L (%) | P I (%) | REC. (%) | SAMPLE NO. | CURVE (S.P.T.) 20 40 60 80 |
|---|---|---|---|---|---|---|---|---|---|---|
| 0 | 26 / 15<br>33 / 15<br>35 / 15 | SM | Silty Sand Interbeded with Rock Fragments from Coral Limestone. Brown, very dense, dry. | 68 | 1.2 | | | | B-17-1 | |
| -1 | | | | | | | | | | |
| -2 | 29 / 15<br>35 / 15<br>40 / 15 | | | 75 | 1.3 | 19 | 2 | | B-17-2 | |
| -3 | 30 / 15<br>36 / 15<br>42 / 15 | | | 78 | 1.5 | | | | B-17-3 | |
| -4 | | | Coral Limestone. Yellowish brown to creamy white, fine grained, very highly weathered, very highly fractured. R.Q.D. = 0.0 % | | | | | 58 | BOX-17-1 | |
| -5 | | | | | | | | | | |
| -6 | | | R.Q.D. = 0.0 % | | | | | 60 | BOX-17-2 | |
| -7 | | | R.Q.D. = 8.0 % | | | | | 63 | BOX-17-3 | |
| -8 | | | | | | | | | | |
| -9 | | | R.Q.D. = 9.0 % | | | | | 64 | BOX-17-4 | |

*Drilling performed by tricon bits.*
*Coring in rock performed by Double tube core barrels.*

Figure [redacted]

# TEST BORING LOG

**BORING NO.: B-17**

**PROJECT** : URGENT BUILDING IN TABUK UNI. IN DUBA.
**CLIENT** : [redacted]
**LOCATION** : DUBA, TABUK AREA, K.S.A.
**PROJECT NO.** : T/SM-2407 **ELEVATION** : 0.0
**G.W.D.** : **NORTH** :
**G.W.L.** : **EAST** :

**DATE STARTED** : 28-01-2014
**DATE FINISHED** : 28-01-2014
**DRILL RIG** : B-53
**DRILLIER** : M. R.
**GEOLOGIST** : [redacted]
**TOTAL DEPTH** : 15.0M

| ELEV/ DEPTH | SOIL SYMBOLS, SAMPLERS AND TEST DATA | USCS | Description | SPT (N) | W.C. (%) | L L (%) | P I (%) | REC. (%) | SAMPLE NO. | CURVE (S.P.T.) 20 40 60 80 |
|---|---|---|---|---|---|---|---|---|---|---|
| -10 — 10 | | | R.Q.D. = 0.0 % | | | | | 58 | BOX-17-5 | |
| -11 — 11 | | | | | | | | | | |
| -12 — 12 | | | R.Q.D. = 7.0 % | | | | | 61 | BOX-17-6 | |
| -13 — 13 | | | R.Q.D. = 9.0 % | | | | | 65 | BOX-17-7 | |
| -14 — 14 | | | | | | | | | | |
| -15 — 15 | | | R.Q.D. = 0.0 % | | | | | 57 | BOX-17-8 | |
| -16 — 16 | | | END OF BORING. | | | | | | | |
| -17 — 17 | | | | | | | | | | |
| -18 — 18 | | | | | | | | | | |
| -19 — 19 | | | | | | | | | | |

Figure [redacted]

# APPENDIX C

## GPS Data for Survey Lines

GPS receivers were positioned over the established Benchmark and allowed to equilibrate before GPS measurements were collected. Data were gathered at each electrode location for each survey line with an accompanying transmitter.

**GPS data for survey lines**: Each GPS data point corresponds to a specific survey line location (i.e. Line 1) and electrode (i.e. EL-01 is for electrode number one). Table C.1 below provides a summary of all the lines of survey data for which GPS data are listed in the following tables.

**Table C.2: Summary of survey parameters for electrical resistivity data collected at the site.**

| SURVEY INFORMATION | | | | | |
|---|---|---|---|---|---|
| **Line ID** | **Array type** | **No. of Electrodes** | **Spacing (m)** | **Estimated depth of investigation (m)** | **Antecedent Moisture** |
| **2D Survey Lines** | | | | | |
| Line 1 | Wenner-Schlumberger | 72 | 1.6 | 12 | dry |
| | Pole-dipole | 72 | 1.6 | 20 | dry |
| Line 2 | Wenner-Schlumberger | 72 | 1.6 | 12 | dry |
| | Pole-dipole | 72 | 1.6 | 20 | dry |
| Line 3 | Wenner-Schlumberger | 72 | 1.6 | 12 | dry |
| | Pole-dipole | 72 | 1.6 | 20 | dry |

| | | | | | |
|---|---|---|---|---|---|
| Line 4 | Wenner-Schlumberger | 72 | 1.6 | 12 | dry |
| | Pole-dipole | 72 | 1.6 | 20 | dry |
| Line 5 | Wenner-Schlumberger | 72 | 1.6 | 12 | dry |
| | Pole-dipole | 72 | 1.6 | 20 | dry |
| Line 6 | Wenner-Schlumberger | 72 | 1.6 | 12 | dry |
| | Pole-dipole | 72 | 1.6 | 20 | dry |
| Line 7 | Wenner-Schlumberger | 72 | 1.6 | 12 | dry |
| | Pole-dipole | 72 | 1.6 | 20 | dry |
| Line 8 | Wenner-Schlumberger | 72 | 1.6 | 12 | dry |
| | Pole-dipole | 72 | 1.6 | 20 | dry |
| Line 9 | Wenner-Schlumberger | 72 | 1.6 | 12 | dry |
| | Pole-dipole | 72 | 1.6 | 20 | dry |
| Line 10 | Wenner-Schlumberger | 72 | 1.6 | 12 | dry |
| | Pole-dipole | 72 | 1.6 | 20 | dry |
| Line 11 | Wenner-Schlumberger | 72 | 1.6 | 12 | dry |
| | Pole-dipole | 72 | 1.6 | 20 | dry |
| Line 12 | Wenner-Schlumberger | 72 | 1.6 | 12 | dry |
| | Pole-dipole | 72 | 1.6 | 20 | dry |
| **3D Loops** | | | | | |
| Loop-1 | Pole-dipole | 72 | 2.5 | 25 | dry |
| Loop-2 | Pole-dipole | 72 | 2.5 | 25 | dry |

| 2D Survey – LINE 1 | | | |
|---|---|---|---|
| **Electrode ID** | **Easting (m)** | **Northing (m)** | **Elevation** |
| EL-01 | 758689.415 | 3035091.974 | 15.351 |
| EL-02 | 758688.400 | 3035093.210 | 15.320 |
| EL-03 | 758687.384 | 3035094.447 | 15.319 |
| EL-04 | 758686.369 | 3035095.684 | 15.470 |
| EL-05 | 758685.354 | 3035096.920 | 15.484 |
| EL-06 | 758684.339 | 3035098.157 | 15.465 |
| EL-07 | 758683.323 | 3035099.393 | 15.039 |
| EL-08 | 758682.308 | 3035100.630 | 15.019 |
| EL-09 | 758681.293 | 3035101.867 | 15.013 |
| EL-10 | 758680.278 | 3035103.103 | 15.018 |
| EL-11 | 758679.262 | 3035104.340 | 15.010 |
| EL-12 | 758678.247 | 3035105.576 | 15.030 |
| EL-13 | 758677.232 | 3035106.813 | 15.146 |
| EL-14 | 758676.217 | 3035108.050 | 15.133 |
| EL-15 | 758675.201 | 3035109.286 | 15.138 |
| EL-16 | 758674.186 | 3035110.523 | 15.151 |
| EL-17 | 758673.171 | 3035111.760 | 15.205 |
| EL-18 | 758672.156 | 3035112.996 | 15.252 |
| EL-19 | 758671.140 | 3035114.233 | 15.264 |
| EL-20 | 758670.125 | 3035115.469 | 15.157 |
| EL-21 | 758669.110 | 3035116.706 | 15.159 |
| EL-22 | 758668.094 | 3035117.943 | 15.109 |
| EL-23 | 758667.079 | 3035119.179 | 15.125 |
| EL-24 | 758666.064 | 3035120.416 | 15.119 |
| EL-25 | 758665.049 | 3035121.653 | 15.119 |
| EL-26 | 758664.033 | 3035122.889 | 15.137 |
| EL-27 | 758663.018 | 3035124.126 | 15.135 |
| EL-28 | 758662.003 | 3035125.362 | 15.333 |
| EL-29 | 758660.988 | 3035126.599 | 15.410 |
| EL-30 | 758659.972 | 3035127.836 | 15.390 |
| EL-31 | 758658.957 | 3035129.072 | 15.294 |
| EL-32 | 758657.942 | 3035130.309 | 15.209 |
| EL-33 | 758656.927 | 3035131.546 | 15.150 |
| EL-34 | 758655.911 | 3035132.782 | 15.188 |
| EL-35 | 758654.896 | 3035134.019 | 15.284 |
| EL-36 | 758653.881 | 3035135.255 | 15.290 |
| EL-37 | 758652.865 | 3035136.492 | 15.347 |
| EL-38 | 758651.850 | 3035137.729 | 15.397 |

| LINE 1 - Continued | | | |
|---|---|---|---|
| EL-39 | 758650.835 | 3035138.965 | 15.394 |
| EL-40 | 758649.820 | 3035140.202 | 15.298 |
| EL-41 | 758648.804 | 3035141.439 | 15.285 |
| EL-42 | 758647.789 | 3035142.675 | 15.249 |
| EL-43 | 758646.774 | 3035143.912 | 15.196 |
| EL-44 | 758645.759 | 3035145.148 | 15.225 |
| EL-45 | 758644.743 | 3035146.385 | 15.162 |
| EL-46 | 758643.728 | 3035147.622 | 15.149 |
| EL-47 | 758642.713 | 3035148.858 | 15.161 |
| EL-48 | 758641.698 | 3035150.095 | 15.185 |
| EL-49 | 758640.682 | 3035151.332 | 15.175 |
| EL-50 | 758639.667 | 3035152.568 | 15.170 |
| EL-51 | 758638.652 | 3035153.805 | 15.178 |
| EL-52 | 758637.637 | 3035155.041 | 15.128 |
| EL-53 | 758636.621 | 3035156.278 | 15.138 |
| EL-54 | 758635.606 | 3035157.515 | 15.127 |
| EL-55 | 758634.591 | 3035158.751 | 15.115 |
| EL-56 | 758633.575 | 3035159.988 | 15.125 |
| EL-57 | 758632.560 | 3035161.225 | 15.136 |
| EL-58 | 758631.545 | 3035162.461 | 15.202 |
| EL-59 | 758630.530 | 3035163.698 | 15.162 |
| EL-60 | 758629.514 | 3035164.934 | 15.082 |
| EL-61 | 758628.499 | 3035166.171 | 15.123 |
| EL-62 | 758627.484 | 3035167.408 | 15.144 |
| EL-63 | 758626.469 | 3035168.644 | 15.134 |
| EL-64 | 758625.453 | 3035169.881 | 15.127 |
| EL-65 | 758624.438 | 3035171.118 | 15.072 |
| EL-66 | 758623.423 | 3035172.354 | 15.035 |
| EL-67 | 758622.408 | 3035173.591 | 15.051 |
| EL-68 | 758621.392 | 3035174.827 | 15.043 |
| EL-69 | 758620.377 | 3035176.064 | 15.017 |
| EL-70 | 758619.362 | 3035177.301 | 15.019 |
| EL-71 | 758618.347 | 3035178.537 | 15.002 |
| EL-72 | 758617.331 | 3035179.774 | 15.001 |
| Remote Pole | 758798.912 | 3034988.221 | 15.157 |

| 2D Survey – LINE 2 | | | |
|---|---|---|---|
| **Electrode ID** | **Easting (m)** | **Northing (m)** | **Elevation** |
| EL-01 | 758692.012 | 3035094.106 | 15.343 |
| EL-02 | 758690.997 | 3035095.342 | 15.317 |
| EL-03 | 758689.981 | 3035096.579 | 15.319 |
| EL-04 | 758688.966 | 3035097.816 | 15.302 |
| EL-05 | 758687.951 | 3035099.052 | 15.301 |
| EL-06 | 758686.936 | 3035100.289 | 15.357 |
| EL-07 | 758685.920 | 3035101.525 | 15.026 |
| EL-08 | 758684.905 | 3035102.762 | 15.009 |
| EL-09 | 758683.890 | 3035103.999 | 15.012 |
| EL-10 | 758682.875 | 3035105.235 | 15.012 |
| EL-11 | 758681.859 | 3035106.472 | 15.019 |
| EL-12 | 758680.844 | 3035107.709 | 15.033 |
| EL-13 | 758679.829 | 3035108.945 | 15.135 |
| EL-14 | 758678.813 | 3035110.182 | 15.394 |
| EL-15 | 758677.798 | 3035111.418 | 15.309 |
| EL-16 | 758676.783 | 3035112.655 | 15.250 |
| EL-17 | 758675.768 | 3035113.892 | 15.151 |
| EL-18 | 758674.752 | 3035115.128 | 15.120 |
| EL-19 | 758673.737 | 3035116.365 | 15.119 |
| EL-20 | 758672.722 | 3035117.602 | 15.270 |
| EL-21 | 758671.707 | 3035118.838 | 15.284 |
| EL-22 | 758670.691 | 3035120.075 | 15.265 |
| EL-23 | 758669.676 | 3035121.311 | 15.139 |
| EL-24 | 758668.661 | 3035122.548 | 15.119 |
| EL-25 | 758667.646 | 3035123.785 | 15.233 |
| EL-26 | 758666.630 | 3035125.021 | 15.158 |
| EL-27 | 758665.615 | 3035126.258 | 15.140 |
| EL-28 | 758664.600 | 3035127.495 | 15.130 |
| EL-29 | 758663.585 | 3035128.731 | 15.146 |
| EL-30 | 758662.569 | 3035129.968 | 15.133 |
| EL-31 | 758661.554 | 3035131.204 | 15.038 |
| EL-32 | 758660.539 | 3035132.441 | 15.051 |
| EL-33 | 758659.523 | 3035133.678 | 15.105 |
| EL-34 | 758658.508 | 3035134.914 | 15.152 |
| EL-35 | 758657.493 | 3035136.151 | 15.264 |
| EL-36 | 758656.478 | 3035137.388 | 15.149 |
| EL-37 | 758655.462 | 3035138.624 | 15.161 |
| EL-38 | 758654.447 | 3035139.861 | 15.185 |

| LINE 1 - Continued | | | |
|---|---|---|---|
| EL-39 | 758653.432 | 3035141.097 | 15.175 |
| EL-40 | 758652.417 | 3035142.334 | 15.170 |
| EL-41 | 758651.401 | 3035143.571 | 15.178 |
| EL-42 | 758650.386 | 3035144.807 | 15.128 |
| EL-43 | 758649.371 | 3035146.044 | 15.138 |
| EL-44 | 758648.356 | 3035147.281 | 15.347 |
| EL-45 | 758647.340 | 3035148.517 | 15.397 |
| EL-46 | 758646.325 | 3035149.754 | 15.394 |
| EL-47 | 758645.310 | 3035150.990 | 15.298 |
| EL-48 | 758644.295 | 3035152.227 | 15.285 |
| EL-49 | 758643.279 | 3035153.464 | 15.249 |
| EL-50 | 758642.264 | 3035154.700 | 15.196 |
| EL-51 | 758641.249 | 3035155.937 | 15.225 |
| EL-52 | 758640.233 | 3035157.174 | 15.162 |
| EL-53 | 758639.218 | 3035158.410 | 15.127 |
| EL-54 | 758638.203 | 3035159.647 | 15.115 |
| EL-55 | 758637.188 | 3035160.883 | 15.125 |
| EL-56 | 758636.172 | 3035162.120 | 15.136 |
| EL-57 | 758635.157 | 3035163.357 | 15.110 |
| EL-58 | 758634.142 | 3035164.593 | 15.142 |
| EL-59 | 758633.127 | 3035165.830 | 15.122 |
| EL-60 | 758632.111 | 3035167.066 | 15.012 |
| EL-61 | 758631.096 | 3035168.303 | 15.144 |
| EL-62 | 758630.081 | 3035169.540 | 15.134 |
| EL-63 | 758629.066 | 3035170.776 | 15.127 |
| EL-64 | 758628.050 | 3035172.013 | 15.072 |
| EL-65 | 758627.035 | 3035173.250 | 15.035 |
| EL-66 | 758626.020 | 3035174.486 | 15.051 |
| EL-67 | 758625.004 | 3035175.723 | 15.233 |
| EL-68 | 758623.989 | 3035176.959 | 15.310 |
| EL-69 | 758622.974 | 3035178.196 | 15.099 |
| EL-70 | 758621.959 | 3035179.433 | 15.188 |
| EL-71 | 758620.943 | 3035180.669 | 15.184 |
| EL-72 | 758619.928 | 3035181.906 | 15.190 |
| Remote Pole | 758798.912 | 3034988.221 | 15.157 |

| 2D Survey – LINE 3 | | | |
|---|---|---|---|
| **Electrode ID** | **Easting (m)** | **Northing (m)** | **Elevation** |
| EL-01 | 758694.609 | 3035096.238 | 15.401 |
| EL-02 | 758693.594 | 3035097.474 | 15.370 |
| EL-03 | 758692.578 | 3035098.711 | 15.369 |
| EL-04 | 758691.563 | 3035099.948 | 15.520 |
| EL-05 | 758690.548 | 3035101.184 | 15.284 |
| EL-06 | 758689.590 | 3035102.350 | 15.265 |
| EL-07 | 758688.517 | 3035103.657 | 15.139 |
| EL-08 | 758687.502 | 3035104.894 | 15.119 |
| EL-09 | 758686.487 | 3035106.131 | 15.013 |
| EL-10 | 758685.471 | 3035107.367 | 15.028 |
| EL-11 | 758684.456 | 3035108.604 | 15.030 |
| EL-12 | 758683.441 | 3035109.841 | 15.230 |
| EL-13 | 758682.426 | 3035111.077 | 15.246 |
| EL-14 | 758681.410 | 3035112.314 | 15.233 |
| EL-15 | 758680.395 | 3035113.550 | 15.338 |
| EL-16 | 758679.380 | 3035114.787 | 15.351 |
| EL-17 | 758678.365 | 3035116.024 | 15.405 |
| EL-18 | 758677.349 | 3035117.260 | 15.452 |
| EL-19 | 758676.334 | 3035118.497 | 15.464 |
| EL-20 | 758675.319 | 3035119.734 | 15.357 |
| EL-21 | 758674.304 | 3035120.970 | 15.359 |
| EL-22 | 758673.288 | 3035122.207 | 15.259 |
| EL-23 | 758672.273 | 3035123.443 | 15.275 |
| EL-24 | 758671.258 | 3035124.680 | 15.269 |
| EL-25 | 758670.242 | 3035125.917 | 15.269 |
| EL-26 | 758669.227 | 3035127.153 | 15.287 |
| EL-27 | 758668.212 | 3035128.390 | 15.285 |
| EL-28 | 758667.197 | 3035129.627 | 15.483 |
| EL-29 | 758666.181 | 3035130.863 | 15.560 |
| EL-30 | 758665.166 | 3035132.100 | 15.490 |
| EL-31 | 758664.151 | 3035133.336 | 15.494 |
| EL-32 | 758663.136 | 3035134.573 | 15.409 |
| EL-33 | 758662.120 | 3035135.810 | 15.350 |
| EL-34 | 758661.105 | 3035137.046 | 15.388 |
| EL-35 | 758660.090 | 3035138.283 | 15.384 |
| EL-36 | 758659.075 | 3035139.520 | 15.490 |
| EL-37 | 758658.059 | 3035140.756 | 15.547 |
| EL-38 | 758657.044 | 3035141.993 | 15.597 |

| LINE 3 - Continued | | | |
|---|---|---|---|
| EL-39 | 758656.029 | 3035143.229 | 15.594 |
| EL-40 | 758655.014 | 3035144.466 | 15.498 |
| EL-41 | 758653.998 | 3035145.703 | 15.485 |
| EL-42 | 758652.983 | 3035146.939 | 15.449 |
| EL-43 | 758651.968 | 3035148.176 | 15.396 |
| EL-44 | 758650.952 | 3035149.413 | 15.425 |
| EL-45 | 758649.937 | 3035150.649 | 15.362 |
| EL-46 | 758648.922 | 3035151.886 | 15.349 |
| EL-47 | 758647.907 | 3035153.122 | 15.361 |
| EL-48 | 758646.891 | 3035154.359 | 15.385 |
| EL-49 | 758645.876 | 3035155.596 | 15.375 |
| EL-50 | 758644.861 | 3035156.832 | 15.370 |
| EL-51 | 758643.846 | 3035158.069 | 15.378 |
| EL-52 | 758642.830 | 3035159.306 | 15.328 |
| EL-53 | 758641.815 | 3035160.542 | 15.338 |
| EL-54 | 758640.800 | 3035161.779 | 15.327 |
| EL-55 | 758639.785 | 3035163.015 | 15.315 |
| EL-56 | 758638.769 | 3035164.252 | 15.325 |
| EL-57 | 758637.754 | 3035165.489 | 15.336 |
| EL-58 | 758636.739 | 3035166.725 | 15.452 |
| EL-59 | 758635.724 | 3035167.962 | 15.412 |
| EL-60 | 758634.708 | 3035169.199 | 15.432 |
| EL-61 | 758633.693 | 3035170.435 | 15.473 |
| EL-62 | 758632.678 | 3035171.672 | 15.494 |
| EL-63 | 758631.662 | 3035172.908 | 15.484 |
| EL-64 | 758630.647 | 3035174.145 | 15.477 |
| EL-65 | 758629.632 | 3035175.382 | 15.422 |
| EL-66 | 758628.617 | 3035176.618 | 15.385 |
| EL-67 | 758627.601 | 3035177.855 | 15.401 |
| EL-68 | 758626.586 | 3035179.092 | 15.393 |
| EL-69 | 758625.571 | 3035180.328 | 15.367 |
| EL-70 | 758624.556 | 3035181.565 | 15.369 |
| EL-71 | 758623.540 | 3035182.801 | 15.352 |
| EL-72 | 758622.525 | 3035184.038 | 15.351 |
| Remote Pole | 758798.912 | 3034988.221 | 15.157 |

| 2D Survey – LINE 4 | | | |
|---|---|---|---|
| **Electrode ID** | **Easting (m)** | **Northing (m)** | **Elevation** |
| EL-01 | 758697.206 | 3035098.370 | 15.251 |
| EL-02 | 758696.190 | 3035099.606 | 15.220 |
| EL-03 | 758695.175 | 3035100.843 | 15.219 |
| EL-04 | 758694.160 | 3035102.080 | 15.370 |
| EL-05 | 758693.145 | 3035103.316 | 15.234 |
| EL-06 | 758692.129 | 3035104.553 | 15.215 |
| EL-07 | 758691.114 | 3035105.790 | 15.089 |
| EL-08 | 758690.099 | 3035107.026 | 15.069 |
| EL-09 | 758689.084 | 3035108.263 | 15.183 |
| EL-10 | 758688.068 | 3035109.499 | 15.108 |
| EL-11 | 758687.053 | 3035110.736 | 15.010 |
| EL-12 | 758686.038 | 3035111.973 | 15.020 |
| EL-13 | 758685.023 | 3035113.209 | 15.296 |
| EL-14 | 758684.007 | 3035114.446 | 15.283 |
| EL-15 | 758682.992 | 3035115.683 | 15.338 |
| EL-16 | 758681.977 | 3035116.919 | 15.351 |
| EL-17 | 758680.962 | 3035118.156 | 15.405 |
| EL-18 | 758679.946 | 3035119.392 | 15.452 |
| EL-19 | 758678.931 | 3035120.629 | 15.464 |
| EL-20 | 758677.916 | 3035121.866 | 15.357 |
| EL-21 | 758676.900 | 3035123.102 | 15.359 |
| EL-22 | 758675.885 | 3035124.339 | 15.309 |
| EL-23 | 758674.870 | 3035125.576 | 15.325 |
| EL-24 | 758673.855 | 3035126.812 | 15.319 |
| EL-25 | 758672.839 | 3035128.049 | 15.319 |
| EL-26 | 758671.824 | 3035129.285 | 15.187 |
| EL-27 | 758670.809 | 3035130.522 | 15.185 |
| EL-28 | 758669.794 | 3035131.759 | 15.383 |
| EL-29 | 758668.778 | 3035132.995 | 15.460 |
| EL-30 | 758667.763 | 3035134.232 | 15.440 |
| EL-31 | 758666.748 | 3035135.469 | 15.444 |
| EL-32 | 758665.733 | 3035136.705 | 15.359 |
| EL-33 | 758664.717 | 3035137.942 | 15.300 |
| EL-34 | 758663.702 | 3035139.178 | 15.338 |
| EL-35 | 758662.687 | 3035140.415 | 15.334 |
| EL-36 | 758661.671 | 3035141.652 | 15.540 |
| EL-37 | 758660.656 | 3035142.888 | 15.597 |
| EL-38 | 758659.641 | 3035144.125 | 15.647 |

| LINE 4 - Continued | | | |
|---|---|---|---|
| EL-39 | 758658.626 | 3035145.362 | 15.644 |
| EL-40 | 758657.610 | 3035146.598 | 15.548 |
| EL-41 | 758656.595 | 3035147.835 | 15.535 |
| EL-42 | 758655.580 | 3035149.071 | 15.499 |
| EL-43 | 758654.565 | 3035150.308 | 15.446 |
| EL-44 | 758653.549 | 3035151.545 | 15.475 |
| EL-45 | 758652.534 | 3035152.781 | 15.412 |
| EL-46 | 758651.519 | 3035154.018 | 15.399 |
| EL-47 | 758650.504 | 3035155.254 | 15.411 |
| EL-48 | 758649.488 | 3035156.491 | 15.435 |
| EL-49 | 758648.473 | 3035157.728 | 15.425 |
| EL-50 | 758647.458 | 3035158.964 | 15.420 |
| EL-51 | 758646.443 | 3035160.201 | 15.428 |
| EL-52 | 758645.427 | 3035161.438 | 15.378 |
| EL-53 | 758644.412 | 3035162.674 | 15.388 |
| EL-54 | 758643.397 | 3035163.911 | 15.420 |
| EL-55 | 758642.381 | 3035165.147 | 15.401 |
| EL-56 | 758641.366 | 3035166.384 | 15.403 |
| EL-57 | 758640.351 | 3035167.621 | 15.159 |
| EL-58 | 758639.336 | 3035168.857 | 15.202 |
| EL-59 | 758638.320 | 3035170.094 | 15.162 |
| EL-60 | 758637.305 | 3035171.331 | 15.182 |
| EL-61 | 758636.290 | 3035172.567 | 15.223 |
| EL-62 | 758635.275 | 3035173.804 | 15.244 |
| EL-63 | 758634.259 | 3035175.040 | 15.234 |
| EL-64 | 758633.244 | 3035176.277 | 15.227 |
| EL-65 | 758632.229 | 3035177.514 | 15.372 |
| EL-66 | 758631.214 | 3035178.750 | 15.335 |
| EL-67 | 758630.198 | 3035179.987 | 15.351 |
| EL-68 | 758629.183 | 3035181.224 | 15.343 |
| EL-69 | 758628.168 | 3035182.460 | 15.317 |
| EL-70 | 758627.153 | 3035183.697 | 15.319 |
| EL-71 | 758626.137 | 3035184.933 | 15.302 |
| EL-72 | 758625.122 | 3035186.170 | 15.301 |
| Remote Pole | 758798.912 | 3034988.221 | 15.157 |

| 2D Survey – LINE 5 | | | |
|---|---|---|---|
| **Electrode ID** | **Easting (m)** | **Northing (m)** | **Elevation** |
| EL-01 | 758699.803 | 3035100.502 | 15.269 |
| EL-02 | 758698.787 | 3035101.738 | 15.420 |
| EL-03 | 758697.772 | 3035102.975 | 15.434 |
| EL-04 | 758696.757 | 3035104.212 | 15.415 |
| EL-05 | 758695.742 | 3035105.448 | 15.089 |
| EL-06 | 758694.726 | 3035106.685 | 15.069 |
| EL-07 | 758693.711 | 3035107.922 | 15.183 |
| EL-08 | 758692.696 | 3035109.158 | 15.108 |
| EL-09 | 758691.681 | 3035110.395 | 15.090 |
| EL-10 | 758690.665 | 3035111.631 | 15.018 |
| EL-11 | 758689.650 | 3035112.868 | 15.011 |
| EL-12 | 758688.635 | 3035114.105 | 15.011 |
| EL-13 | 758687.619 | 3035115.341 | 15.452 |
| EL-14 | 758686.604 | 3035116.578 | 15.464 |
| EL-15 | 758685.589 | 3035117.815 | 15.349 |
| EL-16 | 758684.574 | 3035119.051 | 15.361 |
| EL-17 | 758683.558 | 3035120.288 | 15.335 |
| EL-18 | 758682.543 | 3035121.524 | 15.325 |
| EL-19 | 758681.528 | 3035122.761 | 15.272 |
| EL-20 | 758680.513 | 3035123.998 | 15.262 |
| EL-21 | 758679.497 | 3035125.234 | 15.394 |
| EL-22 | 758678.731 | 3035126.167 | 15.384 |
| EL-23 | 758677.467 | 3035127.708 | 15.377 |
| EL-24 | 758676.452 | 3035128.944 | 15.322 |
| EL-25 | 758675.436 | 3035130.181 | 15.285 |
| EL-26 | 758674.421 | 3035131.417 | 15.301 |
| EL-27 | 758673.406 | 3035132.654 | 15.483 |
| EL-28 | 758672.391 | 3035133.891 | 15.560 |
| EL-29 | 758671.375 | 3035135.127 | 15.299 |
| EL-30 | 758670.360 | 3035136.364 | 15.388 |
| EL-31 | 758669.345 | 3035137.601 | 15.384 |
| EL-32 | 758668.329 | 3035138.837 | 15.390 |
| EL-33 | 758667.314 | 3035140.074 | 15.230 |
| EL-34 | 758666.299 | 3035141.310 | 15.296 |
| EL-35 | 758665.284 | 3035142.547 | 15.283 |
| EL-36 | 758664.268 | 3035143.784 | 15.448 |
| EL-37 | 758663.253 | 3035145.020 | 15.435 |
| EL-38 | 758662.238 | 3035146.257 | 15.399 |

| LINE 5 - Continued | | | |
|---|---|---|---|
| EL-39 | 758661.223 | 3035147.494 | 15.346 |
| EL-40 | 758660.207 | 3035148.730 | 15.375 |
| EL-41 | 758659.192 | 3035149.967 | 15.312 |
| EL-42 | 758658.177 | 3035151.203 | 15.277 |
| EL-43 | 758657.162 | 3035152.440 | 15.265 |
| EL-44 | 758656.146 | 3035153.677 | 15.275 |
| EL-45 | 758655.131 | 3035154.913 | 15.286 |
| EL-46 | 758654.116 | 3035156.150 | 15.260 |
| EL-47 | 758653.100 | 3035157.387 | 15.320 |
| EL-48 | 758652.085 | 3035158.623 | 15.328 |
| EL-49 | 758651.070 | 3035159.860 | 15.228 |
| EL-50 | 758650.055 | 3035161.096 | 15.238 |
| EL-51 | 758649.039 | 3035162.333 | 15.447 |
| EL-52 | 758648.024 | 3035163.570 | 15.497 |
| EL-53 | 758647.009 | 3035164.806 | 15.494 |
| EL-54 | 758645.994 | 3035166.043 | 15.292 |
| EL-55 | 758644.978 | 3035167.280 | 15.293 |
| EL-56 | 758643.963 | 3035168.516 | 15.267 |
| EL-57 | 758642.948 | 3035169.753 | 15.269 |
| EL-58 | 758641.933 | 3035170.989 | 15.252 |
| EL-59 | 758640.917 | 3035172.226 | 15.051 |
| EL-60 | 758639.902 | 3035173.463 | 15.107 |
| EL-61 | 758638.887 | 3035174.699 | 15.109 |
| EL-62 | 758637.872 | 3035175.936 | 15.059 |
| EL-63 | 758636.706 | 3035177.356 | 15.051 |
| EL-64 | 758635.841 | 3035178.409 | 15.269 |
| EL-65 | 758634.826 | 3035179.646 | 15.269 |
| EL-66 | 758633.810 | 3035180.882 | 15.287 |
| EL-67 | 758632.950 | 3035181.930 | 15.285 |
| EL-68 | 758631.780 | 3035183.356 | 15.544 |
| EL-69 | 758630.765 | 3035184.592 | 15.459 |
| EL-70 | 758629.749 | 3035185.829 | 15.400 |
| EL-71 | 758628.734 | 3035187.066 | 15.301 |
| EL-72 | 758627.719 | 3035188.302 | 15.270 |
| Remote Pole | 758798.912 | 3034988.221 | 15.157 |

| 2D Survey – LINE 6 | | | |
|---|---|---|---|
| **Electrode ID** | **Easting (m)** | **Northing (m)** | **Elevation** |
| EL-01 | 758702.400 | 3035102.634 | 15.269 |
| EL-02 | 758701.384 | 3035103.871 | 15.420 |
| EL-03 | 758700.369 | 3035105.107 | 15.434 |
| EL-04 | 758699.354 | 3035106.344 | 15.415 |
| EL-05 | 758698.339 | 3035107.580 | 15.089 |
| EL-06 | 758697.323 | 3035108.817 | 15.069 |
| EL-07 | 758697.323 | 3035110.054 | 15.183 |
| EL-08 | 758695.293 | 3035111.290 | 15.158 |
| EL-09 | 758694.277 | 3035112.527 | 15.140 |
| EL-10 | 758693.262 | 3035113.764 | 15.088 |
| EL-11 | 758692.247 | 3035115.000 | 15.101 |
| EL-12 | 758691.232 | 3035116.237 | 15.155 |
| EL-13 | 758690.216 | 3035117.473 | 15.202 |
| EL-14 | 758689.201 | 3035118.710 | 15.364 |
| EL-15 | 758688.186 | 3035119.947 | 15.249 |
| EL-16 | 758687.171 | 3035121.183 | 15.261 |
| EL-17 | 758686.155 | 3035122.420 | 15.385 |
| EL-18 | 758685.140 | 3035123.657 | 15.375 |
| EL-19 | 758684.125 | 3035124.893 | 15.322 |
| EL-20 | 758683.110 | 3035126.130 | 15.312 |
| EL-21 | 758682.094 | 3035127.366 | 15.444 |
| EL-22 | 758681.079 | 3035128.603 | 15.434 |
| EL-23 | 758680.002 | 3035129.706 | 15.427 |
| EL-24 | 758679.048 | 3035131.076 | 15.372 |
| EL-25 | 758678.033 | 3035132.313 | 15.335 |
| EL-26 | 758677.018 | 3035133.550 | 15.351 |
| EL-27 | 758676.003 | 3035134.786 | 15.533 |
| EL-28 | 758674.987 | 3035136.023 | 15.610 |
| EL-29 | 758673.972 | 3035137.259 | 15.249 |
| EL-30 | 758672.957 | 3035138.496 | 15.338 |
| EL-31 | 758671.942 | 3035139.733 | 15.334 |
| EL-32 | 758670.926 | 3035140.969 | 15.490 |
| EL-33 | 758669.911 | 3035142.206 | 15.330 |
| EL-34 | 758668.896 | 3035143.442 | 15.346 |
| EL-35 | 758667.881 | 3035144.679 | 15.333 |
| EL-36 | 758666.865 | 3035145.916 | 15.548 |
| EL-37 | 758665.850 | 3035147.152 | 15.535 |
| EL-38 | 758664.835 | 3035148.389 | 15.499 |

| LINE 6 - Continued | | | |
|---|---|---|---|
| EL-39 | 758663.820 | 3035149.626 | 15.446 |
| EL-40 | 758662.804 | 3035150.862 | 15.475 |
| EL-41 | 758661.789 | 3035152.099 | 15.412 |
| EL-42 | 758660.774 | 3035153.335 | 15.377 |
| EL-43 | 758659.758 | 3035154.572 | 15.365 |
| EL-44 | 758658.743 | 3035155.809 | 15.375 |
| EL-45 | 758657.728 | 3035157.045 | 15.386 |
| EL-46 | 758656.713 | 3035158.282 | 15.360 |
| EL-47 | 758655.697 | 3035159.519 | 15.420 |
| EL-48 | 758654.682 | 3035160.755 | 15.428 |
| EL-49 | 758653.667 | 3035161.992 | 15.328 |
| EL-50 | 758652.652 | 3035163.228 | 15.338 |
| EL-51 | 758651.636 | 3035164.465 | 15.547 |
| EL-52 | 758650.621 | 3035165.702 | 15.597 |
| EL-53 | 758649.606 | 3035166.938 | 15.594 |
| EL-54 | 758648.591 | 3035168.175 | 15.342 |
| EL-55 | 758647.575 | 3035169.412 | 15.243 |
| EL-56 | 758646.560 | 3035170.648 | 15.217 |
| EL-57 | 758645.545 | 3035171.885 | 15.219 |
| EL-58 | 758644.530 | 3035173.121 | 15.202 |
| EL-59 | 758643.514 | 3035174.358 | 15.101 |
| EL-60 | 758642.499 | 3035175.595 | 15.157 |
| EL-61 | 758641.484 | 3035176.831 | 15.159 |
| EL-62 | 758640.468 | 3035178.068 | 15.109 |
| EL-63 | 758639.453 | 3035179.305 | 15.001 |
| EL-64 | 758638.438 | 3035180.541 | 15.369 |
| EL-65 | 758637.423 | 3035181.778 | 15.369 |
| EL-66 | 758636.407 | 3035183.014 | 15.387 |
| EL-67 | 758635.392 | 3035184.251 | 15.385 |
| EL-68 | 758634.377 | 3035185.488 | 15.644 |
| EL-69 | 758633.362 | 3035186.724 | 15.559 |
| EL-70 | 758632.346 | 3035187.961 | 15.500 |
| EL-71 | 758631.521 | 3035188.966 | 15.401 |
| EL-72 | 758630.316 | 3035190.434 | 15.370 |
| Remote Pole | 758798.912 | 3034988.221 | 15.157 |

| 2D Survey – LINE 7 | | | |
|---|---|---|---|
| **Electrode ID** | **Easting (m)** | **Northing (m)** | **Elevation** |
| EL-01 | 758704.996 | 3035104.766 | 15.293 |
| EL-02 | 758703.981 | 3035106.003 | 15.267 |
| EL-03 | 758702.966 | 3035107.239 | 15.269 |
| EL-04 | 758701.951 | 3035108.476 | 15.252 |
| EL-05 | 758700.935 | 3035109.712 | 15.251 |
| EL-06 | 758699.920 | 3035110.949 | 15.307 |
| EL-07 | 758698.905 | 3035112.186 | 15.509 |
| EL-08 | 758697.890 | 3035113.422 | 15.459 |
| EL-09 | 758696.874 | 3035114.659 | 15.475 |
| EL-10 | 758695.859 | 3035115.896 | 15.469 |
| EL-11 | 758694.844 | 3035117.132 | 15.469 |
| EL-12 | 758693.829 | 3035118.369 | 15.337 |
| EL-13 | 758692.813 | 3035119.605 | 15.335 |
| EL-14 | 758691.798 | 3035120.842 | 15.594 |
| EL-15 | 758690.783 | 3035122.079 | 15.709 |
| EL-16 | 758689.768 | 3035123.315 | 15.650 |
| EL-17 | 758688.752 | 3035124.552 | 15.551 |
| EL-18 | 758687.737 | 3035125.789 | 15.570 |
| EL-19 | 758686.722 | 3035127.025 | 15.569 |
| EL-20 | 758685.706 | 3035128.262 | 15.720 |
| EL-21 | 758684.691 | 3035129.498 | 15.734 |
| EL-22 | 758683.676 | 3035130.735 | 15.715 |
| EL-23 | 758682.661 | 3035131.972 | 15.589 |
| EL-24 | 758681.645 | 3035133.208 | 15.569 |
| EL-25 | 758680.630 | 3035134.445 | 15.683 |
| EL-26 | 758679.615 | 3035135.682 | 15.558 |
| EL-27 | 758678.600 | 3035136.918 | 15.540 |
| EL-28 | 758677.584 | 3035138.155 | 15.530 |
| EL-29 | 758676.569 | 3035139.391 | 15.346 |
| EL-30 | 758675.554 | 3035140.628 | 15.333 |
| EL-31 | 758674.539 | 3035141.865 | 15.338 |
| EL-32 | 758673.523 | 3035143.101 | 15.551 |
| EL-33 | 758672.508 | 3035144.338 | 15.605 |
| EL-34 | 758671.493 | 3035145.575 | 15.652 |
| EL-35 | 758670.477 | 3035146.811 | 15.664 |
| EL-36 | 758669.462 | 3035148.048 | 15.549 |
| EL-37 | 758668.447 | 3035149.284 | 15.661 |
| EL-38 | 758667.432 | 3035150.521 | 15.685 |

| LINE 7 - Continued | | | |
|---|---|---|---|
| EL-39 | 758666.416 | 3035151.758 | 15.675 |
| EL-40 | 758665.437 | 3035152.951 | 15.670 |
| EL-41 | 758664.386 | 3035154.231 | 15.678 |
| EL-42 | 758663.371 | 3035155.468 | 15.628 |
| EL-43 | 758662.355 | 3035156.704 | 15.538 |
| EL-44 | 758661.340 | 3035157.941 | 15.747 |
| EL-45 | 758660.325 | 3035159.177 | 15.797 |
| EL-46 | 758659.310 | 3035160.414 | 15.794 |
| EL-47 | 758658.294 | 3035161.651 | 15.698 |
| EL-48 | 758657.279 | 3035162.887 | 15.485 |
| EL-49 | 758656.264 | 3035164.124 | 15.449 |
| EL-50 | 758655.249 | 3035165.361 | 15.396 |
| EL-51 | 758654.233 | 3035166.597 | 15.425 |
| EL-52 | 758653.218 | 3035167.834 | 15.362 |
| EL-53 | 758652.203 | 3035169.070 | 15.327 |
| EL-54 | 758651.187 | 3035170.307 | 15.315 |
| EL-55 | 758650.172 | 3035171.544 | 15.025 |
| EL-56 | 758649.157 | 3035172.780 | 15.036 |
| EL-57 | 758648.142 | 3035174.017 | 15.010 |
| EL-58 | 758647.126 | 3035175.254 | 15.042 |
| EL-59 | 758646.111 | 3035176.490 | 15.022 |
| EL-60 | 758645.096 | 3035177.727 | 15.012 |
| EL-61 | 758644.081 | 3035178.963 | 15.494 |
| EL-62 | 758643.065 | 3035180.200 | 15.484 |
| EL-63 | 758642.050 | 3035181.437 | 15.477 |
| EL-64 | 758641.035 | 3035182.673 | 15.422 |
| EL-65 | 758640.020 | 3035183.910 | 15.385 |
| EL-66 | 758639.004 | 3035185.147 | 15.401 |
| EL-67 | 758637.989 | 3035186.383 | 15.583 |
| EL-68 | 758636.974 | 3035187.620 | 15.660 |
| EL-69 | 758635.959 | 3035188.856 | 15.449 |
| EL-70 | 758634.943 | 3035190.093 | 15.638 |
| EL-71 | 758633.928 | 3035191.330 | 15.634 |
| EL-72 | 758632.913 | 3035192.566 | 15.640 |
| Remote Pole | 758798.912 | 3034988.221 | 15.157 |

| 2D Survey – LINE 8 | | | |
|---|---|---|---|
| **Electrode ID** | **Easting (m)** | **Northing (m)** | **Elevation** |
| EL-01 | 758707.593 | 3035106.898 | 15.643 |
| EL-02 | 758706.578 | 3035108.135 | 15.617 |
| EL-03 | 758705.563 | 3035109.371 | 15.619 |
| EL-04 | 758704.548 | 3035110.608 | 15.502 |
| EL-05 | 758703.532 | 3035111.845 | 15.501 |
| EL-06 | 758702.517 | 3035113.081 | 15.557 |
| EL-07 | 758701.502 | 3035114.318 | 15.259 |
| EL-08 | 758700.487 | 3035115.554 | 15.209 |
| EL-09 | 758699.471 | 3035116.791 | 15.225 |
| EL-10 | 758698.456 | 3035118.028 | 15.319 |
| EL-11 | 758697.441 | 3035119.264 | 15.319 |
| EL-12 | 758696.425 | 3035120.501 | 15.337 |
| EL-13 | 758695.410 | 3035121.738 | 15.335 |
| EL-14 | 758694.395 | 3035122.974 | 15.844 |
| EL-15 | 758693.380 | 3035124.211 | 15.759 |
| EL-16 | 758692.364 | 3035125.447 | 15.700 |
| EL-17 | 758691.349 | 3035126.684 | 15.451 |
| EL-18 | 758690.334 | 3035127.921 | 15.420 |
| EL-19 | 758689.319 | 3035129.157 | 15.419 |
| EL-20 | 758688.303 | 3035130.394 | 15.570 |
| EL-21 | 758687.547 | 3035131.315 | 15.584 |
| EL-22 | 758686.273 | 3035132.867 | 15.565 |
| EL-23 | 758685.258 | 3035134.104 | 15.439 |
| EL-24 | 758684.242 | 3035135.340 | 15.419 |
| EL-25 | 758683.227 | 3035136.577 | 15.533 |
| EL-26 | 758682.212 | 3035137.814 | 15.458 |
| EL-27 | 758681.197 | 3035139.050 | 15.540 |
| EL-28 | 758680.181 | 3035140.287 | 15.530 |
| EL-29 | 758679.166 | 3035141.523 | 15.546 |
| EL-30 | 758678.151 | 3035142.760 | 15.483 |
| EL-31 | 758677.135 | 3035143.997 | 15.488 |
| EL-32 | 758676.120 | 3035145.233 | 15.551 |
| EL-33 | 758675.105 | 3035146.470 | 15.605 |
| EL-34 | 758674.090 | 3035147.707 | 15.652 |
| EL-35 | 758673.074 | 3035148.943 | 15.664 |
| EL-36 | 758672.059 | 3035150.180 | 15.549 |
| EL-37 | 758671.044 | 3035151.416 | 15.561 |
| EL-38 | 758670.029 | 3035152.653 | 15.585 |

| LINE 8 - Continued | | | |
|---|---|---|---|
| EL-39 | 758669.013 | 3035153.890 | 15.575 |
| EL-40 | 758667.998 | 3035155.126 | 15.570 |
| EL-41 | 758666.983 | 3035156.363 | 15.578 |
| EL-42 | 758665.968 | 3035157.600 | 15.528 |
| EL-43 | 758664.952 | 3035158.836 | 15.538 |
| EL-44 | 758663.937 | 3035160.073 | 15.747 |
| EL-45 | 758662.922 | 3035161.309 | 15.747 |
| EL-46 | 758661.906 | 3035162.546 | 15.744 |
| EL-47 | 758660.891 | 3035163.783 | 15.648 |
| EL-48 | 758659.876 | 3035165.019 | 15.635 |
| EL-49 | 758658.861 | 3035166.256 | 15.599 |
| EL-50 | 758657.845 | 3035167.493 | 15.496 |
| EL-51 | 758656.830 | 3035168.729 | 15.525 |
| EL-52 | 758655.815 | 3035169.966 | 15.462 |
| EL-53 | 758654.800 | 3035171.202 | 15.427 |
| EL-54 | 758653.784 | 3035172.439 | 15.015 |
| EL-55 | 758652.769 | 3035173.676 | 15.025 |
| EL-56 | 758651.754 | 3035174.912 | 15.036 |
| EL-57 | 758650.739 | 3035176.149 | 15.102 |
| EL-58 | 758649.723 | 3035177.386 | 15.042 |
| EL-59 | 758648.708 | 3035178.622 | 15.432 |
| EL-60 | 758647.693 | 3035179.859 | 15.473 |
| EL-61 | 758646.678 | 3035181.095 | 15.494 |
| EL-62 | 758645.662 | 3035182.332 | 15.484 |
| EL-63 | 758644.647 | 3035183.569 | 15.527 |
| EL-64 | 758643.632 | 3035184.805 | 15.472 |
| EL-65 | 758642.616 | 3035186.042 | 15.435 |
| EL-66 | 758641.601 | 3035187.279 | 15.451 |
| EL-67 | 758640.586 | 3035188.515 | 15.633 |
| EL-68 | 758639.571 | 3035189.752 | 15.910 |
| EL-69 | 758638.555 | 3035190.988 | 15.699 |
| EL-70 | 758637.540 | 3035192.225 | 15.788 |
| EL-71 | 758636.525 | 3035193.462 | 15.784 |
| EL-72 | 758635.510 | 3035194.698 | 15.790 |
| Remote Pole | 758798.912 | 3034988.221 | 15.157 |

| 2D Survey – LINE 9 | | | |
|---|---|---|---|
| **Electrode ID** | **Easting (m)** | **Northing (m)** | **Elevation** |
| EL-01 | 758710.190 | 3035109.030 | 15.651 |
| EL-02 | 758709.175 | 3035110.267 | 15.620 |
| EL-03 | 758707.990 | 3035111.710 | 15.619 |
| EL-04 | 758707.144 | 3035112.740 | 15.770 |
| EL-05 | 758706.129 | 3035113.977 | 15.584 |
| EL-06 | 758705.114 | 3035115.213 | 15.565 |
| EL-07 | 758704.099 | 3035116.450 | 15.439 |
| EL-08 | 758703.083 | 3035117.686 | 15.419 |
| EL-09 | 758702.068 | 3035118.923 | 15.333 |
| EL-10 | 758701.053 | 3035120.160 | 15.258 |
| EL-11 | 758700.038 | 3035121.396 | 15.240 |
| EL-12 | 758699.022 | 3035122.633 | 15.230 |
| EL-13 | 758698.007 | 3035123.870 | 15.246 |
| EL-14 | 758696.992 | 3035125.106 | 15.233 |
| EL-15 | 758695.977 | 3035126.343 | 15.338 |
| EL-16 | 758694.961 | 3035127.579 | 15.351 |
| EL-17 | 758693.946 | 3035128.816 | 15.405 |
| EL-18 | 758692.931 | 3035130.053 | 15.452 |
| EL-19 | 758691.916 | 3035131.289 | 15.714 |
| EL-20 | 758690.900 | 3035132.526 | 15.607 |
| EL-21 | 758689.885 | 3035133.763 | 15.609 |
| EL-22 | 758688.870 | 3035134.999 | 15.559 |
| EL-23 | 758687.854 | 3035136.236 | 15.575 |
| EL-24 | 758686.839 | 3035137.472 | 15.569 |
| EL-25 | 758685.824 | 3035138.709 | 15.619 |
| EL-26 | 758684.809 | 3035139.946 | 15.637 |
| EL-27 | 758683.793 | 3035141.182 | 15.635 |
| EL-28 | 758682.778 | 3035142.419 | 15.833 |
| EL-29 | 758681.763 | 3035143.656 | 15.910 |
| EL-30 | 758680.748 | 3035144.892 | 15.740 |
| EL-31 | 758679.732 | 3035146.129 | 15.744 |
| EL-32 | 758678.717 | 3035147.365 | 15.659 |
| EL-33 | 758677.702 | 3035148.602 | 15.600 |
| EL-34 | 758676.687 | 3035149.839 | 15.638 |
| EL-35 | 758675.671 | 3035151.075 | 15.684 |
| EL-36 | 758674.656 | 3035152.312 | 15.690 |
| EL-37 | 758673.641 | 3035153.549 | 15.747 |
| EL-38 | 758672.626 | 3035154.785 | 15.797 |

| LINE 9 - Continued | | | |
|---|---|---|---|
| EL-39 | 758671.610 | 3035156.022 | 15.794 |
| EL-40 | 758670.595 | 3035157.258 | 15.698 |
| EL-41 | 758669.580 | 3035158.495 | 15.535 |
| EL-42 | 758668.564 | 3035159.732 | 15.499 |
| EL-43 | 758667.549 | 3035160.968 | 15.446 |
| EL-44 | 758666.534 | 3035162.205 | 15.475 |
| EL-45 | 758665.519 | 3035163.442 | 15.412 |
| EL-46 | 758664.503 | 3035164.678 | 15.349 |
| EL-47 | 758663.488 | 3035165.915 | 15.361 |
| EL-48 | 758662.473 | 3035167.151 | 15.385 |
| EL-49 | 758661.458 | 3035168.388 | 15.375 |
| EL-50 | 758660.442 | 3035169.625 | 15.370 |
| EL-51 | 758659.427 | 3035170.861 | 15.078 |
| EL-52 | 758658.412 | 3035172.098 | 15.028 |
| EL-53 | 758657.397 | 3035173.335 | 15.038 |
| EL-54 | 758656.381 | 3035174.571 | 15.027 |
| EL-55 | 758655.366 | 3035175.808 | 15.315 |
| EL-56 | 758654.548 | 3035176.805 | 15.325 |
| EL-57 | 758653.335 | 3035178.281 | 15.386 |
| EL-58 | 758652.320 | 3035179.518 | 15.452 |
| EL-59 | 758651.305 | 3035180.754 | 15.412 |
| EL-60 | 758650.290 | 3035181.991 | 15.432 |
| EL-61 | 758649.274 | 3035183.228 | 15.473 |
| EL-62 | 758648.259 | 3035184.464 | 15.544 |
| EL-63 | 758647.244 | 3035185.701 | 15.534 |
| EL-64 | 758646.229 | 3035186.937 | 15.527 |
| EL-65 | 758645.213 | 3035188.174 | 15.472 |
| EL-66 | 758644.198 | 3035189.411 | 15.435 |
| EL-67 | 758643.183 | 3035190.647 | 15.451 |
| EL-68 | 758642.168 | 3035191.884 | 15.993 |
| EL-69 | 758641.152 | 3035193.120 | 15.967 |
| EL-70 | 758640.137 | 3035194.357 | 15.969 |
| EL-71 | 758639.122 | 3035195.594 | 15.952 |
| EL-72 | 758638.107 | 3035196.830 | 15.951 |
| Remote Pole | 758798.912 | 3034988.221 | 15.157 |

| 2D Survey – LINE 10 | | | |
|---|---|---|---|
| **Electrode ID** | **Easting (m)** | **Northing (m)** | **Elevation** |
| EL-01 | 758712.787 | 3035111.162 | 15.551 |
| EL-02 | 758711.772 | 3035112.399 | 15.520 |
| EL-03 | 758710.757 | 3035113.635 | 15.519 |
| EL-04 | 758709.741 | 3035114.872 | 15.670 |
| EL-05 | 758708.726 | 3035116.109 | 15.684 |
| EL-06 | 758707.711 | 3035117.345 | 15.665 |
| EL-07 | 758706.696 | 3035118.582 | 15.539 |
| EL-08 | 758705.680 | 3035119.818 | 15.319 |
| EL-09 | 758704.665 | 3035121.055 | 15.433 |
| EL-10 | 758703.650 | 3035122.292 | 15.358 |
| EL-11 | 758702.635 | 3035123.528 | 15.440 |
| EL-12 | 758701.619 | 3035124.765 | 15.430 |
| EL-13 | 758700.604 | 3035126.002 | 15.446 |
| EL-14 | 758699.589 | 3035127.238 | 15.333 |
| EL-15 | 758698.574 | 3035128.475 | 15.338 |
| EL-16 | 758697.558 | 3035129.711 | 15.351 |
| EL-17 | 758696.543 | 3035130.948 | 15.405 |
| EL-18 | 758695.528 | 3035132.185 | 15.602 |
| EL-19 | 758694.512 | 3035133.421 | 15.614 |
| EL-20 | 758693.497 | 3035134.658 | 15.507 |
| EL-21 | 758692.482 | 3035135.895 | 15.609 |
| EL-22 | 758691.467 | 3035137.131 | 15.559 |
| EL-23 | 758690.451 | 3035138.368 | 15.575 |
| EL-24 | 758689.436 | 3035139.604 | 15.569 |
| EL-25 | 758688.421 | 3035140.841 | 15.569 |
| EL-26 | 758687.406 | 3035142.078 | 15.587 |
| EL-27 | 758686.390 | 3035143.314 | 15.585 |
| EL-28 | 758685.375 | 3035144.551 | 15.733 |
| EL-29 | 758684.360 | 3035145.788 | 15.810 |
| EL-30 | 758683.345 | 3035147.024 | 15.790 |
| EL-31 | 758682.329 | 3035148.261 | 15.794 |
| EL-32 | 758681.314 | 3035149.497 | 15.709 |
| EL-33 | 758680.299 | 3035150.734 | 15.650 |
| EL-34 | 758679.283 | 3035151.971 | 15.638 |
| EL-35 | 758678.268 | 3035153.207 | 15.634 |
| EL-36 | 758677.253 | 3035154.444 | 15.640 |
| EL-37 | 758676.238 | 3035155.681 | 15.697 |
| EL-38 | 758675.222 | 3035156.917 | 15.747 |

| LINE 10 - Continued | | | |
|---|---|---|---|
| EL-39 | 758674.207 | 3035158.154 | 15.744 |
| EL-40 | 758673.192 | 3035159.390 | 15.748 |
| EL-41 | 758672.177 | 3035160.627 | 15.735 |
| EL-42 | 758671.161 | 3035161.864 | 15.549 |
| EL-43 | 758670.146 | 3035163.100 | 15.496 |
| EL-44 | 758669.131 | 3035164.337 | 15.525 |
| EL-45 | 758668.116 | 3035165.574 | 15.362 |
| EL-46 | 758667.100 | 3035166.810 | 15.349 |
| EL-47 | 758666.085 | 3035168.047 | 15.361 |
| EL-48 | 758665.070 | 3035169.283 | 15.385 |
| EL-49 | 758664.055 | 3035170.520 | 15.375 |
| EL-50 | 758663.039 | 3035171.757 | 15.370 |
| EL-51 | 758662.024 | 3035172.993 | 15.378 |
| EL-52 | 758661.009 | 3035174.230 | 15.328 |
| EL-53 | 758659.993 | 3035175.467 | 15.188 |
| EL-54 | 758658.978 | 3035176.703 | 15.027 |
| EL-55 | 758657.963 | 3035177.940 | 15.015 |
| EL-56 | 758656.948 | 3035179.176 | 15.025 |
| EL-57 | 758655.932 | 3035180.413 | 15.036 |
| EL-58 | 758654.917 | 3035181.650 | 15.552 |
| EL-59 | 758653.902 | 3035182.886 | 15.512 |
| EL-60 | 758652.887 | 3035184.123 | 15.382 |
| EL-61 | 758651.871 | 3035185.360 | 15.423 |
| EL-62 | 758650.856 | 3035186.596 | 15.444 |
| EL-63 | 758649.841 | 3035187.833 | 15.284 |
| EL-64 | 758648.826 | 3035189.069 | 15.277 |
| EL-65 | 758647.810 | 3035190.306 | 15.222 |
| EL-66 | 758646.795 | 3035191.543 | 15.835 |
| EL-67 | 758645.780 | 3035192.779 | 15.851 |
| EL-68 | 758644.764 | 3035194.016 | 15.693 |
| EL-69 | 758643.749 | 3035195.253 | 15.667 |
| EL-70 | 758642.734 | 3035196.489 | 15.669 |
| EL-71 | 758641.719 | 3035197.726 | 15.652 |
| EL-72 | 758640.703 | 3035198.962 | 15.301 |
| Remote Pole | 758798.912 | 3034988.221 | 15.157 |

| 2D Survey – LINE 11 | | | |
|---|---|---|---|
| **Electrode ID** | **Easting (m)** | **Northing (m)** | **Elevation** |
| EL-01 | 758715.384 | 3035113.294 | 15.690 |
| EL-02 | 758714.369 | 3035114.531 | 15.680 |
| EL-03 | 758713.354 | 3035115.767 | 15.396 |
| EL-04 | 758712.338 | 3035117.004 | 15.583 |
| EL-05 | 758711.323 | 3035118.241 | 15.588 |
| EL-06 | 758710.308 | 3035119.477 | 15.601 |
| EL-07 | 758709.293 | 3035120.714 | 15.655 |
| EL-08 | 758708.277 | 3035121.951 | 15.602 |
| EL-09 | 758707.262 | 3035123.187 | 15.614 |
| EL-10 | 758706.247 | 3035124.424 | 15.507 |
| EL-11 | 758705.231 | 3035125.660 | 15.401 |
| EL-12 | 758704.216 | 3035126.897 | 15.393 |
| EL-13 | 758703.201 | 3035128.134 | 15.367 |
| EL-14 | 758702.186 | 3035129.370 | 15.269 |
| EL-15 | 758701.170 | 3035130.607 | 15.252 |
| EL-16 | 758700.155 | 3035131.844 | 15.251 |
| EL-17 | 758699.140 | 3035133.080 | 15.409 |
| EL-18 | 758698.125 | 3035134.317 | 15.359 |
| EL-19 | 758697.109 | 3035135.553 | 15.375 |
| EL-20 | 758696.094 | 3035136.790 | 15.378 |
| EL-21 | 758695.079 | 3035138.027 | 15.688 |
| EL-22 | 758694.064 | 3035139.263 | 15.720 |
| EL-23 | 758693.048 | 3035140.500 | 15.701 |
| EL-24 | 758692.033 | 3035141.737 | 15.669 |
| EL-25 | 758691.018 | 3035142.973 | 15.669 |
| EL-26 | 758690.003 | 3035144.210 | 15.687 |
| EL-27 | 758688.987 | 3035145.446 | 15.685 |
| EL-28 | 758687.972 | 3035146.683 | 15.883 |
| EL-29 | 758686.957 | 3035147.920 | 15.960 |
| EL-30 | 758685.941 | 3035149.156 | 15.940 |
| EL-31 | 758684.926 | 3035150.393 | 15.844 |
| EL-32 | 758683.911 | 3035151.630 | 15.759 |
| EL-33 | 758682.896 | 3035152.866 | 15.700 |
| EL-34 | 758681.880 | 3035154.103 | 15.738 |
| EL-35 | 758680.865 | 3035155.339 | 15.884 |
| EL-36 | 758679.850 | 3035156.576 | 15.890 |
| EL-37 | 758678.835 | 3035157.813 | 15.947 |
| EL-38 | 758677.819 | 3035159.049 | 15.997 |

| LINE 11 - Continued | | | |
|---|---|---|---|
| EL-39 | 758676.804 | 3035160.286 | 15.994 |
| EL-40 | 758675.789 | 3035161.523 | 15.848 |
| EL-41 | 758674.774 | 3035162.759 | 15.835 |
| EL-42 | 758673.758 | 3035163.996 | 15.799 |
| EL-43 | 758672.743 | 3035165.232 | 15.746 |
| EL-44 | 758671.728 | 3035166.469 | 15.675 |
| EL-45 | 758670.712 | 3035167.706 | 15.612 |
| EL-46 | 758669.697 | 3035168.942 | 15.599 |
| EL-47 | 758668.682 | 3035170.179 | 15.611 |
| EL-48 | 758667.667 | 3035171.416 | 15.635 |
| EL-49 | 758666.651 | 3035172.652 | 15.525 |
| EL-50 | 758665.636 | 3035173.889 | 15.520 |
| EL-51 | 758664.621 | 3035175.125 | 15.528 |
| EL-52 | 758663.606 | 3035176.362 | 15.051 |
| EL-53 | 758662.590 | 3035177.599 | 15.020 |
| EL-54 | 758661.575 | 3035178.835 | 15.019 |
| EL-55 | 758660.560 | 3035180.072 | 15.320 |
| EL-56 | 758659.545 | 3035181.308 | 15.334 |
| EL-57 | 758658.529 | 3035182.545 | 15.315 |
| EL-58 | 758657.514 | 3035183.782 | 15.639 |
| EL-59 | 758656.499 | 3035185.018 | 15.619 |
| EL-60 | 758655.484 | 3035186.255 | 15.733 |
| EL-61 | 758654.468 | 3035187.492 | 15.708 |
| EL-62 | 758653.453 | 3035188.728 | 15.703 |
| EL-63 | 758652.539 | 3035189.842 | 15.809 |
| EL-64 | 758651.422 | 3035191.201 | 15.852 |
| EL-65 | 758650.407 | 3035192.438 | 15.812 |
| EL-66 | 758649.392 | 3035193.675 | 15.732 |
| EL-67 | 758648.377 | 3035194.911 | 15.773 |
| EL-68 | 758647.361 | 3035196.148 | 15.794 |
| EL-69 | 758646.346 | 3035197.385 | 15.784 |
| EL-70 | 758645.331 | 3035198.621 | 15.777 |
| EL-71 | 758644.316 | 3035199.858 | 15.622 |
| EL-72 | 758643.300 | 3035201.094 | 15.585 |
| Remote Pole | 758798.912 | 3034988.221 | 15.157 |

| 2D Survey – LINE 12 | | | |
|---|---|---|---|
| **Electrode ID** | **Easting (m)** | **Northing (m)** | **Elevation** |
| EL-01 | 758718.012 | 3035115.452 | 15.640 |
| EL-02 | 758716.997 | 3035116.688 | 15.630 |
| EL-03 | 758715.981 | 3035117.925 | 15.646 |
| EL-04 | 758714.966 | 3035119.161 | 15.633 |
| EL-05 | 758713.951 | 3035120.398 | 15.638 |
| EL-06 | 758712.936 | 3035121.635 | 15.651 |
| EL-07 | 758711.920 | 3035122.871 | 15.455 |
| EL-08 | 758710.905 | 3035124.108 | 15.502 |
| EL-09 | 758709.890 | 3035125.345 | 15.514 |
| EL-10 | 758708.875 | 3035126.581 | 15.507 |
| EL-11 | 758707.859 | 3035127.818 | 15.501 |
| EL-12 | 758706.844 | 3035129.054 | 15.493 |
| EL-13 | 758705.829 | 3035130.291 | 15.467 |
| EL-14 | 758704.814 | 3035131.528 | 15.569 |
| EL-15 | 758703.798 | 3035132.764 | 15.552 |
| EL-16 | 758702.783 | 3035134.001 | 15.551 |
| EL-17 | 758701.768 | 3035135.238 | 15.609 |
| EL-18 | 758700.752 | 3035136.474 | 15.559 |
| EL-19 | 758699.737 | 3035137.711 | 15.575 |
| EL-20 | 758698.722 | 3035138.947 | 15.578 |
| EL-21 | 758697.707 | 3035140.184 | 15.588 |
| EL-22 | 758696.691 | 3035141.421 | 15.620 |
| EL-23 | 758695.399 | 3035142.995 | 15.601 |
| EL-24 | 758694.661 | 3035143.894 | 15.619 |
| EL-25 | 758693.646 | 3035145.131 | 15.619 |
| EL-26 | 758692.630 | 3035146.367 | 15.637 |
| EL-27 | 758691.615 | 3035147.604 | 15.635 |
| EL-28 | 758690.600 | 3035148.840 | 15.833 |
| EL-29 | 758689.585 | 3035150.077 | 15.910 |
| EL-30 | 758688.569 | 3035151.314 | 15.890 |
| EL-31 | 758687.554 | 3035152.550 | 15.894 |
| EL-32 | 758686.539 | 3035153.787 | 15.809 |
| EL-33 | 758685.523 | 3035155.024 | 15.750 |
| EL-34 | 758684.508 | 3035156.260 | 15.738 |
| EL-35 | 758683.493 | 3035157.497 | 15.734 |
| EL-36 | 758682.478 | 3035158.733 | 15.740 |
| EL-37 | 758681.462 | 3035159.970 | 15.797 |
| EL-38 | 758680.447 | 3035161.207 | 15.847 |

| LINE 12 - Continued | | | |
|---|---|---|---|
| EL-39 | 758679.432 | 3035162.443 | 15.794 |
| EL-40 | 758678.417 | 3035163.680 | 15.698 |
| EL-41 | 758677.401 | 3035164.917 | 15.685 |
| EL-42 | 758676.386 | 3035166.153 | 15.649 |
| EL-43 | 758675.371 | 3035167.390 | 15.546 |
| EL-44 | 758674.356 | 3035168.626 | 15.575 |
| EL-45 | 758673.340 | 3035169.863 | 15.512 |
| EL-46 | 758672.325 | 3035171.100 | 15.499 |
| EL-47 | 758671.310 | 3035172.336 | 15.511 |
| EL-48 | 758670.295 | 3035173.573 | 15.535 |
| EL-49 | 758669.279 | 3035174.810 | 15.175 |
| EL-50 | 758668.264 | 3035176.046 | 15.170 |
| EL-51 | 758667.249 | 3035177.283 | 15.078 |
| EL-52 | 758666.233 | 3035178.519 | 15.113 |
| EL-53 | 758665.218 | 3035179.756 | 15.202 |
| EL-54 | 758664.203 | 3035180.993 | 15.294 |
| EL-55 | 758663.188 | 3035182.229 | 15.270 |
| EL-56 | 758662.172 | 3035183.466 | 15.284 |
| EL-57 | 758661.157 | 3035184.703 | 15.315 |
| EL-58 | 758660.142 | 3035185.939 | 15.189 |
| EL-59 | 758659.127 | 3035187.176 | 15.169 |
| EL-60 | 758658.111 | 3035188.412 | 15.833 |
| EL-61 | 758657.096 | 3035189.649 | 15.758 |
| EL-62 | 758656.081 | 3035190.886 | 15.753 |
| EL-63 | 758655.066 | 3035192.122 | 15.759 |
| EL-64 | 758654.050 | 3035193.359 | 15.852 |
| EL-65 | 758653.035 | 3035194.596 | 15.812 |
| EL-66 | 758652.020 | 3035195.832 | 15.832 |
| EL-67 | 758651.004 | 3035197.069 | 15.823 |
| EL-68 | 758649.989 | 3035198.305 | 15.844 |
| EL-69 | 758648.974 | 3035199.542 | 15.834 |
| EL-70 | 758647.959 | 3035200.779 | 15.827 |
| EL-71 | 758646.943 | 3035202.015 | 15.772 |
| EL-72 | 758645.928 | 3035203.252 | 15.735 |
| Remote Pole | 758798.912 | 3034988.221 | 15.157 |

| 3D Survey – LOOP 1 | | | |
|---|---|---|---|
| **Electrode ID** | **Easting (m)** | **Northing (m)** | **Elevation** |
| EL-01 | 758616.435 | 3035180.866 | 15.001 |
| EL-02 | 758618.368 | 3035182.452 | 15.190 |
| EL-03 | 758620.301 | 3035184.038 | 15.351 |
| EL-04 | 758622.233 | 3035185.623 | 15.301 |
| EL-05 | 758624.164 | 3035187.212 | 15.270 |
| EL-06 | 758626.096 | 3035188.798 | 15.370 |
| EL-07 | 758628.028 | 3035190.384 | 15.640 |
| EL-08 | 758629.964 | 3035191.966 | 15.790 |
| EL-09 | 758631.893 | 3035193.557 | 15.951 |
| EL-10 | 758633.830 | 3035195.137 | 15.301 |
| EL-11 | 758635.763 | 3035196.723 | 15.585 |
| EL-12 | 758637.696 | 3035198.309 | 15.735 |
| EL-13 | 758639.622 | 3035199.903 | 15.320 |
| EL-14 | 758641.561 | 3035201.480 | 15.319 |
| EL-15 | 758643.494 | 3035203.066 | 15.470 |
| EL-16 | 758646.626 | 3035202.402 | 15.484 |
| EL-17 | 758648.213 | 3035200.470 | 15.465 |
| EL-18 | 758649.799 | 3035198.537 | 15.039 |
| EL-19 | 758651.385 | 3035196.605 | 15.019 |
| EL-20 | 758652.972 | 3035194.673 | 15.013 |
| EL-21 | 758654.558 | 3035192.741 | 15.018 |
| EL-22 | 758656.144 | 3035190.808 | 15.010 |
| EL-23 | 758657.757 | 3035188.897 | 15.030 |
| EL-24 | 758659.317 | 3035186.944 | 15.146 |
| EL-25 | 758660.903 | 3035185.012 | 15.133 |
| EL-26 | 758662.490 | 3035183.079 | 15.138 |
| EL-27 | 758664.099 | 3035181.166 | 15.151 |
| EL-28 | 758665.685 | 3035179.234 | 15.205 |
| EL-29 | 758667.271 | 3035177.301 | 15.252 |
| EL-30 | 758668.835 | 3035175.351 | 15.264 |
| EL-31 | 758670.421 | 3035173.418 | 15.157 |
| EL-32 | 758672.028 | 3035171.502 | 15.159 |
| EL-33 | 758673.594 | 3035169.554 | 15.109 |
| EL-34 | 758675.199 | 3035167.637 | 15.125 |
| EL-35 | 758676.767 | 3035165.689 | 15.119 |
| EL-36 | 758678.370 | 3035163.771 | 15.119 |
| EL-37 | 758679.956 | 3035161.838 | 15.137 |
| EL-38 | 758681.542 | 3035159.906 | 15.135 |

| LOOP 1 - Continued | | | |
|---|---|---|---|
| EL-39 | 758683.127 | 3035157.973 | 15.333 |
| EL-40 | 758684.699 | 3035156.028 | 15.410 |
| EL-41 | 758686.299 | 3035154.107 | 15.390 |
| EL-42 | 758687.871 | 3035152.164 | 15.294 |
| EL-43 | 758689.458 | 3035150.232 | 15.209 |
| EL-44 | 758691.056 | 3035148.309 | 15.150 |
| EL-45 | 758692.641 | 3035146.376 | 15.188 |
| EL-46 | 758694.227 | 3035144.443 | 15.284 |
| EL-47 | 758695.803 | 3035142.503 | 15.290 |
| EL-48 | 758697.398 | 3035140.578 | 15.347 |
| EL-49 | 758698.976 | 3035138.638 | 15.397 |
| EL-50 | 758700.562 | 3035136.706 | 15.394 |
| EL-51 | 758702.148 | 3035134.774 | 15.298 |
| EL-52 | 758703.741 | 3035132.847 | 15.285 |
| EL-53 | 758705.327 | 3035130.914 | 15.249 |
| EL-54 | 758706.912 | 3035128.981 | 15.196 |
| EL-55 | 758708.498 | 3035127.048 | 15.225 |
| EL-56 | 758710.080 | 3035125.113 | 15.162 |
| EL-57 | 758711.667 | 3035123.181 | 15.149 |
| EL-58 | 758713.253 | 3035121.248 | 15.161 |
| EL-59 | 758714.839 | 3035119.316 | 15.185 |
| EL-60 | 758716.426 | 3035117.384 | 15.175 |
| EL-61 | 758716.426 | 3035114.151 | 15.640 |
| EL-62 | 758714.534 | 3035112.596 | 15.690 |
| EL-63 | 758712.602 | 3035111.010 | 15.551 |
| EL-64 | 758710.670 | 3035109.423 | 15.651 |
| EL-65 | 758708.737 | 3035107.837 | 15.643 |
| EL-66 | 758706.805 | 3035106.251 | 15.293 |
| EL-67 | 758704.869 | 3035104.669 | 15.293 |
| EL-68 | 758702.941 | 3035103.078 | 15.269 |
| EL-69 | 758701.008 | 3035101.492 | 15.251 |
| EL-70 | 758699.076 | 3035099.905 | 15.401 |
| EL-71 | 758697.144 | 3035098.319 | 15.343 |
| EL-72 | 758695.205 | 3035096.741 | 15.351 |
| Remote Pole | 758618.368 | 3035182.452 | 15.190 |

| 3D Survey – LOOP 2 | | | |
|---|---|---|---|
| **Electrode ID** | **Easting (m)** | **Northing (m)** | **Elevation** |
| EL-01 | 758716.426 | 3035117.384 | 15.640 |
| EL-02 | 758716.466 | 3035114.182 | 15.690 |
| EL-03 | 758714.534 | 3035112.596 | 15.551 |
| EL-04 | 758712.602 | 3035111.010 | 15.651 |
| EL-05 | 758710.670 | 3035109.423 | 15.643 |
| EL-06 | 758708.735 | 3035107.840 | 15.293 |
| EL-07 | 758706.802 | 3035106.255 | 15.293 |
| EL-08 | 758704.869 | 3035104.669 | 15.269 |
| EL-09 | 758702.936 | 3035103.083 | 15.251 |
| EL-10 | 758701.003 | 3035101.498 | 15.401 |
| EL-11 | 758699.076 | 3035099.905 | 15.343 |
| EL-12 | 758697.144 | 3035098.319 | 15.351 |
| EL-13 | 758695.212 | 3035096.733 | 15.351 |
| EL-14 | 758693.272 | 3035095.155 | 15.320 |
| EL-15 | 758691.339 | 3035093.569 | 15.319 |
| EL-16 | 758687.820 | 3035093.916 | 15.470 |
| EL-17 | 758686.234 | 3035095.848 | 15.484 |
| EL-18 | 758684.648 | 3035097.780 | 15.465 |
| EL-19 | 758683.061 | 3035099.713 | 15.039 |
| EL-20 | 758681.475 | 3035101.645 | 15.019 |
| EL-21 | 758679.889 | 3035103.577 | 15.013 |
| EL-22 | 758678.302 | 3035105.509 | 15.018 |
| EL-23 | 758676.716 | 3035107.442 | 15.010 |
| EL-24 | 758675.130 | 3035109.374 | 15.030 |
| EL-25 | 758673.543 | 3035111.306 | 15.146 |
| EL-26 | 758671.957 | 3035113.238 | 15.133 |
| EL-27 | 758670.371 | 3035115.170 | 15.138 |
| EL-28 | 758668.784 | 3035117.103 | 15.151 |
| EL-29 | 758667.198 | 3035119.035 | 15.205 |
| EL-30 | 758665.612 | 3035120.967 | 15.252 |
| EL-31 | 758664.025 | 3035122.899 | 15.264 |
| EL-32 | 758662.439 | 3035124.832 | 15.157 |
| EL-33 | 758660.852 | 3035126.764 | 15.159 |
| EL-34 | 758659.266 | 3035128.696 | 15.109 |
| EL-35 | 758657.680 | 3035130.628 | 15.125 |
| EL-36 | 758656.094 | 3035132.561 | 15.119 |

| LOOP 2 - Continued | | | |
|---|---|---|---|
| EL-37 | 758654.507 | 3035134.493 | 15.119 |
| EL-38 | 758652.921 | 3035136.425 | 15.137 |
| EL-39 | 758651.334 | 3035138.357 | 15.135 |
| EL-40 | 758649.748 | 3035140.289 | 15.333 |
| EL-41 | 758648.162 | 3035142.222 | 15.410 |
| EL-42 | 758646.575 | 3035144.154 | 15.390 |
| EL-43 | 758644.989 | 3035146.086 | 15.294 |
| EL-44 | 758643.403 | 3035148.018 | 15.209 |
| EL-45 | 758641.816 | 3035149.950 | 15.150 |
| EL-46 | 758640.230 | 3035151.883 | 15.188 |
| EL-47 | 758638.643 | 3035153.815 | 15.284 |
| EL-48 | 758637.057 | 3035155.747 | 15.290 |
| EL-49 | 758635.471 | 3035157.680 | 15.347 |
| EL-50 | 758633.885 | 3035159.612 | 15.397 |
| EL-51 | 758632.298 | 3035161.544 | 15.394 |
| EL-52 | 758630.712 | 3035163.476 | 15.298 |
| EL-53 | 758629.126 | 3035165.409 | 15.285 |
| EL-54 | 758627.539 | 3035167.341 | 15.249 |
| EL-55 | 758625.953 | 3035169.273 | 15.196 |
| EL-56 | 758624.366 | 3035171.205 | 15.225 |
| EL-57 | 758622.780 | 3035173.137 | 15.162 |
| EL-58 | 758621.194 | 3035175.069 | 15.149 |
| EL-59 | 758619.607 | 3035177.002 | 15.161 |
| EL-60 | 758618.021 | 3035178.934 | 15.185 |
| EL-61 | 758618.368 | 3035182.452 | 15.144 |
| EL-62 | 758620.301 | 3035184.038 | 15.134 |
| EL-63 | 758622.233 | 3035185.623 | 15.127 |
| EL-64 | 758624.166 | 3035187.209 | 15.072 |
| EL-65 | 758626.099 | 3035188.795 | 15.001 |
| EL-66 | 758628.032 | 3035190.380 | 15.190 |
| EL-67 | 758629.964 | 3035191.966 | 15.351 |
| EL-68 | 758631.893 | 3035193.557 | 15.301 |
| EL-69 | 758633.825 | 3035195.143 | 15.270 |
| EL-70 | 758635.763 | 3035196.723 | 15.370 |
| EL-71 | 758637.696 | 3035198.309 | 15.640 |
| EL-72 | 758639.628 | 3035199.894 | 15.790 |
| Remote Pole | 758618.368 | 3035182.452 | 15.190 |

# VITAE

| | | |
|---|---|---|
| Name | : | Muhammad Haroon Tayyab |
| Nationality | : | Pakistani |
| Date of Birth | : | 09-Mar-1987 |
| Email | : | harooni2@hotmail.com<br>g201301230@kfupm.edu.sa |
| Address | : | House No. 122, Parklane Homes, Paragon City<br>Burki Road, Lahore, Pakistan. |
| Academic background | : | M.S. in Geophysics, 2016, King Fahd University of Petroleum & Minerals.<br>B.S. in Geological Engineering, 2009, University of Engineering & Technology, Lahore, Pakistan. |
| Research papers | : | An integrated approach to study karstic terrain for construction suitability using electrical resistivity tomography, rock quality and aerial imagery. Journal of Environmental Earth Sciences (ENGE) (1st Revision submitted - under consideration).<br><br>Investigation of Seepage through Embankment Dam Using 3D Electrical Resistivity Tomography and 3D Ground Penetrating Radar Imaging. SAGEEP |

Denver USA (2017). (Published-conference proceedings), Journal of Geophysics and Engineering. (Submitted - under review).

Application of ΔLogR technique for quantification of Total Organic Carbon TOC from wireline logs – for lower Goru and Sembar Formation, Middle Indus Basin Pakistan. 16th Formation Evaluation Symposium, JOGMEC-TRC, Chiba, Japan (2010) (presented and published in conference proceedings)